SISSA/ISAS, International School for Advanced Studies
via Beirut 4 - 34014 Trieste - Italy

Physical interpretations of observations of Core Collapse SNe

Thesis submitted for the degree of
"Doctor Philosophiæ"

In
Astrophysics

CANDIDATE

Abouazza Elmhamdi

SUPERVISORS

Prof. I. John. Danziger
Prof. John Miller

October 2003

Abstract

My Ph.D work was dedicated mainly to the study of Core Collapse SNe (CCSNe), both their observational properties and their physical interpretation. I have been particularly involved in the study of SN 1999em in NGC 1637, a type II Plateau event (SN IIP), possibly the most well studied event among CCSNe after SN 1987A. In fact a large study, covering more than 600 days after outburst, photometrically and spectroscopically, has been presented (**Elmhamdi A. et al. 2003, MNRAS, 338, 939**). The widely spaced and critical observations of this object have provided a unique opportunity to test our knowledges of the physics of CCSNe and as well an understanding of the different parameters that characterize the pre-SN evolution. In particular we have argued for dust condensation, spectroscopically and photometrically, between days 465 and 510. Support for our finding of dust formation comes from the more recent late optical photometric observations sampling 679 to 738 days after explosion date presented by Leonard et al. (2003; astro-ph/0305259). We have also pointed out the differences between SN 1999em compared to SN 1987A in manifesting the same events (e.g. Bochum event, asymmetry, dust formation), and have discussed the physical interpretations of such diversities. The bolometric properties of the SN have also been presented and discussed, providing an estimate of the ejected ^{56}Ni mass, which was lower ($\sim$ 0.02 $M_{\odot}$) compared to a typical value for SNe IIP ($\sim$ 0.07 $M_{\odot}$). An estimate of the oxygen mass has also been provided. Interestingly, two correlations are hinted at when analysing the observational behaviour of SN 1999em and other IIP events, namely, a curious flattening in the light curves, just after the steep decline from the plateau phase, clearer for the blue bands. This behaviour is also reported in other events, having all lower ejected ^{56}Ni mass (SNe 1997D, 1991G and 1999eu), indicating this behaviour to be a common feature in faint SNe IIP. In addition the duration of the flattening period seems to be correlated to the amount of ejected ^{56}Ni. The second hinted correlation is between the measured Hα luminosities and ^{56}Ni mass when compared to SN 1987A at later phases. Indeed this second hinted correlation was the real incentive for a following project in which our main goal was to check the possibility of using Hα luminosity at the nebular epoch as a tracer of ^{56}Ni mass in SNe IIP.

My second project was a study of a sample of type IIP SNe on the basis of available photometry and spectra, especially at latter epochs (**Elmhamdi A., Chugai N. N. and Danziger I. J. 2003, A&A, 404, 1077**). The main goal of the work was to check the idea of using Hα luminosity as tracer of ^{56}Ni mass in type IIP SNe. We make use of collected published photometry while the utilized spectra have been taken from

Asiago/ESO Catalogue. Additional spectra were provided kindly by R. Stathakis. Once we fix the points related to the extinction and distance, which are crucial when dealing with a SN-sample study, we proceed with computing the amounts of ejected ^{56}Ni photometrically using the absolute V-light curve of SN 1987A as template (in the 120−400 days time range). We found a range from lower values for SN 1999eu and SN 1997D to a higher one for SN 1992H, with an average of about 0.05 $M_{\odot}$. Analysing the absolute light curves of the events, we introduced a new parameter, called "*steepness*" and dubbed S, which describes the shape of the light curves and provides a way to measure the decay rate at the inflection point. A confirmation of the correlation between the ^{56}Ni mass and plateau M_V found by Hamuy (2003, ApJ, 582, 905) is evident, while an interesting by-product of the sample photometry analysis is the demonstrated correlation between ^{56}Ni mass and the steepness parameter S. The correlation is such that the steeper the decline at the inflection point the lower is the mass of ^{56}Ni. This correlation is interesting in the sense that, if confirmed, will provide distance and extinction independent estimates of the ^{56}Ni mass in SNe IIP. We then applied a two-zone model of the Hα luminosity in SN IIP to explore the sensitivity of the Hα behaviour to variation of model parameters. The primary purpose of the upgraded model is to specify better the early nebular phase compared to the previous version (Chugai 1990, SvAL, 16, 457). We found that if mass, energy and mixing conditions do not vary strongly among SNe IIP (less than factor 1.4) then with an accuracy better than 10% Hα luminosity is proportional to ^{56}Ni mass during the 200 – 400 days after explosion. Hα luminosities were then used to derive ^{56}Ni masses. This was done employing two approaches: first, using the Hα light curve in SN 1987A as template and, second, applying the model computations. Both approaches agree within 15% unless we are dealing with extreme cases such as SN 1970G (type IIP/L) and underluminous SN 1997D. In both these cases we should possess additional information about ejecta mass and energy to derive the ^{56}Ni mass from Hα. The ^{56}Ni mass values derived from the photometry and Hα luminosity agree within 20%, which thus gives us confidence that Hα is a good indicator of the amount of ^{56}Ni in SNe IIP. Simultaneously, this consistency suggests that parameters of SNe IIP (mass, energy and mixing) are not very different. In fact this is consistent with the uniformity of plateau luminosities and plateau lengths of SNe IIP. Worth noting is the simple approach of using Hα light curve of SN 1987A as a template to estimate the ^{56}Ni mass. Indeed this simple approach has been applied for three SNe for which we have late spectra but no photometry (SNe 1995ad, 1995V and 1995W), where we obtained reasonable values, demonstrating the usefulness of the method.

The last part of my Ph.D program was devoted to the study and analysis of observational properties of some type Ib/c SNe. Indeed, an analysis of photometry and spectra of the type Ib SN 1990I have been completed (**A. Elmhamdi** & **I. J. Danziger**

2003; In preparation). We investigate many particular observational aspects this event showed during its evolution. SN 1990I is found to show higher expansion velocities compared to the type Ib sample studied by Branch et al. (2002, ApJ, 566, 1005). We show evidence of helium lines in the ejecta. This event provides further understanding of some features that may or may not be common in this class of objects (i.e. possible dust condensation, observational evidence of asymmetry), and as well gives a check on the present believable physical scenario behind CCSNe that lack hydrogen lines in their spectra at the level of the progenitor stars. We give an estimate of the ejecta and ^{56}Ni masses ($M(^{56}Ni) = 0.11$ M$_\odot$ and $M_{ej} = 3.7$ M$_\odot$) by applying a simplified γ-ray deposition model to the recovered quasi-bolometric "$BVRI$" light curve. This latter shows a change of slope at late phases, with an e-folding time of 60 $\pm$2 d in the [50 : 200] d time interval, clearly faster than the one of ^{56}Co decay (i.e. 111.3 d), suggestive of the γ-rays escape with lower deposition, consistent with the low mass nature of the ejecta. At early phases ([30 : 100] d), the pseudo-light curves of SNe 1990I and 1993J are found to display a high degree of similarity. After day 200 they behave differently: while SN 1993J tends to flatten, SN 1990I demonstrates a dramatic fall with a deficit in luminosity estimated around day 308 to be about 50%. Spectroscopically, SN 1990I shows evidence for asymmetry and clumping. A blueshift in some nebular lines is reported, which we interpret as due to dust condensation in the ejecta when combined with the rapid and sudden drop in both the pseudo-bolometric light curve and $(B - V)$ colour around day 250.

In an appendix I outline a possible method for determining O/Fe yields from CCSNe. At the moment the uncertainties in estimates of oxygen masses are too large to draw safe conclusions about progenitor masses.

Contents

List of Figures

List of Tables

Chapter 1

Introduction: General review on supernova

The appearance of the term "*Supernovae*" (SNe) as a definition of new astrophysical objects had been introduced first in 1934 by Baade & Zwickey[1] in order to distinguish them from the bright stellar outbursts called "Novae". The fundamental classification scheme of SNe was recognized by Minkowski (1941)[20], who distinguished, on the basis of the presence (or not) of hydrogen lines in the SNe spectra, two different classes, namely: type II and type I. These objects, being as bright as the whole galaxy and having a fundamental role in synthesizing and distributing heavy elements through the interstellar medium, have been shown to deserve special interest from astronomers (both theorists and observers) over the last decades.

1.1 Taxonomy and observational characteristics

To account for the diversities in the SNe observations, spectroscopically and photometrically, the SNe taxonomy has evolved with time, becoming more rich and complex (Wheeler & Harkness 1990[29]; Filippenko 1997[11]). Figure 1.1 shows the general subdivision within SNe types based on the element abundances in their spectra and the shape of their light curves.

Here, I will describe the main properties of each SN class on the level of our present understanding of their physics (i.e. explosion mechanisms, environments, progenitors and possible remnants). Further detailed descriptions will be provided through the chapters of the thesis, especially for the core collapse objects (SNe II, Ib/c).

1.1.1 Thermonuclear class: SNe Ia

At early phases, type Ia SNe are spectroscopically distinguishable by the absence of hydrogen lines and the presence of a deep absorption feature near 6150 Å produced by

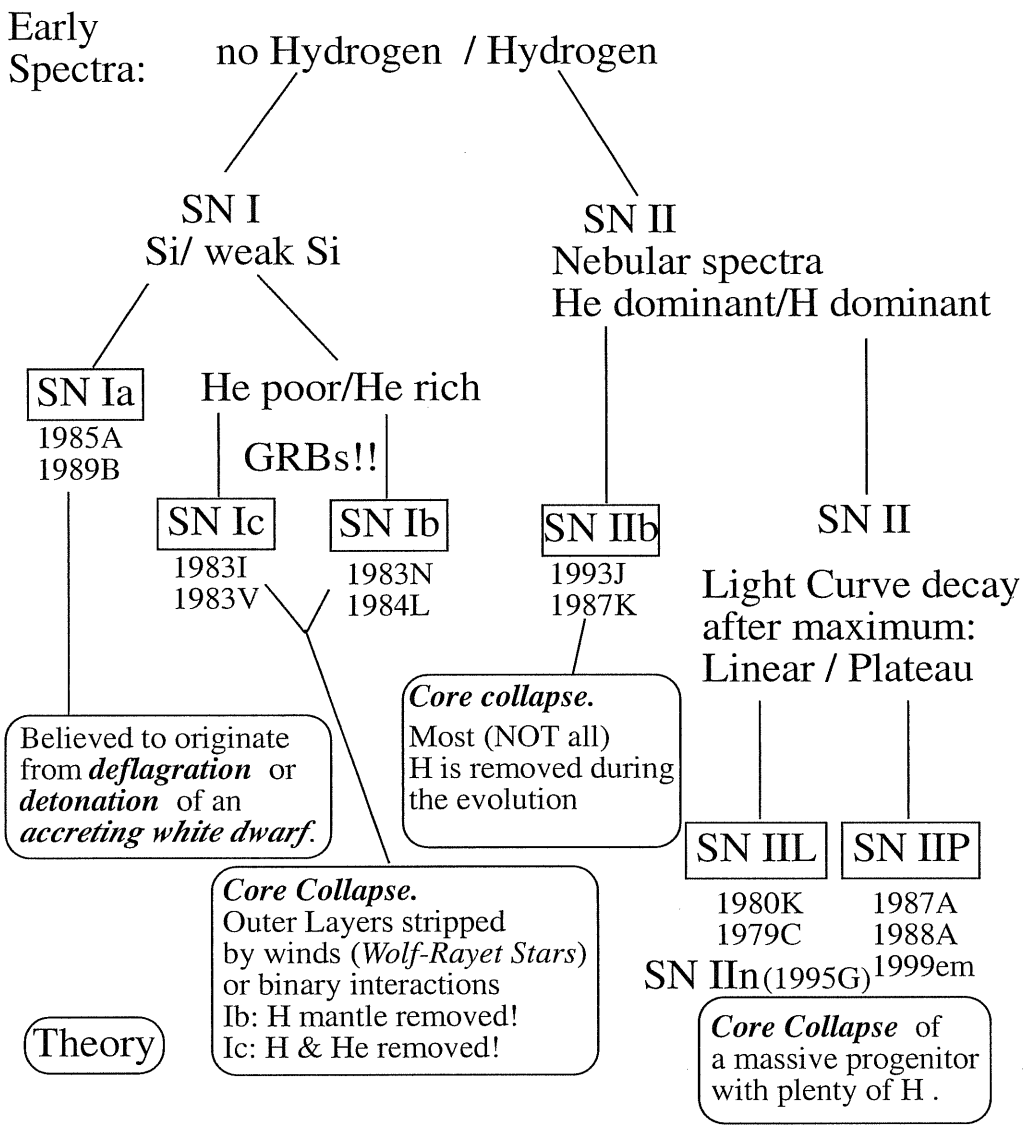

Figure 1.1: Summary of the present understanding of the SNe classification and their possible progenitors. From M. J. Montes home page with modifications (http://rsd-www.nrl.navy.mil/7212/montes/).

blueshifted Si II 6355 Å. Features due to Fe II, S II and Ca II are clearly recognized around maximum. At late phases, however, iron group emission lines dominate (Fig 1.2). The weakness of intermediate elements, especially oxygen, during the nebular phase possibly indicates the low mass nature of the progenitor. Photometrically, SNe Ia light curves are found to display small dispersion in absolute magnitude (see Fig. 1.3 for a B-band template). Except for rare cases of individual differences among type Ia SNe, e.g. SNe 1991bg and 1991T, the observed homogeneity (i.e. spectral evolution, light curves shape, colours) is explained as a consequence of the progenitor (white dwarfs "WD"), being well defined (Leibundgut 2000 [17]). In addition, the small peak width light curve and the lack of radio emission demonstrates, respectively, the compactness nature of the progenitor star and the low mass loss during its evolution.

Based on thermonuclear explosion mechanism, the most accepted scenario adopted to account for many observed features of SNe Ia is an accreting WD in a binary system. Despite the nature of the donor star the final picture is the same: explosion of a C/O-WD with a mass close to M_{Ch} (Chandrasekhar mass). The star is disrupted completely, leaving no compact object remnant behind. Neutrinos, apparently do not play an important role in type Ia SNe since they carry away only $\sim$ 1% of the thermonuclear energy released, in contrast to core collapse SNe where neutrinos play a fundamental role.

We note here the very recent and interesting observations of the type Ia SN 2002ic. This event shows strong and narrow-peaked hydrogen emission lines, similar to what is observed in type IIn SNe. These facts are interpreted as the first observational evidence of large amounts of "CSM" around a type Ia SN, suggesting a progenitor system formed by C/O-WD and a massive asymptotic giant branch star ($\sim$ $3-7$ $M_{\odot}$) as a donor (Hamuy et al. 2003 [15]).

Type Ia SNe are found to occur in all morphological types of galaxies, and their homogeneity (physics and observations) makes them good probes for cosmological use. Worth noticing is that type Ia SNe are the main iron-producers in the universe (typically $M(^{56}Ni) \simeq 0.6 M_{\odot}$), providing an important source of metal enrichment.

1.1.2 Core collapse class: SNe Ib/c and II

Type II and Ib/c SNe are believed to result from gravitational core collapse in massive stars ($M_{initial} \geq 8 M_{\odot}$). This fact is supported by the occurrence of these events in spiral galaxies and star forming regions, generally in/or near spiral arms and HII regions, and never being seen in elliptical galaxies. Type Ib/c show relatively strong radio emission (e.g. SNe 1983N and 1984L), while type II SNe are quite diverse, with type IIP (e.g. SN 1999em) being weak radio emitters, consistent with their low mass loss rate (Sramek & Weiler, 2003 [28]).

The liberated gravitational energy by the core collapse is of the order $\sim 10^{53}$ erg, which represents the difference in binding energy between the core and the remnant (generally a neutron star). Only a fraction of about 1% of this released huge energy is

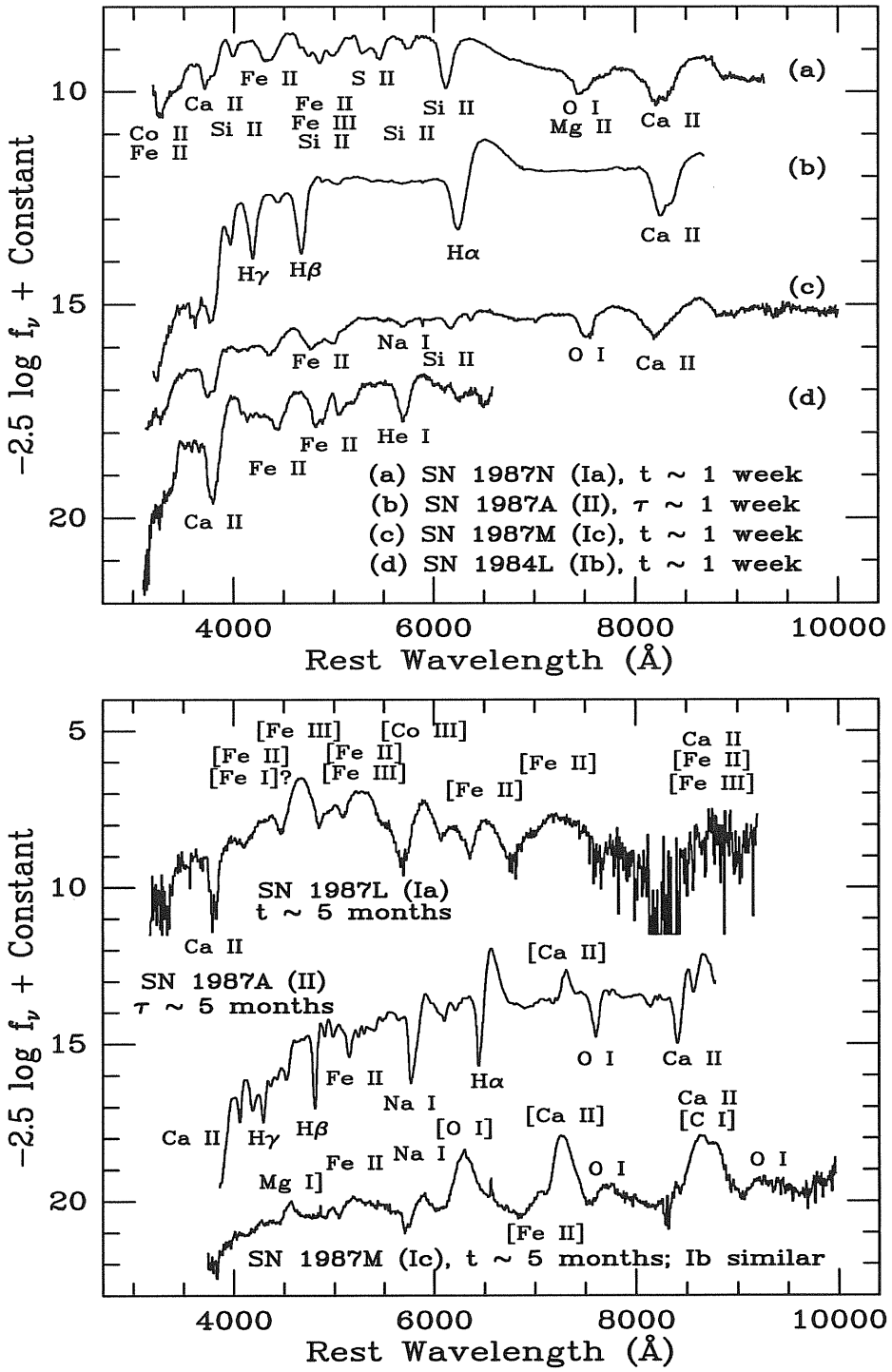

Figure 1.2: Photospheric (upper panel) and nebular (lower panel) spectra of different SN types. Prominent lines are shown (taken from Filippenko 2000 [12]).

in form of kinetic energy ($\sim 10^{51}$ erg) and $\sim$0.01% is in form of optical radiation ($\sim 10^{49}$ erg), while 99% account for energy emitted by neutrinos. Two principle mechanisms are responsible to trigger the collapse in massive stars, namely: electron capture and iron photodissociation. The envelope then rebounds possibly with help from neutrinos.

Type Ib/c

Type Ib/c SNe lost their hydrogen envelopes prior to the core collapse. Two scenarios may lead to such observed properties: a high mass progenitor with an extreme mass loss preceding the explosion (generally Wolf Rayet stars that shed their hydrogen in massive stellar wind) or less massive star being striped of its outer envelope in a binary system once it exceeds its Roche lobe.

The early time spectra of this class of objects are illustrated in Fig. 1.2 (upper panel). The basic feature that distinguishes type Ib from Ic is the presence of He I lines, indicating an additional loss of helium envelope for type Ic SNe. On the other hand the claims of the presence of He I 10830 Å in some type Ic spectra, e.g. SN 1990W (Wheeler et al. 1994 [30]) and SN 1994I (Filippenko et al. 1995 [10]), points to the presence of some amount of helium in type Ic SNe and highlights the difficulty of differentiating the nature of the progenitor stars of these two objects. The presence of hydrogen (small amount) is as well of high importance in this class of objects since it reflects the nature and the composition of the progenitor star prior the explosion, especially for type Ib SNe. It has been a matter of debate concerning the identification of Hα in the 6000 – 6500 Å spectral region in some type Ib events (SN 1999dn, Deng et al. 2000 [5]; SN 1991D, Benetti et al. 2002 [2]) or even in some extreme SNe Ic cases (SN 1987M, Filippenko 1992 [9]). The possible presence of hydrogen in type Ib/c SNe combined with the discovery of transition events that evolve from normal type II to type Ib as they aged (e.g. SN 1987K and 1993J, dubbed IIb) suggests a clear link between SNe of type II and Ib/c. At the nebular phase, SNe Ib/c are similar and both show presence of unblended intermediate mass elements (Fig 1.2, lower panel) as well as iron.

Photometrically SNe Ib/c are fainter than type Ia. This is essentially because of their lower ejected ^{56}Ni mass ($\sim 0.1\ M_{\odot}$). Typical B-light curves of type Ib and Ic SNe are shown in Fig. 1.3. A simple comparison reveals the fact that type Ib show broader peak width and small peak-to-tail contrast, while type Ic SNe have narrower width and greater peak-to-tail contrast. This may point to a correlation between the peak-width and the way the SN declines from maximum light. I will discuss the different behaviour displayed by the type Ib/c V-light curves in Chap. 4 when analysing a sample of SNe Ib/c light curves. A large sample of SNe Ib/c light curves are needed to draw any conclusion about the use of light curve shape, during the first 100 days since explosion, to distinguish type Ib from type Ic events.

Finally, the possible connection of the highly energetic events (e.g. SN 1998bw and SN 2003dh) with Gamma ray bursts (GRBs) have opened a new window on the study of a new class called "Hypernovae" (Woosley et al. 1999 [31]; Nomoto et al. 2000 [23])

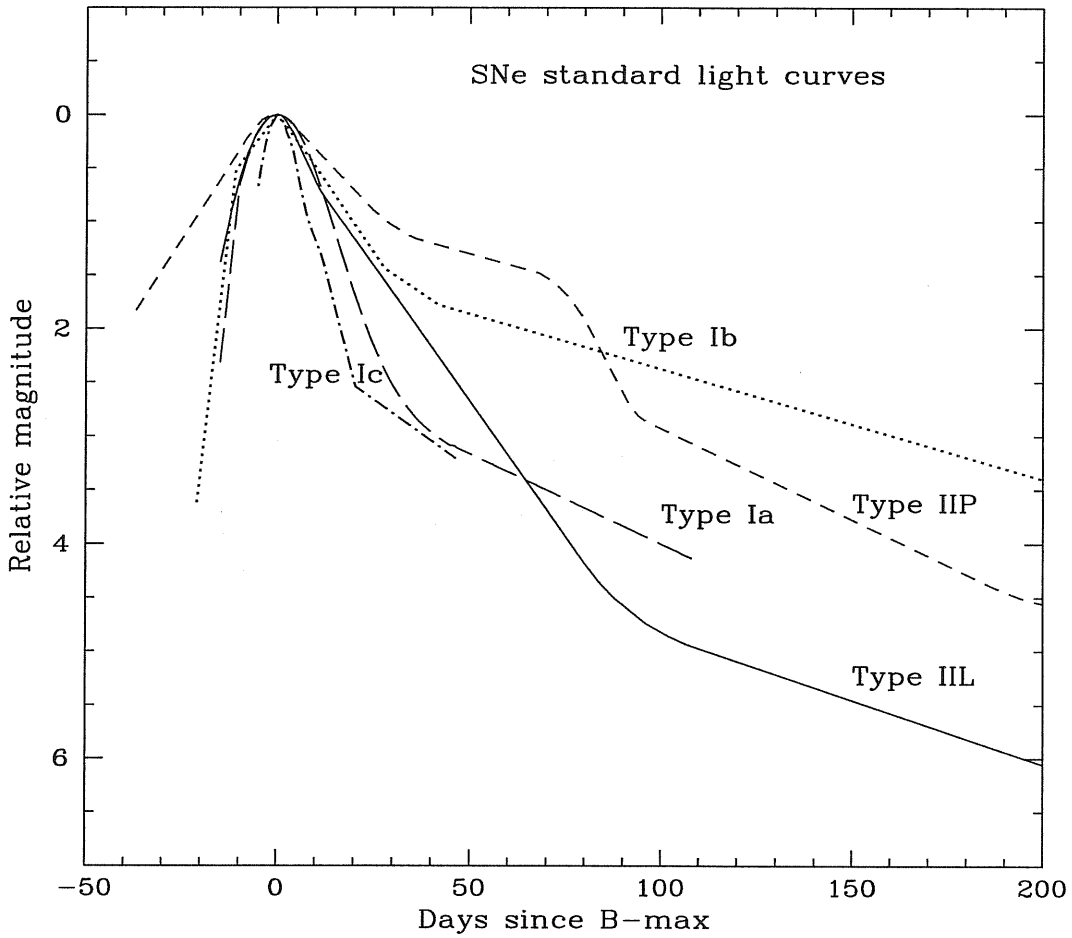

Figure 1.3: Variety of SNe light curves. The light curves are normalized to B-maximum. Type IIL, IIP: mean B-light curves from Doggett & Branch (1985)[6]. Type Ia: from Leibundgut et al. (1991)[16]. Type Ib: we use combined light curves of 1984L and 1985F. Type Ic: we use the typical SN 1994I.

Type II

Type II SNe surely embrace the widest range of properties among the SN panorama. Spectroscopically, the unique characteristic which all the SNe II share is the presence of hydrogen lines. During the photospheric phase, type II SNe display broad P-Cygni profiles of hydrogen Balmer lines superimposed on a blue continuum (Fig. 1.2, upper panel). The nebular spectra, on the other hand, are dominated by a very strong Hα and prominent [O I], [Ca II] and Ca II emission lines (Fig. 1.2, lower panel). According to the shape of the light curves, SNe II are generally divided into two main groups: type IIP (plateau) and type IIL (linear) and they are basically fainter than SN type Ia. Representative light curves are shown in Fig. 1.3.

No difference is so far clear in the spectral display between type IIP and IIL SNe, although the absence of the absorption component in the Hα P-Cygni profile around maximum has been claimed as an intrinsic property of type IIL (Wheeler & Harkness 1990 [29]). Large samples of type IIL spectra are needed, however, to draw any conclusion about this possibility.

An additional subclass of type II objects that display narrow components in their spectra on top of broader or intermediate emissions are labeled type IIn SNe (e.g. SNe 1988Z and 1995G). These narrow features are believed to result from the interaction of the ejecta with a dense circumstellar environment (Chugai & Danziger 1994 [4]). We note here the existence of an event that changes its behaviour from an interacting event (IIn) at early time to a normal type IIP later on, namely SN 1987C (Schlegel & Kirshner 1998 [26]).

The different photometric evolutionary phases in type II SNe have been well studied thanks to the high quality data of SN 1987A. The initial increase to the peak and the following decrease are related to the shock breakout and the cooling of the envelope. A phase of almost constant luminosity followed in type IIP, lasting about 2-3 months (e.g. SN 1999em, Elmhamdi et al. 2003a [7]). This phase is produced by the balance between the expansion of the photosphere and the cooling. A hydrogen recombination wave propagates inward, in mass, through the supernova envelope keeping the photospheric parameters (i.e. radius, velocity and temperature) almost constant. In this context, it is easy to see that the type II L progenitors have less massive hydrogen envelops ($\sim 1-2\ M_{\odot}$) compared to type IIP ($\sim 8\ M_{\odot}$). In fact, a model in which a common envelope evolution in massive binary systems with varying mass ratios and separations of the components has been argued to lead to various degrees of stripping of the envelope (Nomoto et al. 1995 [22]). Within this scenario the decrease in the hydrogen envelope mass matches the following sequence of SNe types: IIL–IIb–Ib–Ic.

The physics of the plateau phase in type IIP SNe have been well analysed and successfully modeled (Litvinova & Nadyozhin 1985 (LN85)[18]; Chugai 1991 [3]; Popov 1993 (P93)[24]). These models have provided simple approximation formulae which allow to estimate energy (E), ejecta mass (M) and the presupernova radius (R) from observational parameters of individual events, namely: the plateau duration t_p, a representative

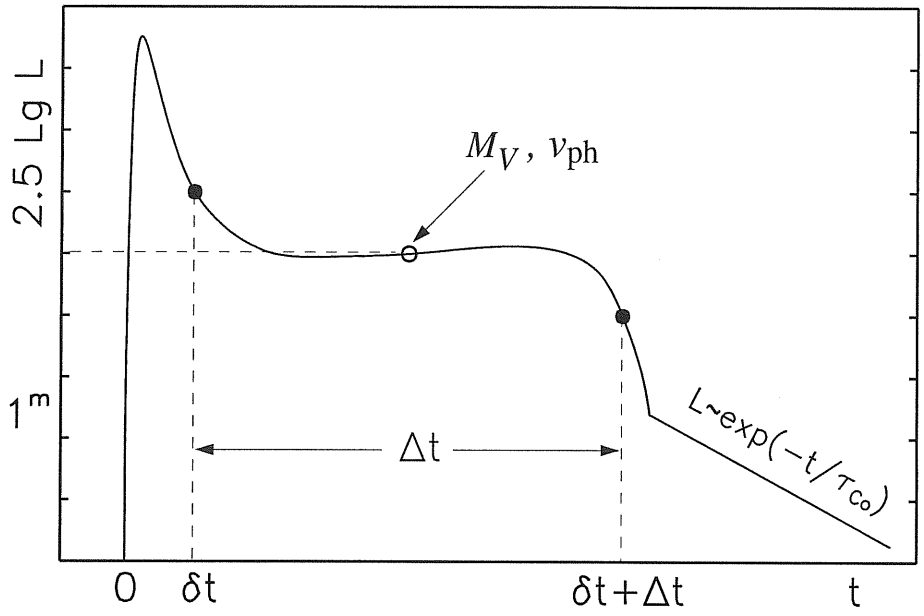

Figure 1.4: An example of a type IIP light curve. The open circle marks the middle of the plateau. From Nadyozhin (2003)[21]

photospheric velocity v_{ph} and the absolute plateau V−magnitude M_V. Figure 1.4. displays a schematic SN IIP light curve. Shown are the plateau duration boundaries and the time at which the absolute V−magnitude and the photospheric velocity can be measured according to LN85.

According to the P93 analytical model, the plateau duration is more sensitive to the envelope mass than energy and radius ($t_p \propto M^{1/2}R^{1/6}E^{-1/6}$). This dependence combined with the observed similarity in the plateau lengths is suggestive of the uniformity in the ejecta masses in type IIP SNe.

The plateau phase is followed by a steep decline, indicative of the onset of the nebular phase and the start of the radioactive decline. The way the SN declines from the plateau phase to reach the radioactive tail is highly correlated with the mass of ^{56}Ni. This finding and other interesting correlations will be discussed in details in Chap. 4. At late phases SNe IIP V−light curves are found to decline with an e−folding time close to the one of the ^{56}Co decay, indicating the radioactive decay, ^{56}Co→^{56}Fe, with the consequent trapping of γ−rays is the main source of energy powering the light curve at late epochs. At the same time, this fact provides a solid basis for the use of the V−light curves for the recovery of the ejected ^{56}Ni masses.

An important issue is the amount of ^{56}Ni ejected by this class of objects. This has been statistically studied in several works (e.g. Sollerman 2002), claiming that a typical value is about 0.07 $M_\odot$. This view has been recently changed with more detailed studies (Hamuy 2003 [14]; Elmhamdi et al. 2003b [8]), indicating a wide range of variation, from $\sim$ 0.003 $M_\odot$ (SN 1997D) to $\sim$ 0.29 $M_\odot$ (SN 1992am). The emergence of type IIP faint objects has also altered our understanding about iron yields. These peculiar

objects have in common some characteristics that may be summarized as: 1. They show lower expansion velocities at all epochs, especially at the end of the recombination phase ($v_{ph} \sim 1000$ km s^{-1}, a factor $3-4$ lower than normal type II SNe). 2. They have lower explosion energies ($< 10^{51}$ erg) and ^{56}Ni masses ($<0.01 M_{\odot}$). In this class different events are found, namely SNe 1997D, 1999br, 1999eu, 2001dc (Pastorello et al. 2003, in preparation). These unusually faint objects have attracted considerable attention in connection with the possibility of black hole formation as a remnant and the fallback mechanism (Zampieri et al. 2003 [32]).

The above facts may point to a continuous range in the iron yield in core collapse SNe, rather than typical values for each class with an "*empty*" gap in between. In this sense we propose the following sequence with increasing ^{56}Ni mass: Faint IIP ($<0.01 M_{\odot}$; SN 1997D)–Intermediate IIP ($\sim 0.03\ M_{\odot}$; SN 1999em)–Normal IIP, IIL ($\sim 0.07\ M_{\odot}$; SN 1987A)–Bright IIP ($>0.1\ M_{\odot}$; SN 1992am) and Ib/c ($\sim 0.1\ M_{\odot}$; SN 1994I)–Hypernovae ($\sim 0.4\ M_{\odot}$; SN 1998bw). These new results are extremely important for modeling the chemical evolution of galaxies since they impose constraints on the iron production (Matteucci. 2001 [19]). The iron and oxygen yields in core collapse SNe will be presented and discussed in Appendix "A".

Although they are not so luminous as type Ia SNe, the high degree of homogeneity in type IIP SNe is very encouraging to use them as cosmological probes. In fact they were used as distance indicators by means of the Expanding Photosphere Method (*EPM*; Schmidt et al. 1994 [27]). Recently, Hamuy & Pinto (2002)[13] have presented clear evidence of a correlation between expansion velocities of the ejecta of type IIP SNe and their bolometric luminosities during the plateau phase ($v_{ph} \propto L_p^{0.33(\pm 0.04)}$). The authors have used this correlation to decrease the scatter in the Hubble diagram and obtained satisfactory estimates for the Hubble constant $H_0 = 54 \pm 12$ km s^{-1} Mpc^{-1}, in agreement with some Cepheids/SNe Ia results ($H_0 = 65 \pm 5$ km s^{-1} Mpc^{-1}). This is surely a new method in cosmology and with large and well sampled type IIP SNe data it will be possible to improve the results and even get estimates for other cosmological parameters using *high-z* events.

Bibliography

[1] Baade W. & Zwicky F, 1934, PNAS, 20, 254

[2] Benetti S., Branch D., Turatto M. et al. 2002, MNRAS, 336, 91

[3] Chugai N. N., 1991, SvAL, 17, 210

[4] Chugai N. N. & Danziger I. J., 1994, MNRAS, 268, 173

[5] Deng J. S., Qiu Y. L., Hu J. Y., Hatano K. & Branch D. 2000, ApJ, 540, 452

[6] Doggett J. B., & Branch D., 1985, AJ, 90, 2303

[7] Elmhamdi A., Danziger I. J., Chugai N. N. et al. 2003a, MNRAS, 338, 939

[8] Elmhamdi A., Chugai N. N. and Danziger I. J. et al. 2003b, A&A, 404, 1077

[9] Filippenko A. V., 1992, ApJ, 384, 37

[10] Filippenko et al. 1995, ApJ, 450, 11

[11] Filippenko A. V. 1997, ARA&A, 35, 309

[12] Filippenko A. V. 2000 , (astro-ph/0002264), "Cosmic Explosions" – eds. S. Holt and W. W. Zhang (New York: American Institute of Physics), 2000

[13] Hamuy M. & Pinto P. A., 2002, ApJ, 566, 63

[14] Hamuy M. 2003, ApJ, 582, 905

[15] Hamuy M. 2003, accepted by Nature (astro-ph/0306270)

[16] Leibundgut B. et al. 1991, A&AS, 89, 537

[17] Leibundgut B, 2000, A&ARv, 10, 179

[18] Litvinova I.Y. & Nadozhin D.K., 1985, SVAL, 11, 145

[19] Matteucci F., 2001, In "The chemical evolution of the Galaxy", Book Review (Kluwer Academic Publishers)

[20] Minkowski R., 1941, PASP, 53, 224

[21] Nadyozhin D. K., 2003, (astro-ph/0303411)

[22] Nomoto K., Iwamoto K., Suzuki T., 1995, Phys. Reports, 256, 173

[23] Nomoto K., Maeda K., Nakamura T. et al. 2000, hgrb.symp, 622

[24] Popov D.V. 1993, ApJ, 414, 712

[25] Sollerman J., 2002, NewAR, 46, 493

[26] Schlegel E. M. & Kirshner R. P., 1998, NewA, 3, 125

[27] Schmidt B. P. et al. 1994, ApJ, 432, 42

[28] Sramek R. A. & Weiler K., 2003, in "*Supernovae and Gamma – Ray – Bursts*", ed . by Weiler K.(Washington, DC, USA), p.145

[29] Wheeler J. C. & Harkness R. P. 1990, Rep. Prog. Phys., 53, 1467

[30] Wheeler J. C. et al. 1994, ApJ, 436, 135

[31] Woosley S. E., Eastman R. G. & Schmidt B. P. 1999, ApJ, 5167, 88

[32] Zampieri L. et al. 2003, MNRAS, 338, 711

Chapter 2

SN IIP 1999em: photometry and spectroscopy from outburst to dust formation.

This work have been done in collaboration with I. J. Danziger, N. N. Chugai and A. Pastorello.

"The most beautiful thing we can experience is the mysterious. It is the source of all true art and science."

Albert Einstein (1879 - 1955)

Abstract

We present photometry and spectra of the type IIP supernova 1999em in NGC 1637 from several days after the outburst till day 642. The radioactive tail of the recovered bolometric light curve of SN 1999em indicates the amount of the ejected ^{56}Ni to be $\approx 0.02\ M_{\odot}$. The Hα and He I 10830 Å lines at the nebular epoch show that the distribution of the bulk of ^{56}Ni can be represented approximately by a sphere of ^{56}Ni with a velocity of 1500 km s^{-1}, which is shifted towards the far hemisphere by about 400 km s^{-1}. The fine structure of the Hα at the photospheric epoch reminiscent of the "Bochum event" in SN 1987A is analysed in terms of two plausible models: bi-polar ^{56}Ni jets and non-monotonic behaviour of the Hα optical depth combined with the one-sided ^{56}Ni ejection. The late time spectra show a dramatic transformation of the [O I] 6300 Å line profile between days 465 and 510, which we interpret as an effect of dust condensation during this period. Late time photometry supports the dust formation scenario after day 465. The [O I] line profile suggests that the dust occupies a sphere with velocity $\approx$ 800 km s^{-1} and optical depth $\gg 10$. The latter exceeds the optical depth of the dusty zone in SN 1987A by more than 10 times. Use is made of the Expanding Photosphere Method to estimate the distance and the explosion time, $D \approx 7.83$ Mpc and $t_0 \simeq$ 1999 October 24.5 UT, in accord with observational constraints on the explosion time and with other results of detailed studies of the method (Hamuy et al. 2001; Leonard et al. 2002). The plateau brightness and duration combined with the expansion velocity suggest a presupernova radius of $120 - 150\ R_{\odot}$, ejecta mass of $10 - 11\ M_{\odot}$ and explosion energy of $(0.5 - 1) \times 10^{51}$ erg. The ejecta mass combined with the neutron star and a conservative assumption about mass loss implies the main sequence progenitor of $M_{\rm ms} \approx 12 - 14\ M_{\odot}$. The derived mass range is in agreement with the upper limit to the mass found using pre-supernova field images by Smartt et al. (2001). From the [O I] 6300,6364 Å doublet luminosity we infer the oxygen mass to be a factor four lower than in SN 1987A which is consistent with the estimated SN 1999em progenitor mass according to nucleosynthesis and stellar evolution theory. We note a "second-plateau" behaviour of the light curve after the main plateau at the beginning of the radioactive tail. This feature seems to be common to SNe IIP with low ^{56}Ni mass.

2.1 Introduction

Type II (and Ib/Ic) SNe are generally associated with regions of recent star formation in spiral galaxies, suggesting that they represent the final episode in the life of massive stars ($M > 8M_{\odot}$) which explode owing to core collapse (Filippenko 2001 [27]). The study of core collapse events is important for understanding the range of progenitor masses which produce them, the consequent nucleosynthesis for its effect on galactic chemical evolution and the explosion energy which remains an ill-determined quantity for the vast majority of SNe, and which is also relevant for gas dynamical processes and ejection of material from galaxies. Detailed photometric and spectroscopic observations of SNe II on a long time scale are still rare, especially for SNe IIP (plateau). Meanwhile from the recent experience with SN 1987A we know, how valuable can be extended sets of photometric and spectroscopic data for understanding what really happens to the massive ($M > 8M_{\odot}$) star when its central iron core collapses. In this way one obtained information on the amount of ejected ^{56}Ni and oxygen, and their mixing and clumpiness, possible asymmetry of ^{56}Ni ejecta, "Bochum event", dust formation. The case of SN 1987A also provided us with the possibility for testing and revising the theory of stellar evolution, SN hydrodynamical models and models of spectra formation.

Supernova 1999em, discovered by the Lick observatory Supernova Search on Oct 29 UT at an unfiltered magnitude $\sim$ 13.5 mag in the nearby galaxy NGC 1637 ($D = 7.8$ Mpc; IAUC 7294 [40]), has become another well observed type IIP event. Detected very soon after the explosion and followed for more that 600 days this event gives another boost to studies of SNe II. SN 1999em is the first type IIP detected at both radio and X-ray wavelengths at early time (Pooley et al. [49]). However it is the least radio luminous and among the least X-ray luminous SNe (*Chandra* X-ray and radio NRAO observations; Fox & Lewin 1999 [25]; Lacey et al. 1999 [36]). This early and weak radio emission is consistent with a low mass loss shortly before the explosion for SNe IIP (Baron et al. 2000 [6]). The analysis of the spectra at the early photospheric epoch already emphasized the problem of He abundance in the hydrogen envelope of SN IIP progenitors (Baron et al. 2000 [6]) and permitted one to check and upgrade the method of the expanding photosphere (EPM) for the distance determination (Hamuy et al. 2001 [32]; Leonard et al. 2002 [39]). The spectropolarimetry on the other hand has been studied at 5 different epochs (till day 163 after discovery; Leonard et al. 2000 [38]). The authors estimated the broadband polarization at day 7 to be $\sim$ 0.2 %, rising to $\sim$ 0.5 % on day 161. The low polarization found for SN 1999em and hence the small implied asphericity especially at early photospheric phase is another encouraging reason for the validity of the EPM for this class of object (SNe IIP). The progenitor nature of SN 1999em was discussed by Smartt et al. (2002)[55], who used pre-explosion *CFHT* images to derive bolometric luminosity limits and thus constraints on the mass of the progenitor star of SN 1999em. They concluded that the main-sequence mass should be $< 12 \pm 1M_{\odot}$.

Here we present photometry and spectroscopy of SN 1999em from the phase of several days after the explosion till day 642. In what follows we describe the photometry and spectral evolution and provide estimates of the ^{56}Ni and oxygen mass in SN 1999em; we will analyse fine structures of the line profiles at the photospheric and nebular epoch

in an attempt to determine the effects of the ^{56}Ni mixing and asymmetry. The last spectra are used as diagnostics of possible dust formation in the ejecta. The photometry and spectroscopy at the plateau phase will be used to recover global parameters of SN (presupernova radius, mass and energy of SN). We then discuss the main sequence mass of the progenitor and some important correlations.

2.2 Photometric Evolution and bolometric light curve

Figure 2.1 shows the position of SN 1999em in its host galaxy NGC 1637. It is located at R.A=4:41:27.13, a Decl=-02:51:45.2, about 15″ west and 17″ south of the nucleus of its host galaxy NGC 1637. NGC 1637 is an SABc late type spiral galaxy having a heliocentric recession velocity of $V_{hel} \sim 717$ km s^{-1}. According to Sohn & Davidge (1998)[56] it has a distance of $7.8^{+1.0}_{-0.9}$ Mpc. A KAIT[1] image of the field taken on Oct 20.45 showed nothing at the position of SN 1999em, limiting the magnitude to about 19.0, suggesting that it was discovered shortly after the explosion.

2.2.1 Interstellar extinction

Galactic extinction towards NGC 1637 is known to be $A_V^{gal} = 0.134$ (Schlegel et al. 1998 [54]) corresponding to a colour excess E(B − V)=0.04 (adopting the standard reddening laws of Cardelli et al. 1989 [12]). However estimating the extinction due to the host galaxy is more complicated.

Recently Baron et al. (2000)[6] have provided constraints on the total colour excess using theoretical modelling of two early time spectra, namely their 29 Oct & 4-5 Nov spectra. They found that E(B − V) = 0.05 − 0.10 and E(B − V) ≤ 0.15. A value of E(B − V)=0.05, as derived from their SYNOW fit to their Oct 29 spectrum, implies an amount of E(B − V)=0.01 due to the host galaxy corresponding to $A_V^{host} = 0.031$ and $A_B^{host} = 0.041$. Adopting, for example, these values one finds $M^B_{max} \leq -15.8$, which places SN 1999em at the lower extremity of the regular type II-plateau SNe in the classification of Patat et al. 1994 [46].

On the other hand we note the presence of a narrow Na I D interstellar absorption line in our first spectra at the redshift of NGC 1637 with an equivalent width (EW) ∼ 1.3 Å, and therefore we would expect significant additional reddening in the host galaxy. In fact some correlations in the literature relating the equivalent width of Na I D to the reddening within the host galaxy indicate values of the order E(B − V) ∼ 0.32 (Barbon et al. 1990 [4]) and E(B − V) ∼ 0.17 (Benetti et al., in preparation), corresponding to $A_V^{host} = 0.99$ and $A_V^{host} = 0.52$, respectively. If, for instance, we assume this last value, we obtain $M^B_{max} \leq -16.48$, which implies that SN 1999em is a regular SN IIP but with significant reddening. Uncertainties in the calibration of absorption line strengths prevent a confident determination of reddening by this method.

[1] 0.8-m Katzman Automatic Imaging Telescope

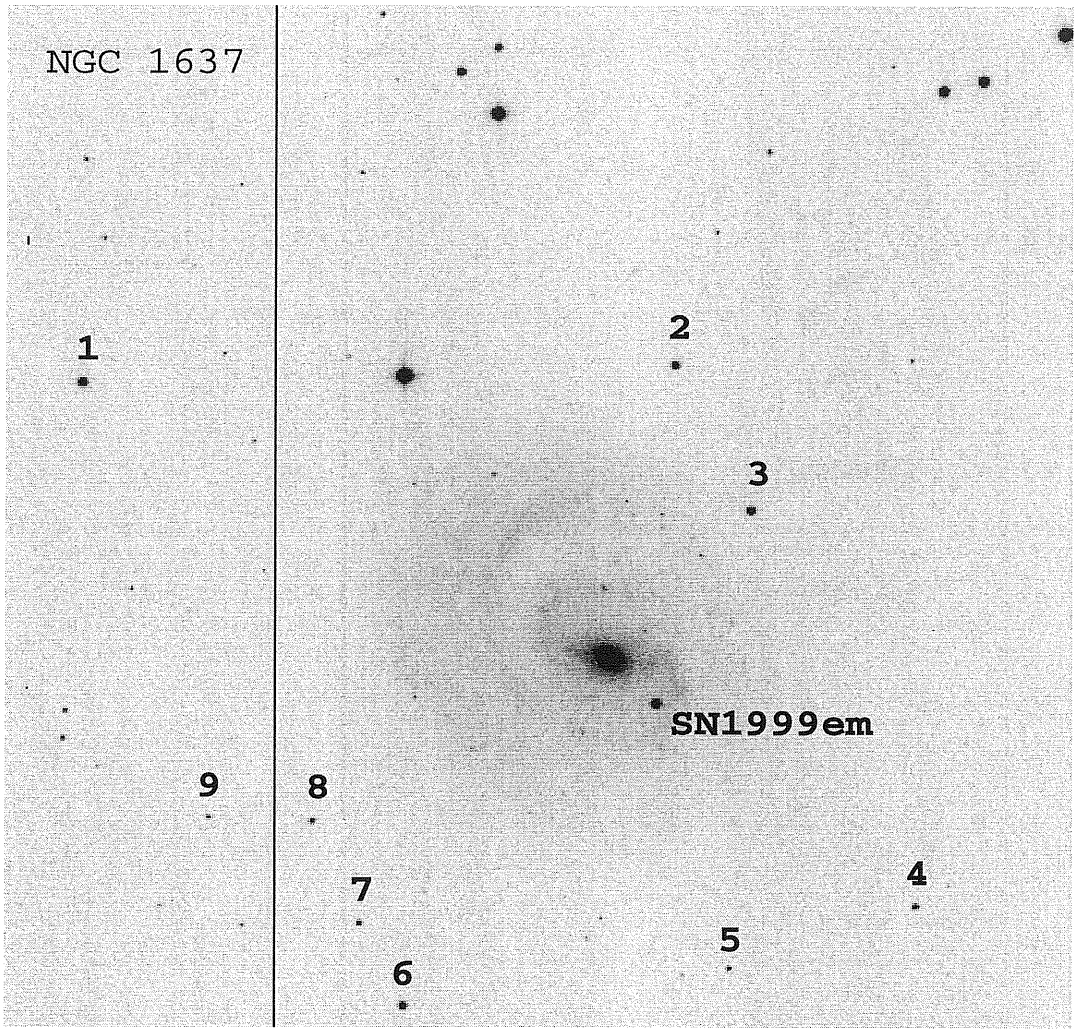

Figure 2.1: SN 1999em in NGC 1637. Image taken at ESO on Mar 27. 2000, about 150 days after discovery (in the R band). The SN position is indicated, also shown are the reference sequence stars. North is up, East is to the left.

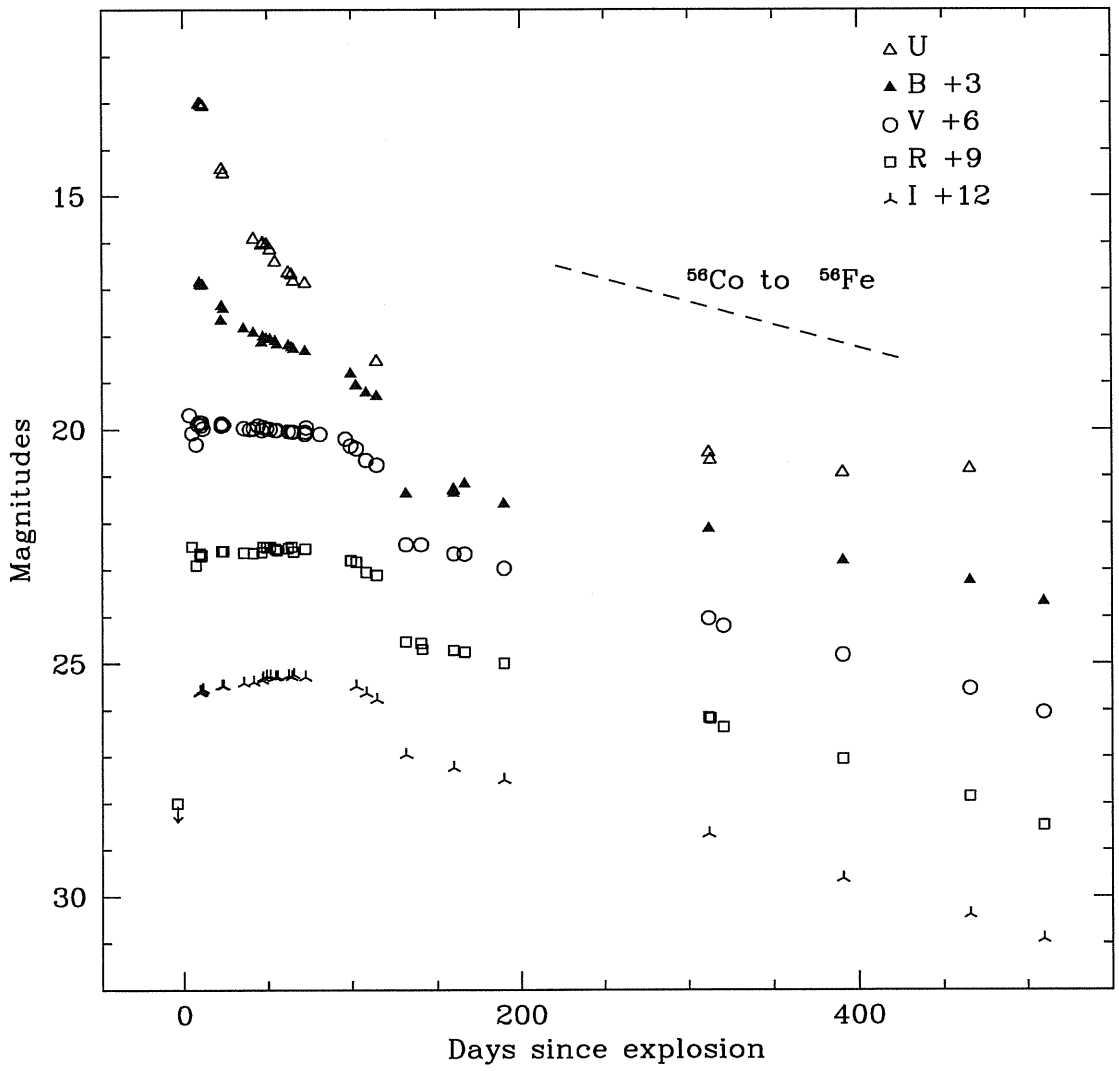

Figure 2.2: UBVRI Light curves of SN 1999em. The light curves have been shifted by the reported amounts. Also shown is the slope of ^{56}Co to ^{56}Fe decay. Reddening corrections have not been applied.

To overcome this disagreement between theoretical modelling and empirical calibration, Hamuy et al. 2001 [32] have tested the sensitivity of the Expanding Photosphere Method (EPM) to reddening caused by the host galaxy in deriving the distance to the supernova (using different filter subsets, their Figure 12). They conclude a consistent value for the extinction in the host galaxy is $A_V^{\rm host} = 0.18$ and thus a total extinction $A_V^{\rm tot} = 0.31$ and $A_B^{\rm tot} = 0.41$, which we adopt as the best estimate for our present analysis.

2.2.2 Light curves

The UBVRI photometry data are reported in Table 2.1 together with the different telescopes and instruments with which the observations were obtained. Our photometry started at ~9 d and extended to ~508 d (after explosion time). The reduction was carried out within the IRAF environment, applying bias, overscan and flat-field corrections. The contamination of the galaxy has been removed using PSF substraction. The photometric calibration of the SN was made relative to the local sequence of stars (see Figure 2.1) in the field of the host galaxy NGC 1637 and calibrated using observations of Landolt standard stars (Landolt 1992 [37]), obtained when the nights were photometric. The SN magnitudes have been measured using a point-spread-function fitting technique.

The UBVRI light curves of SN 1999em are illustrated in Figure 2.2. The Figure includes also data from Hamuy et al. (2001)[32] as well some data from circulars and VSNET service[2]. We have also plotted the decay slope of ^{56}Co : 0.98 mag (100 d)$^{-1}$, which corresponds to the late-phase decline rate of most normal SNe II L-P, especially for the V-band (Turatto et al. 1990 [61]; Patat et al. 1994 [46]).

At early times, especially in the V band, one notes that SN 1999em rises to a brief peak, then drops by about 0.6 mag in $\sim$ 3.5 days, then rises again to a brief second maximum followed by a settling onto the plateau phase. Here the expansion of the photosphere and the cooling balance each other to produce a phase of almost constant magnitude, $m_V \sim 14$ and $M_V \sim -15.76$. The plateau phase lasts about 80 days, after which the light curve displays a steep decline ($\sim$ 2 mag in $\sim$ 40 days for the V-band), signaling the onset of the nebular phase and the start of the exponential decline. Similar early short duration rapid change was seen in SN IIP 1988A (Ruiz-Lapuente et al. 1990 [51]) as well as for SN 1993J (Barbon et al. 1995 [5]), and can be interpreted to be a consequence of low mass loss in the immediate presupernova phase (see discussion of the bolometric light curve).

After the steep decline from the plateau phase and starting around 130 days after explosion the shapes of the light curves evolve with time: firstly there is a clear flattening from day 130 lasting about 50 days, especially at blue wavelengths, which is then followed by the exponential decline. Similar flattening is also seen in the data for the faint SN IIP 1997D (Benetti et al. 2001 [7]) and is present in the light curves of SN IIP 1991G (Blanton et al. 1995 [9]).

A linear fit to the tail (from ~180 to $\sim$ 510) gives the following decline rates (in mag

[2]http://www.kusastro.kyoto-u.ac.jp/vsnet/

Table 2.1: Photometric observations of SN 1999em

Date (UT)	JD 2400000+	U(σ)	B(σ)	V(σ)	R(σ)	I(σ)	Instrument
28/10/99	51479.51	—	—	13.69 .06	—	—	0
03/11/99	51485.62	13.02 .03	13.85 .03	13.84 .03	13.67 .03	13.63 .03	4
03/11/99	51485.81	—	13.89 .03	13.84 .03	13.65 .03	13.61 .03	2
04/11/99	51486.62	13.04 .03	13.90 .03	13.91 .03	13.71 .03	13.59 .03	4
04/11/99	51486.73	—	13.93 .03	13.85 .03	13.68 .03	13.61 .06	2
05/11/99	51487.57	13.07 .12	13.90 .06	13.98 .03	13.83 .09	13.55 .12	4
05/12/99	51517.80	15.92	14.93	13.98	13.64	13.40	1
08/12/99	51520.56	—	—	13.92 .12	—	—	5
11/12/99	51523.54	16.01 .03	15.01 .03	13.95 .03	13.50 .03	13.30 .03	4
13/12/99	51525.51	16.04 .03	15.06 .03	13.98 .03	13.52 .03	13.27 .03	4
15/12/99	51527.57	16.15 .03	15.07 .03	13.99 .03	13.50 .03	13.27 .03	4
18/12/99	51530.73	16.41 .27	15.11 .09	14.02 .03	13.55 .03	13.29 .03	1
25/12/99	51538.59	16.64 .06	15.20	14.04	13.54	13.26	4
27/12/99	51540.50	16.68 .03	15.25	14.05	13.51	13.28	4
28/12/99	51541.71	16.82 .09	15.28 .06	14.05 .03	13.61 .03	13.24 .03	2
05/01/00	51548.51	16.87 .03	15.33 .03	14.05 .03	13.55 .03	13.29 .03	4
31/01/00	51575.44	—	15.81 .12	14.35 .09	13.80 .03	—	5
09/02/00	51584.32	—	16.22 .39	14.66 .09	14.05 .06	13.64 .06	5
16/02/00	51590.53	18.55	16.29	14.76	14.11	13.77	2
13/03/00	51616.50	—	—	16.46 .06	15.57 .06	—	2
08/04/00	51642.52	—	18.17	16.66	15.76	—	1
31/08/00	51787.71	—	—	18.04 .06	17.16 .03	—	3
31/08/00	51787.74	20.51 .21	19.13 .06	—	—	16.66 .06	3
01/09/00	51788.90	20.66 1.05	—	—	17.18 .06	—	1
08/09/00	51796.60	—	—	18.20 .15	17.37 .09	—	5
17/11/00	51866.77	20.94 .72	19.81 .54	18.82 .24	18.05 .12	17.62 .24	2
01/02/01	51941.65	20.85 .12	20.24 .18	19.54 .12	18.86 .12	18.39 .09	1
16/03/01	51985.53	—	20.69 .27	20.05 .18	19.47 .24	18.91 .21	2

0 = WHT(Image provided by Smartt.); 1 = ESO 3.6m+EFOSC2; 2 = Danish 1.54m+DFOSC
3 = TNG+DOLORES; 4 = TNG+OIG; 5 = Asiago 1.82m+AFOSC

$\star$ The reported errors are 1σ.

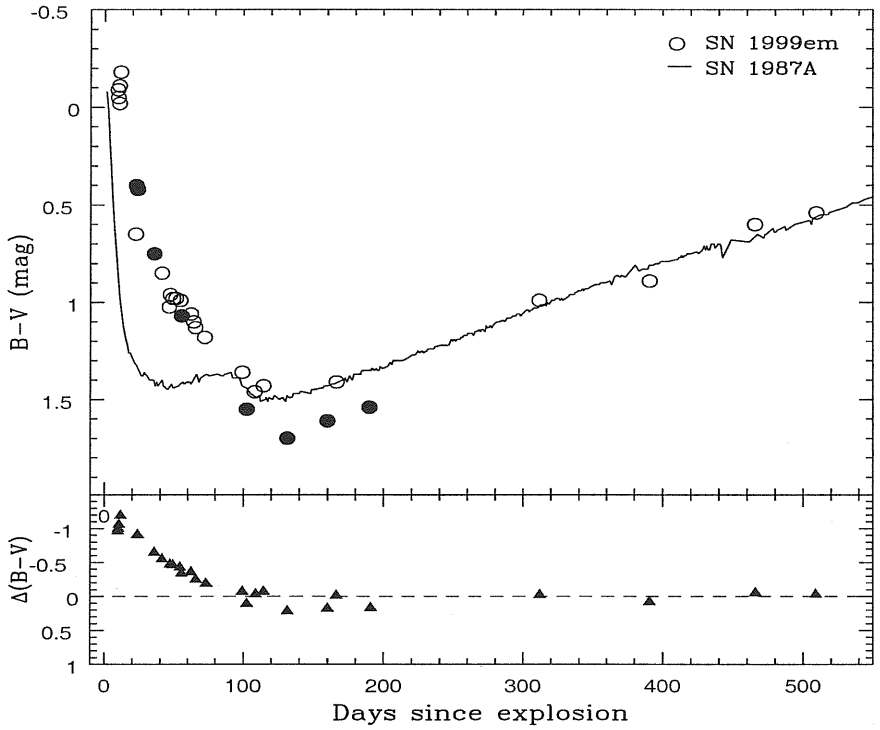

Figure 2.3: B−V colour of SN 1999em and SN 1987A. Bottom panel shows the difference $\Delta(\mathrm{B}-\mathrm{V}) = (\mathrm{B}-\mathrm{V})_{99\mathrm{em}} - (\mathrm{B}-\mathrm{V})_{87\mathrm{A}}$. Both SNe have been corrected for reddening. For SN 1987A we use $A_V = 0.6$ (Filippenko 1988 [26]). Filled circles represent data from Hamuy et al. 2001 [32].

$(100\mathrm{d})^{-1}$): $\gamma_B \sim 0.66$, $\gamma_V \sim 0.97$, $\gamma_R \sim 1.08$ and $\gamma_I \sim 1.07$ which are close to the values found for the typical SN IIP 1969L (Turatto et al. 1990 [61]). Especially for the V-light curve this indicates that radioactive decay of ^{56}Co with consequent trapping of γ-rays is the main source of energy powering the light curve at late times, at least until $\sim$ 510 days after explosion.

We note also that the late U light curve remains almost flat, similar in behaviour to that reported for SN 1987A until $\sim$ 400 days after explosion (Suntzeff et al. 1988 [60]).

2.2.3 Colour evolution

In Figure 2.3 we show the (B − V) colour curve of SN 1999em, together with that of SN 1987A for comparison. The explosion date of SN 1987A is well established to be February 23.316 from the Kamiokande and IMB neutrino detections (Hirata et al. 1987 [34]; Bionta et al. 1987 [8]), while for SN 1999em the explosion date is assumed to be October 24.5 ($\sim$ JD 2451476) derived from the EPM, to be discussed later.

The (B − V) colour varies at different rates according to phase. During the first 40

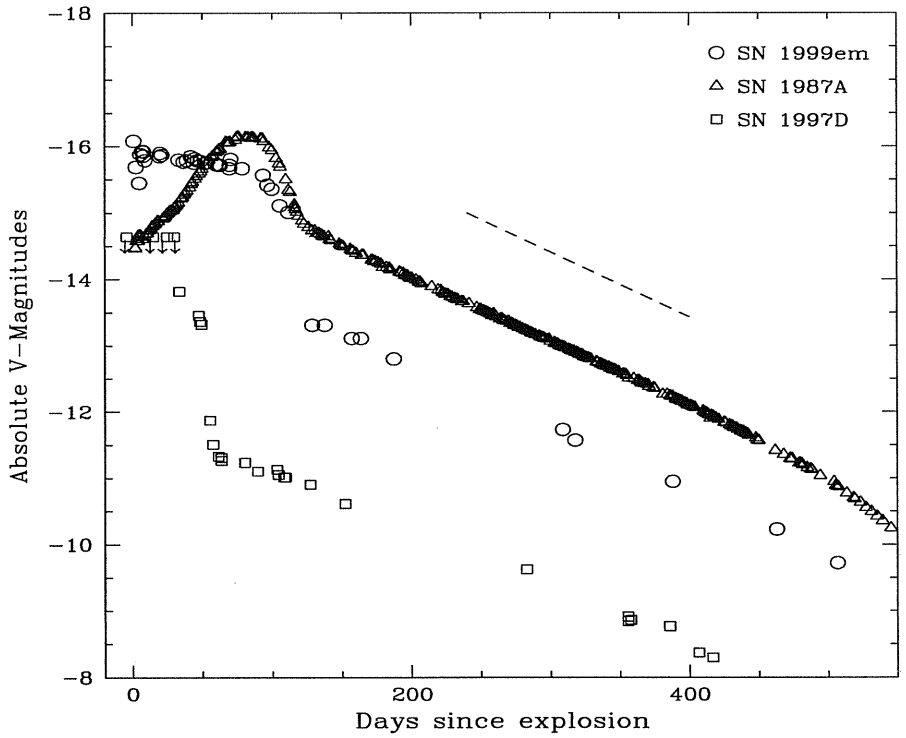

Figure 2.4: Comparison of the V absolute light curve of SN 1999em with those of SN 1987A and SN 1997D. Distances moduli of $\mu = 29.46$, $\mu = 18.49$ and $\mu = 30.64$ are assumed for the three SNe, respectively. Dashed line shows the luminosity dependence due to ^{56}Co decay for arbitrary mass of ^{56}Ni.

days, it exhibits a steep and rapid decline from blue (high temperatures) to red (low temperatures) as the supernova envelope expands and cools. Subsequently the (B − V) colour varies more slowly as the rate of cooling decreases. At ∼130 d the (B − V) colour reaches a value around 1.7, then it turns blue again (rate ~ -0.33 mag $(100\ \mathrm{d})^{-1}$), as the light curve settles into the exponential tail.

Note the general similarity of (B − V) colour evolution of SN 1999em with that of SN 1987A especially at late phases, where the Δ(B − V) approaches zero (the bottom box in Figure 2.3). This fact gives us confidence that comparison of absolute V-light curves should be reliable for the estimation of ^{56}Ni mass, released in the explosion of SN 1999em, because the bolometric light-curves are liable to be similar also. There is little doubt that the difference of the colour behaviour of both supernovae at the early epoch (faster cooling of SN 1987A) is related to the difference in presupernovae radii. The smaller radius of SN 1987A presupernova leads to a faster adiabatic cooling of the radiation trapped in the expanding envelope. The details of the colour behaviour of SN 1999em should be reproduced in future hydrodynamical modelling.

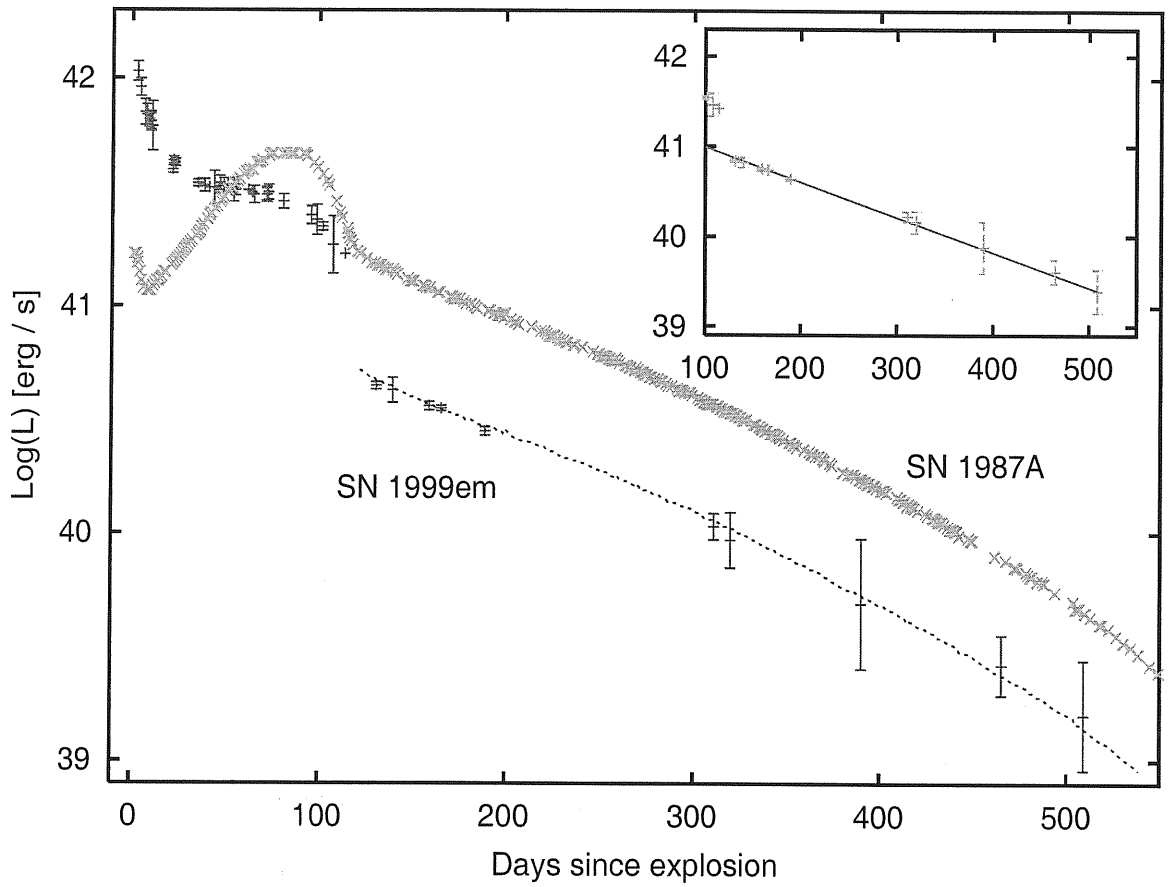

Figure 2.5: The UBVRI bolometric light curve of SN 1999em together with that of SN 1987A for comparison. The dotted line corresponds to the best fit of SN 1999em late data by SN 1987A tail. The window on the right shows the resulting tail scaled up by an amount of 0.19 dex (provided by integrated J,H,K fluxes) along with the ^{56}Co decay for 0.02 of ^{56}Ni. The reported error bars are 1σ.

2.2.4 The bolometric light curve and ^{56}Ni mass

In Figure 2.4, we present the absolute light curve of SN 1999em in the V band. The light curve of the double-peaked SN 1987A and the peculiar type IIP SN 1997D are also displayed for comparison. These plots highlight the different behaviour of the photometric evolution of the three SNe, from the explosion until about 550 days. They provide constraints on the explosion energy of SN 1999em as well as on the radioactive ^{56}Ni mass ejected. All the radioactive tails of the three SNe, especially in the V band, follow the ^{56}Co decay slope suggesting that it is the main energy source powering the late phases of the light curves. The fainter object SN 1997D, $M_V^{max} \geq -14.65$ (Turatto et al. 1998 [63]), ejected an extremely small amount of radioactive ^{56}Ni, about 0.002 $M_\odot$, with a low explosion energy of $\sim 10^{50}$ ergs derived from modelling the spectra (Chugai & Utrobin 2000 [18]), while the mass of ^{56}Ni ejected by the well studied SN 1987A and the explosion energy are $\sim$0.075 $M_\odot$ and $\sim 1.3 \times 10^{51}$ ergs, respectively (Danziger et al. 1988 [20];

Woosley et al. 1989 [68]). We therefore conclude that SN 1999em produced a mass of ^{56}Ni intermediate between 0.002 and 0.075 $M_{\odot}$. To obtain a more accurate estimate of the ^{56}Ni mass we constructed the "bolometric" light curve of SN 1999em by integrating the flux in the UBVRI bands. The resulting light curve is shown in Figure 2.5 together with that of SN 1987A.

A least squares fit of the tail (from +140 d to +465 d) yields an e-folding time of $\sim$ 119 days. Comparing the bolometric luminosities of the tail of SN 1999em with SN 1987A we obtain a best fit of SN 1999em data to the tail of SN 1987A for $L(99\mathrm{em})/L(87\mathrm{A}) = 0.30$. With the ^{56}Ni mass 0.075 $M_{\odot}$ in SN 1987A we thus derive for SN 1999em the amount of ejected ^{56}Ni $\sim$ 0.022 $M_{\odot}$. The bolometric luminosity should be corrected for the contribution of the flux in JHK bands. According to our photometric observation on day 440 the contribution of the JHKs flux is about 0.19 dex. Then assuming a similar constant percentage contribution by the infrared flux during the tail phase (which is not precise), we scale up the derived UBVRI light curve by 0.19 dex. The resulting late curve is shown in the window in Figure 2.5 together with the best theoretical fit of the radioactive decay energy input assuming that the envelope is optically thick to γ-rays ($L = L_0 \times (M_{\mathrm{Ni}}/M_{\odot}) e^{-t/\tau_{\mathrm{Co}}}$, with L_0=1.32$\times$ 10^{43} ergs s^{-1} and $\tau_{\mathrm{Co}} = 111.23$ days; Woosley et al. 1989 [68]). The best fit is found for ^{56}Ni mass 0.02 ± 0.0013 $M_{\odot}$. Both methods thus lead to the consistent value of ^{56}Ni mass of 0.02 $M_{\odot}$. This amount is similar to the one derived for SN 1991G ($\sim$ 0.024 $M_{\odot}$; Blanton et al. 1995 [9]) and smaller than the mass determined for the typical SNe IIP 1969L and 1988A ($\sim$ 0.07 $M_{\odot}$; Turatto et al. 1993 [62]).

2.3 Spectroscopic Evolution

The journal of the spectroscopic observations in the optical as well as in the infrared are displayed in Table 2.2. For each spectrum the date (col.1), phase (col.2), range (col.3) and the instrument used (col.4) are presented. The spectra have been wavelength calibrated using comparison arc-spectra of He-Ar or He-Ne lamps, and flux calibrated using observations of spectrophotometric standard stars selected from Stone & Baldwin 1983 [59], Baldwin & Stone 1984 [3]; Hamuy et al. 1992 [30] and Hamuy et al. 1994 [31].

2.3.1 Optical spectra

We present the spectral evolution of SN 1999em which extends from $\sim$ +9 d to $\sim$ +642 d since explosion. The redshift cz=717 km s^{-1} of the parent galaxy NGC 1637 has been removed in all spectra .

In Figure 2.6A we show the evolution during the photospheric phase. The earliest spectra display a blue continuum indicating temperatures exceeding 10^4 K with broad P-Cygni profiles of the hydrogen Balmer lines, He I lines, and the Na I D and Ca II lines. In the first spectrum the blue wing of Hα absorption indicate expansion velocities up to $\sim$ 16000 km s^{-1}.

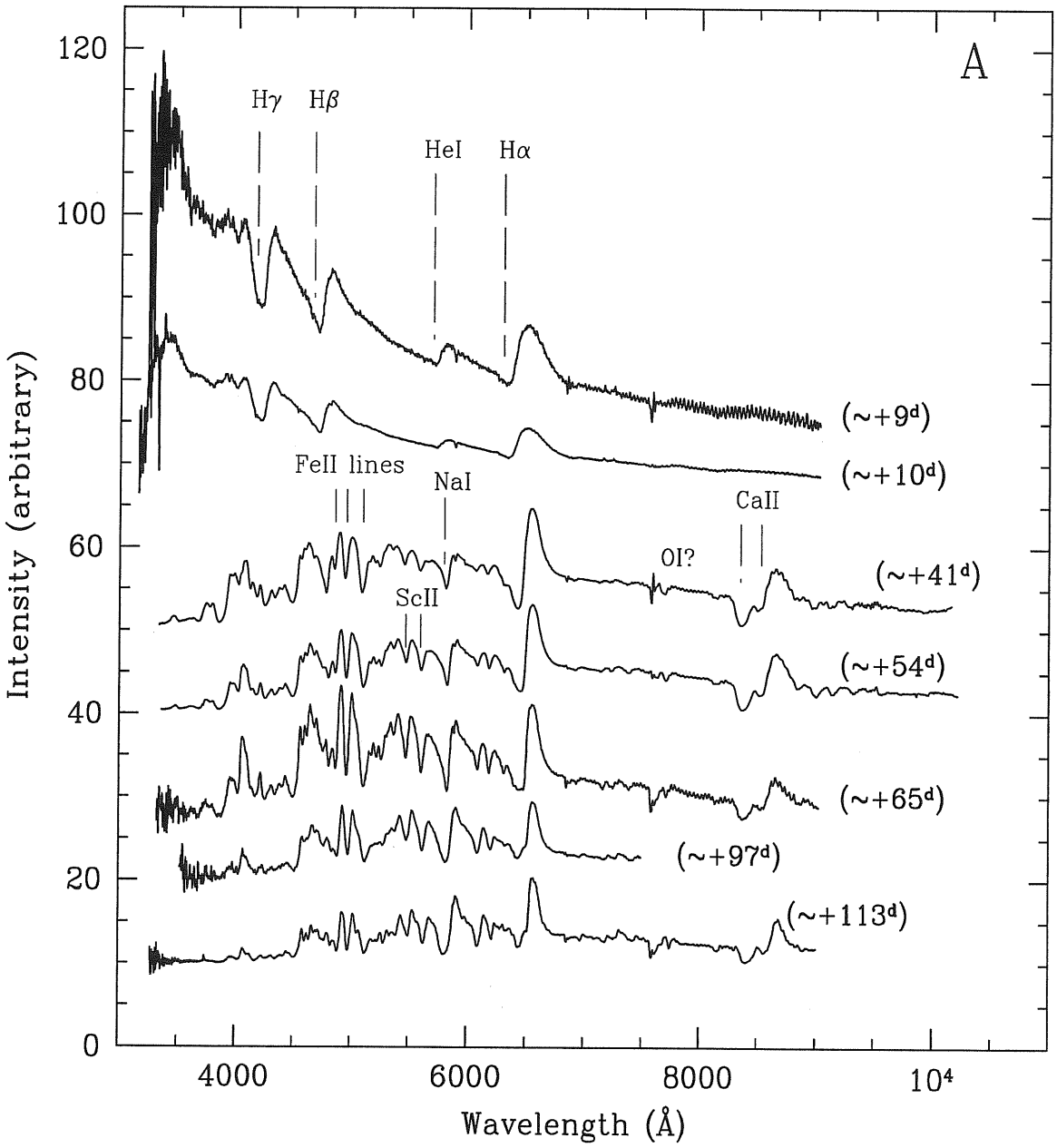
A
Hγ
Hβ
HeI
Hα
FeII lines
NaI
CaII
OI?
ScII
(~+9d)
(~+10d)
(~+41d)
(~+54d)
(~+65d)
(~+97d)
(~+113d)
Intensity (arbitrary)
Wavelength (Å)
0
20
40
60
80
100
120
4000
6000
8000
10⁴

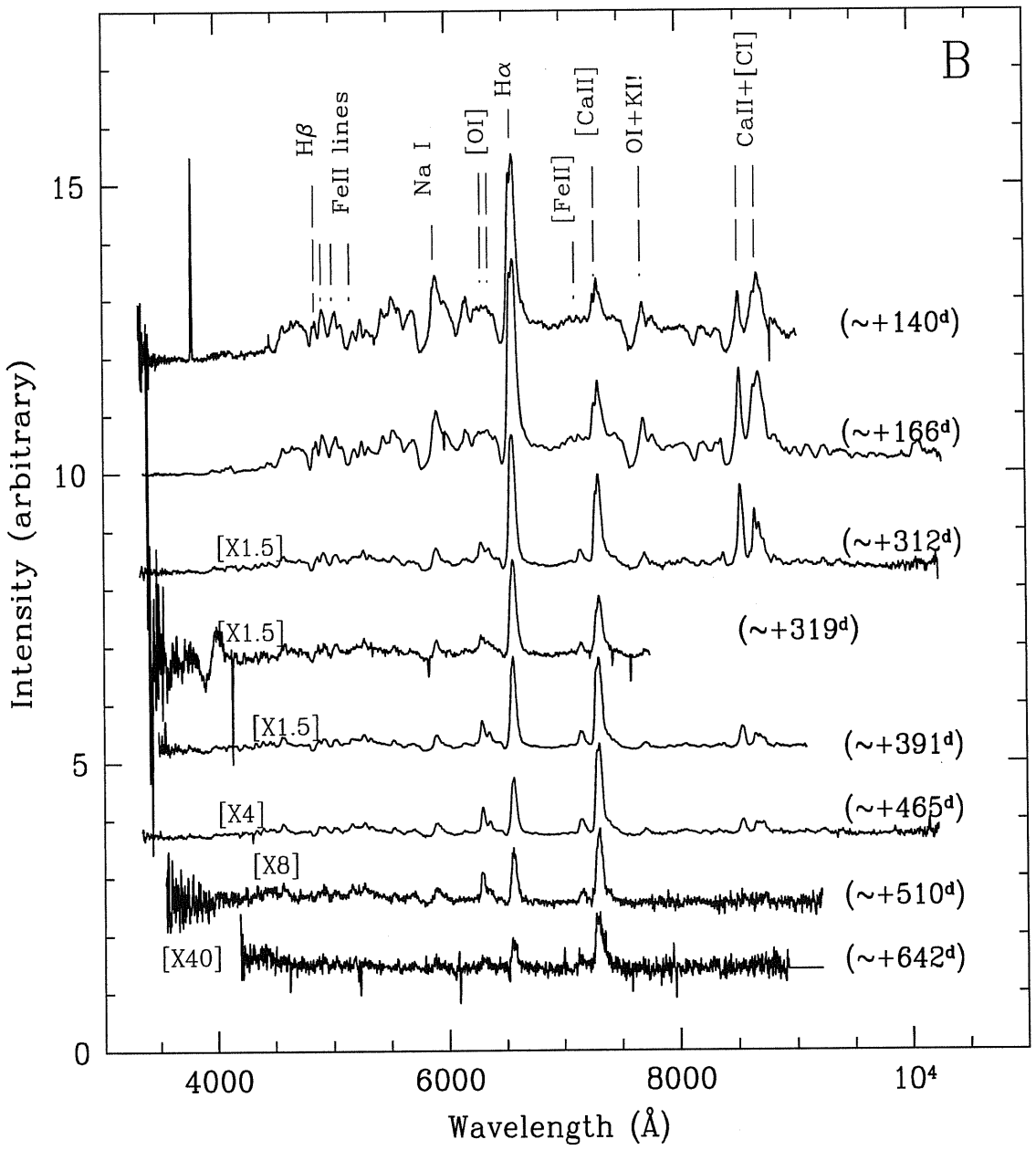

Figure 2.6: Spectral evolution of SN 1999em during the photospheric phase(A), and during the nebular phase(B). All the spectra have been corrected for the recession velocity of the host galaxy NGC 1637 and vertically displaced by an arbitrary constants for clarity. Each spectrum is labelled by the corresponding days after explosion. The strongest features are also marked as absorption in the photospheric phase(A) and at the rest frame in the nebular phase(B).

Table 2.2: Spectroscopic observations of SN 1999em

Date (UT; dd/mm/yy)	Phase†	Range (Å)	Instrument
⋆ Optical observations :			
03/11/99	+9	3240-9060	DI
04/11/99	+10	3160-9050	DI
05/12/99	+41	3340-10190	EI
18/12/99	+54	3370-10200	EI
29/12/99	+65	3340-9050	DI
31/01/00	+97	3530-7520	AI
16/02/00	+113	3280-9030	DI
13/03/00	+140	3340-9050	DI
08/04/00	+166	3380-10300	EI
01/09/00	+312	3350-10260	EI
08/09/00	+319	3410-7770	AI
19/11/00	+391	3500-9110	DI
01/02/01	+465	3360-10260	EI
18/03/01	+510	3560-9240	DI
27/07/01	+642	4200-9940	EII
⋆ IR observations :			
14/11/99	+20	9420-25040	EIII
11/01/01	+444	9430-16540	EIII

† since the explosion time: $\sim$ 24.5/10/1999

AI = Asiago 1.82m+AFOSC; DI = Danish 1.54m+DFOSC;

EI = ESO 3.6m+EFOSC2; EII = ESO-VLT-U1+FORS1 ;

EIII = ESO-NTT+SOFI

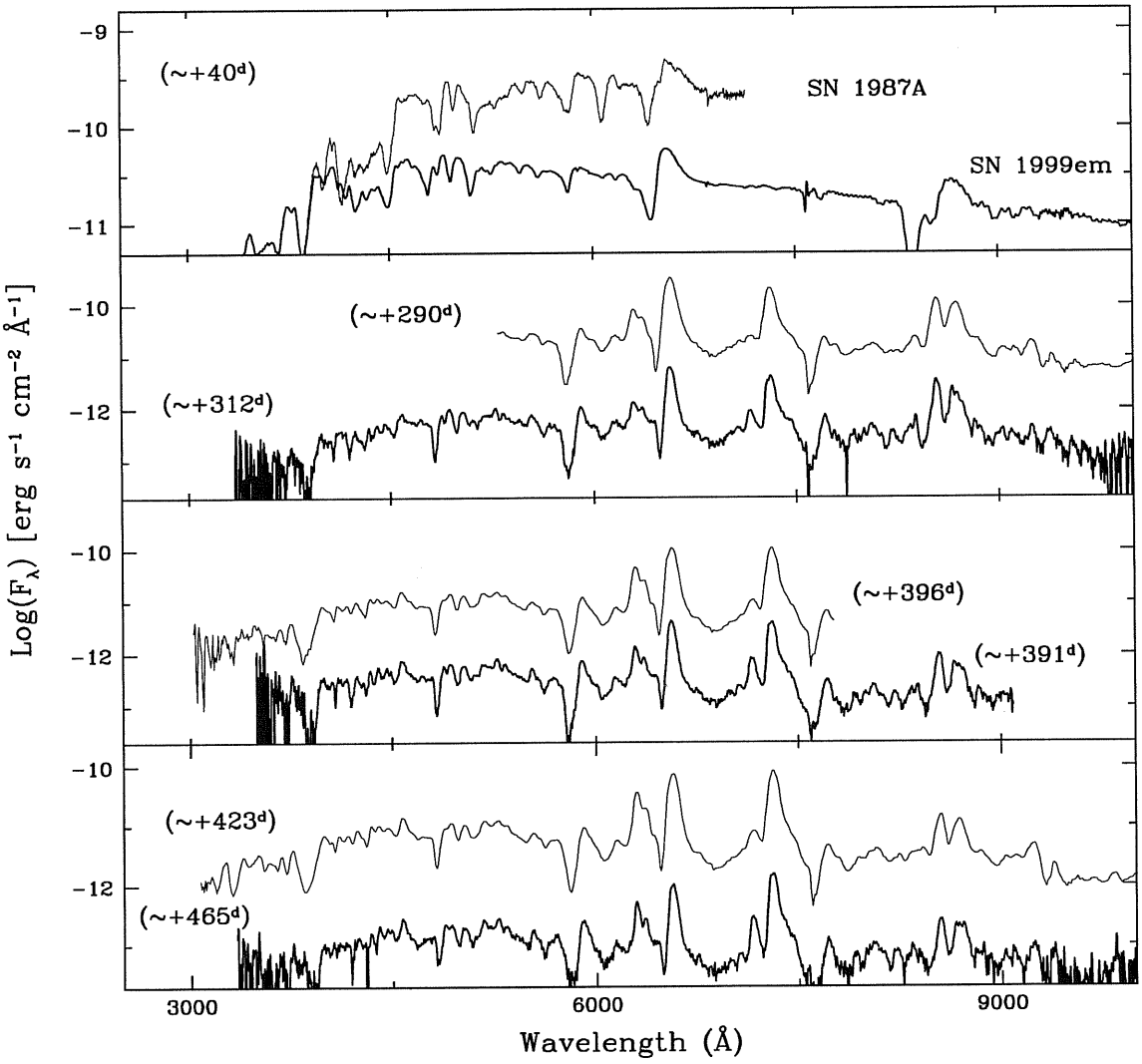

Figure 2.7: The spectral evolution of SN 1999em with that of SN 1987A at similar phases. The spectra of SN 1999em have been shifted by 3.5 dex (log-scale). The flux scales correspond to SN 1987A. The spectra are corrected for redshift as well for reddening by the same amounts as Fig. 2.3.

Those facts, broad P-Cygni profiles of hydrogen lines, high expansion velocities and high temperatures, imply that the supernova is a type II SN with a substantial hydrogen envelope discovered close to the explosion time. Note that the He I 5876 Å with a P-Cygni profile is visible for the 3 and 4 Nov spectra (the same behaviour was seen in SN 1987A). In fact, in early time spectra Baron et al. (2000)[6] have found evidence for helium enhanced by at least a factor of 2 over the solar value as well as a possible nitrogen enhancement. We do not find clear evidence for nitrogen lines in our first spectra. As to the He I line, the interpretation of its strength in terms of He overabundance is premature, since ignored freeze-out effects could lead to the enhanced He excitation compared to the steady-state model (Utrobin & Chugai 2002 [65]).

At the middle of the plateau phase the photosphere cools down to 5000 – 6000 K; at this epoch the spectra (Fig. 2.6A) are dominated by strong lines of H, Ca II, Fe II, Na I with well developed P-Cygni profiles which become narrower as the velocity at the photosphere decreases. We note also the appearance of absorption lines at 5476 Å and 5608 Å which we attribute to lines of Sc II 5526 Å and 5658 Å, respectively although secondary evidence from other lines of these ions is not obvious. As the supernova ages, the internal energy in the form of the trapped radiation is exhausted, the luminosity drops signaling the end of the photospheric epoch and transition to the nebular phase. The continuum formed in the region excited by ^{56}Co decay becomes faint and diluted compared to black-body intensity. As a result the contrast between the net line emission and continuum increases, which is demonstrated *e.g.* by Hα and Ca II 8600 Å triplet (last spectrum in Fig. 2.6A).

Figure 2.6B shows the spectra during the nebular phase, from $\sim$ +140 d until $\sim$ +642 d after explosion. The supernova is now in the radioactive tail phase. The first two spectra signal the onset of the nebular phase, where relatively broad P-Cygni profiles of Hα and Na I 5890,5896 Å were still seen with FWHM of Hα about 3500 km s^{-1}. About five months later, $\sim$ +312 d after explosion, Hα has become still narrower with FWHM of $\sim$ 2400 km s^{-1}. The feature at 7300 Å is identified with [Ca II] 7392, 7324 Å doublet always observed in nebular spectra of SNe IIP. What is unusual is the notable domination of the [Ca II] 7300 Å over Hα in the latest spectra. Note also the emergence of the nebular emission of the [O I] 6300,6364 Å doublet. Its profile evolution can be seen in Figure 2.6B. The 140 d and 166 d spectra showed already the presence of the [O I] although the two components were not yet resolved. As time progresses the [O I] 6300 Å component increases relative to the [O I] 6364 Å one, indicating that the lines become optically thin as the supernova envelope expands.

The spectra of SN 1999em at photospheric and nebular epochs in many respects are similar to those of SN 1987A (Fig. 2.7). Note, however, the line width and hence velocities in SN 1987A are higher e.g. at $\sim$ +40 d: $V_{87A}(H\alpha) \sim 6900$ km s^{-1}, $V_{99em}(H\alpha) \sim 6100$ km s^{-1} from the P-Cygni absorption minima. The Ba II 6142 Å absorption line of an s-process element, is very prominent for SN 1987A, while its presence is only hinted in the spectrum of SN 1999em. The Sc II 6280 Å line, if correctly identified, on the other hand has almost the same strength for the two spectra. The 4554 Å feature, partly due to Ba II 4554 Å, is similar for the two SNe. This is possibly due to a blend

with other lines, in particular Fe II 4555 Å and Ti II 4549 Å. Note also the emergence of the [Fe II] 7155 Å emission line. Indeed we measure the maximum intensities of this line and comparing it with the strong [Ca II] 7291,7324 Å line we obtain at $\sim$ 390 d: $I_{\max}([\text{Ca II}])/I_{\max}([\text{Fe II}]) = 6.98$ for SN 1999em, while it is around 24.68 for SN 1987A. This suggests that the [Fe II] lines do not originate from newly synthesized iron.

In Figure 2.8 we report the luminosity evolution of some nebular lines, namely Hα, [Ca II] 7291,7324 Å (upper panel) and [O I] 6300,64 Å (lower panel) for SN 1999em. The same data for SN 1987A, at similar times, are also shown for comparison. The evolution of Hα and [Ca II] 7291,7324 Å are clearly decreasing in time for both supernovae in a similar and parallel way. This reflects the exponential decline at late times. On the other hand the derived luminosities for SN 1999em are lower than for SN 1987A which must be related to the nature and diversities in the progenitor stars of the two events. It is noteworthy that the ratio of Hα luminosity of SN 1999em and SN 1987A between days 300 and 400 is $\approx$ 0.3, i.e. the same as the ratio of the ^{56}Ni. This is perhaps not surprising since the rate of Hα emission is determined by the rate of radioactive decay. However, we know that hydrogen photoionization from the second level is involved also in producing Hα quanta (Chugai 1987 [13]; Xu et al. 1992 [66]), which, although it also is eventually determined by radioactive decay, might spoil the scaling of Hα luminosity with ^{56}Ni mass especially at the early nebular epoch. Moreover, at the early epoch collisional de-excitation probably plays a role also. On the other hand at later epoch (> 400 d) the escape of γ-rays should be significant, with the escape rate dependent on the mass and explosion energy. Therefore the epoch 300 – 400 days is just the right phase at which the Hα luminosity scales as ^{56}Ni mass in SNe IIP. This suggests to us the idea of using spectrophotometry of SNe IIP around day 300 in the Hα band with low resolution (say 1000 km s^{-1}) to measure ^{56}Ni mass based upon comparison of Hα luminosity with the template SN 1987A, without the need to reconstruct the bolometric light curve, which would be difficult for distant SNe IIP. The behaviour of the luminosity of [O I] doublet in both supernovae is similar with a "plateau-like" maximum from $\sim$ 166 d until $\sim$ 391 d for SN 1999em followed by a clear steep decline later on, as for SN 1987A. We measured this decline rate for SN 1999em to be $\sim$ 0.0166 mag day^{-1}.

Yet the luminosity of [O I] doublet in SN 1999em is a factor of 15 lower between day $\sim$ 300 and $\sim$ 500 which indicates a lower amount of oxygen compared to that of SN 1987A. To get a rough idea of the ratio of oxygen mass in both supernovae one notes that the luminosity of [O I] doublet at the epoch of $\sim$ 1 year is powered by the γ-ray deposition and by ultraviolet emission arising from the deposition of γ-rays in oxygen-poor material. Generally, one may write the [O I] doublet luminosity as:

$$L(6300) = \eta \frac{M_{\rm O}}{M_{\rm ex}} L(^{56}\text{Co}), \tag{2.1}$$

where $M_{\rm O}$ is the mass of oxygen, $M_{\rm ex}$ is the "excited" mass in which the bulk of radioactive energy is deposited, and η is the efficiency of transformation of the energy deposited in oxygen into the [O I] doublet radiation. Given 15 times lower luminosity of [O I] doublet in SN 1999em (before dust formation) and factor 3.4 lower ^{56}Ni mass in SN 1999em (section 2.4), and assuming that in both supernovae η and $M_{\rm ex}$ are similar,

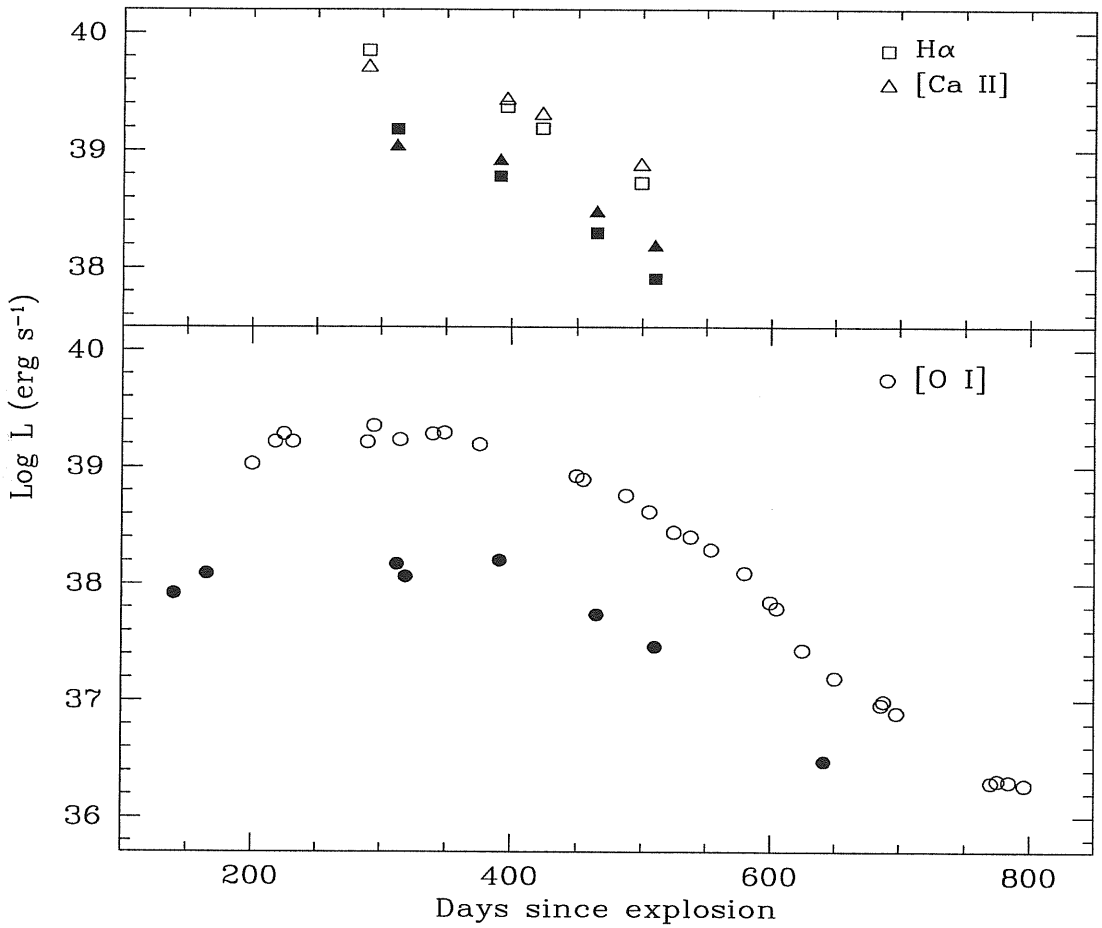

Figure 2.8: The temporal evolution of the luminosity of some nebular lines for SN 1999em with that of SN 1987A at similar times. Upper panel: the [Ca II]7291,7324 Å and Hα evolution. Lower panel: the [O I] 6300,64 Å doublet evolution. Filled symbols correspond to SN 1999em while open symbols represent SN 1987A data.

we derive the rough estimate that the mass of oxygen in SN 1999em is a factor 4.4 lower than in SN 1987A. The oxygen mass in SN 1987A according to different determinations (Fransson & al. 1993 [28]; Chugai 1994 [17]) is in the range $1.5 - 2\ M_{\odot}$, which translates into $\sim 0.3 - 0.4\ M_{\odot}$ of oxygen in SN 1999em. Given the nucleosynthesis computations (Woosley & Weaver 1995 [69]) this mass corresponds to the main-sequence stellar mass of $13 - 14\ M_{\odot}$.

2.3.2 Infrared spectra

The infrared spectra are shown in Figure 2.9 where some line identifications are given. The first spectrum was obtained during the photospheric phase ($\sim$ +20 d) while the second one corresponds to $\sim$ +444 d after explosion during the nebular phase. The earlier spectrum is dominated by a strong continuum with clear evidence of the Paschen series of hydrogen, namely Pβ, Pγ and Pδ displaying P-Cygni profiles as did the optical Balmer lines. The structure of the Pγ profile results from blending with He I 10830Å. The position of the peak emission and the absorption minimum of Pγ are reported in Figure 2.10, using a linear interpolation between the respective positions for Pδ and Pβ. Note the difference in velocity.

The velocity of He I 10830 Å absorption component is in fact similar to that of Hα estimated by interpolation between days 10 and 41. The presence of He I 10830 Å at this epoch may be a result of the non-thermal excitation due to the presence of small amount of ^{56}Ni in the outer layers of the ejecta. Alternatively, excitation can result from the recombination of frozen ionization, the mechanism suggested by Utrobin & Chugai (2002)[65]. The second spectrum is dominated by emission lines as the absorption components of the P-Cygni profiles became weaker.

Combining these IR spectra together with optical spectra obtained at similar phases we have extended spectra at two quite different phases. Figure 2.11 displays the resulting spectra, after being corrected for redshift of the host galaxy as well as for reddening, together with three black-body fits to the photospheric phase spectrum corresponding to different temperatures, yielding a temperature of the order 5500 K as the best fit. Both combinations required no arbitrary shifts between optical and IR sections.

2.3.3 Hα evolution,"Bochum event" and ^{56}Ni asymmetry

The evolution of the Hα profile from the early photospheric epoch through the developed nebular stage is in many respects similar to that of SN 1987A: early photospheric epoch with normal P-Cygni lines expected in the spherically-symmetric case, development in the Hα line of a fine structure resembling "Bochum-event" in SN 1987A at the late photospheric epoch, and the development of fine structure and red-shift in the emission maximum of Hα at the nebular epoch (Fig. 2.12).

The first two spectra show an undisturbed P-Cygni profile of Hα with a clear blueshift of the peak emission, in contrast with the standard picture of line formation in an expanding atmosphere that generally requires an unshifted emission maximum. Similar

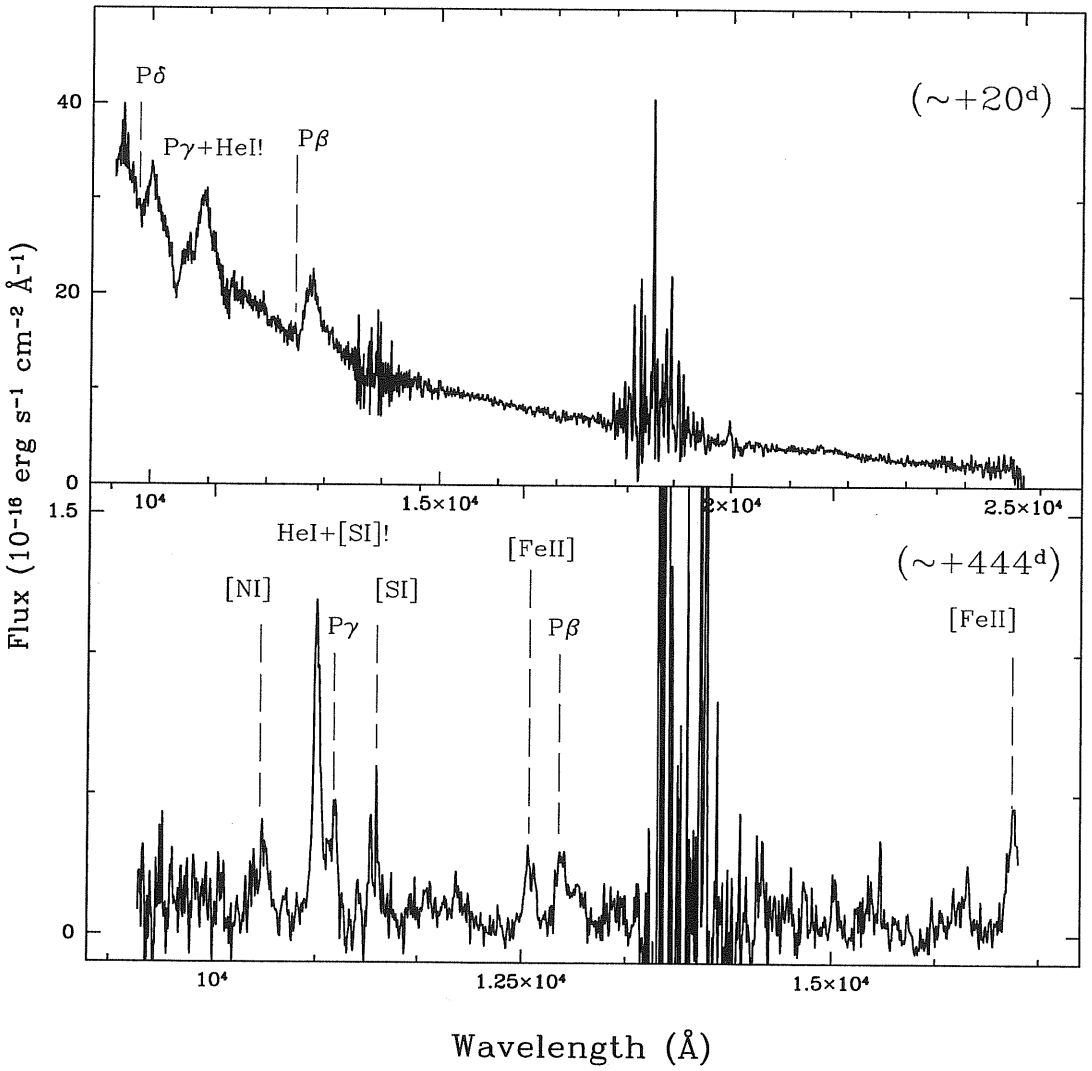

Figure 2.9: The infrared spectra on day 20 and 444 after correcting them from the redshift of the host galaxy. Some line identifications for both phases are also reported.

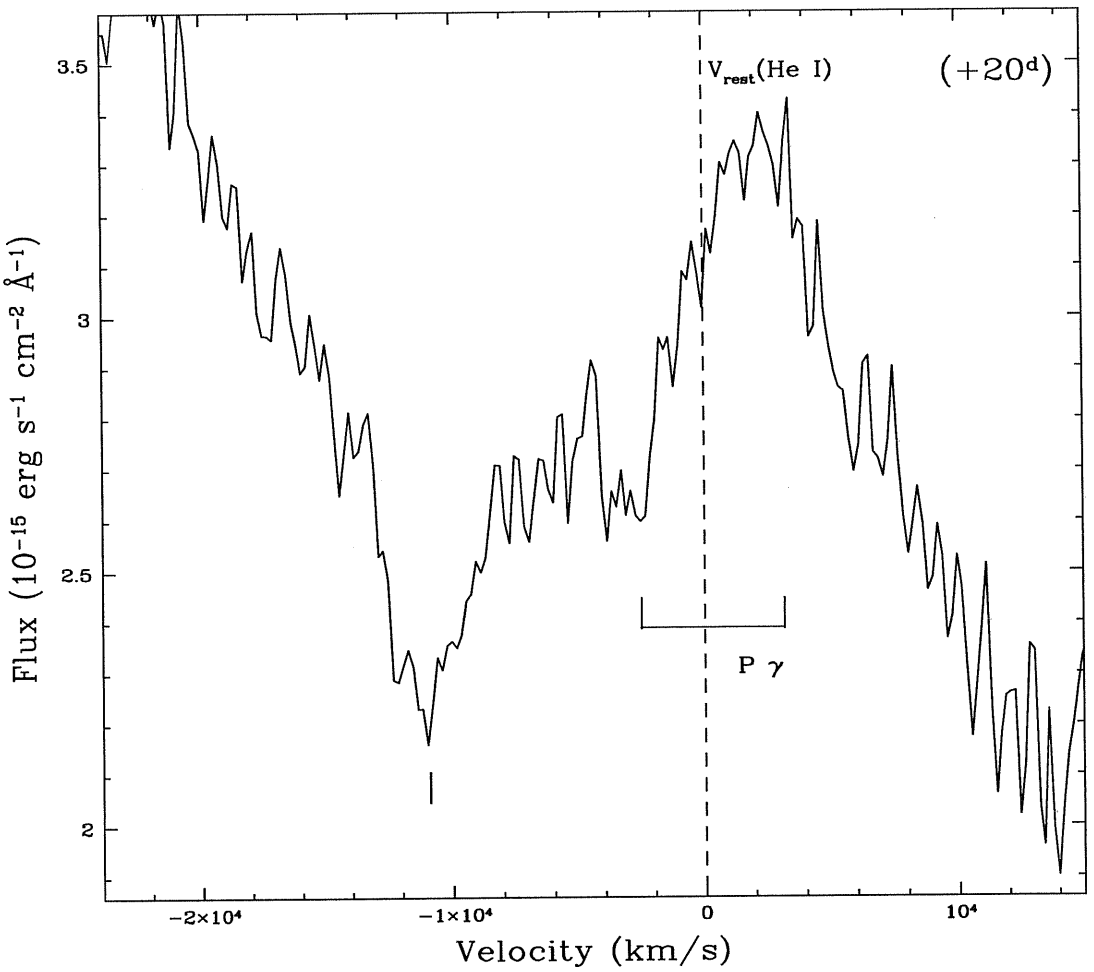

Figure 2.10: He I 10830 Å on day 20. The line is blended with Pγ which strongly affects the He I emission component, but does not affect the absorption component of 10830 Å line whose absorption minimum is shown by a vertical tick at a velocity of $\approx$ 11000 km s^{-1}. The expected positions of absorption and emission components of Pγ are indicated with the "U" shape segment. Note that Pγ and He I 10830 Å velocities are different. The vertical short-dashed line corresponds to the He I 10830 Å rest wavelength.

behaviour is also seen in spectra of other SNe II, namely SN IIP 1988A (Turatto et al. 1993 [62]), SN IIL 1990K (Cappellaro et al. 1995 [11]) and SN 1987A for which this behaviour has been a subject of theoretical studies and has been explained as being due to the reflection of photons by the photosphere (Chugai 1988 [1988]; Jeffery & Branch 1990 [35]). There is a similar blueshift in the emission peak of Hβ, clearer for the first spectra. Figure 2.13(left) displays the amount of the blueshift seen in our spectra.

As the supernova evolves, the blueshift decreases, so that by $\sim$ 65 d it approaches zero, more clearly for Hα than for Hβ where line blending is a complication. The blueshifts for the Paschen hydrogen lines from our first infrared spectrum are also shown to be in good agreement with Hα, indicating similar properties of the photosphere in the optical as well as in the infrared.

In Figure 2.13(right) we display the evolution in time of the Hα velocity of SN 1999em together with that of SN 1987A. Velocities are derived from the minima of the P-Cygni absorption components, and in SN 1999em are lower than in SN 1987A at similar phases. The nature and the similarity of the evolution confirm the initial rapid decline in velocity corresponding to the rapid cooling period, followed by a slowly decreasing velocity period as expected during the plateau phase.

The expansion velocities at $\sim$ 97 d and $\sim$ 113 d and also to a lesser extent at $\sim$ 65 d deviate from an otherwise smooth trend. This is due to the emergence of some structures in the absorption components that make the determination of the minimum absorption complicated and doubtful. The evidence of some structures in SN 1999em spectra has been noted first by Leonard et al. 2000 [38].

Around $\sim$ 65 d we note some flattening of the absorption component with a hint of a weak peak near 6496 Å in the transition between the minimum and maximum flux. This subsequently becomes more pronounced. A less pronounced feature develops on the red side of the emission component at $\sim$ 97 d near 6675 Å. All these features show a tendency to smaller velocities (i.e. they move toward the rest wavelength) as time increases, reaching their maximum prominence around +113 d. Similar but not so clear behaviour is evident for other lines in SN 1999em, in particular Na I D. Figure 2.14 illustrates the structure and the presence of these "bumps" on the lines at day 113. On the Hα profile we mark three detectable structures: 1 blue and 2 red bumps. In the lower plot we show the Na I D profile which reveals clearly the presence of two red bumps at velocities very close to r_1 and r_2 seen in Hα. Moreover we note that the b_1 feature velocity is in agreement with the photospheric velocities as derived from weak metal lines (Fe II 5018 Å and 5169 Å) at corresponding time. For the +113 d spectrum : $V_{\mathrm{Fe\ II}} \sim 2100$ km s^{-1} while the corresponding velocity from the peak of the b_1 feature is of the order $V_{\mathrm{b1}} \sim 2400$ km s^{-1}.

This complicated structure of the Hα profile was also noted for SN 1987A (Hα fine structure and Bochum event; Hanuschick 1988 [33]; Phillips et al. 1989 [47]; Sartori et al. 1990 [53]) and in SN 1988A (Turatto et al. 1993 [62]). It occurred earlier in SN 1987A and has been ascribed to clumping and mixing of radioactive material into the outer envelope with an axially symmetric geometry, two-sided jet, by Lucy (1988)[42]. This possibility is illustrated by Figure 2.15(left) which shows the spectrum on day 97

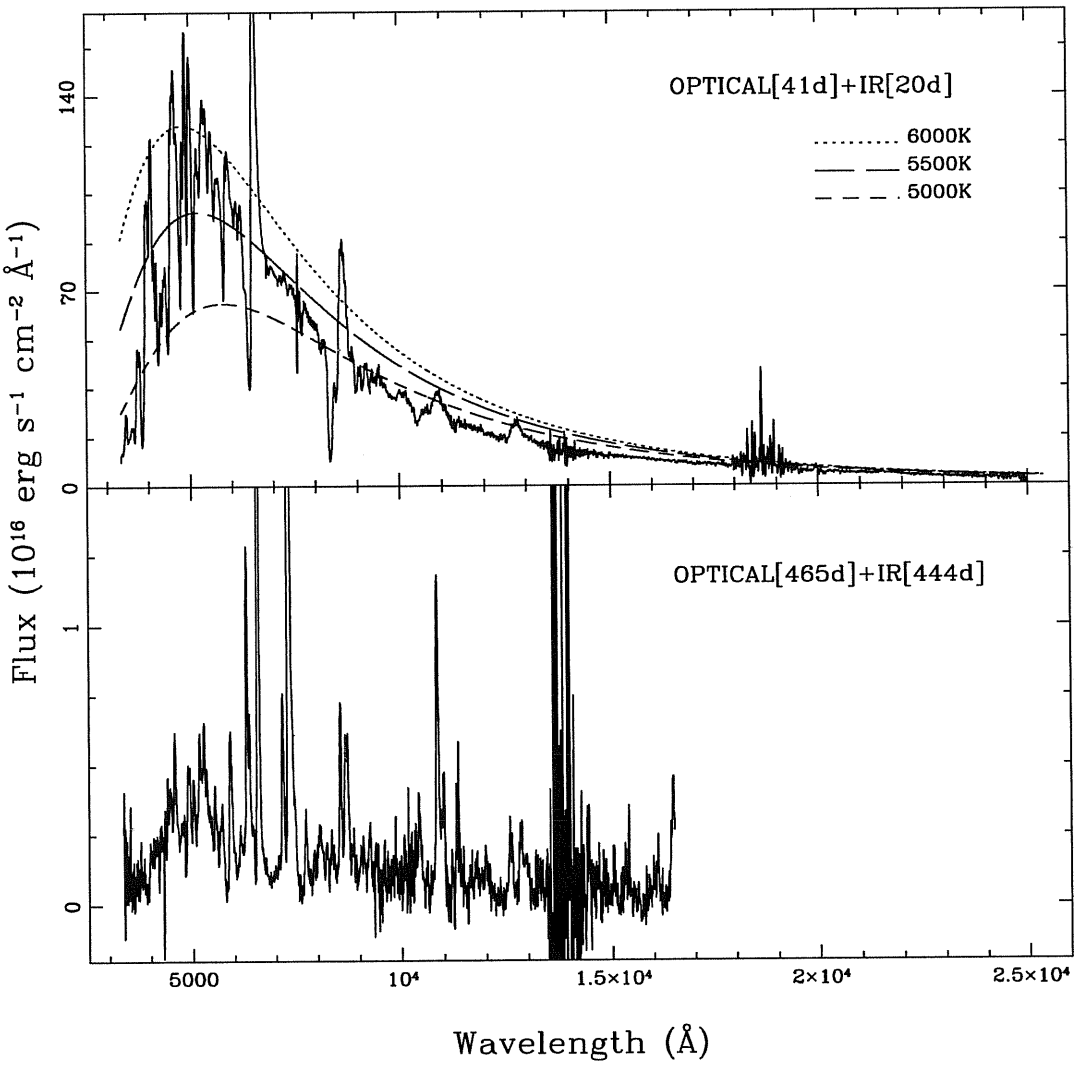

Figure 2.11: The resulted extended spectra from the best combination of infrared and optical spectra. Both spectra are corrected for redshif. The earliest OP(+ 41 d)+IR(+ 20 d) spectrum, shown on the top, is also corrected for reddening. Black-body curves at 3 different temperatures are plotted with the best fit corresponding to a temperature of the order ~5500 K .

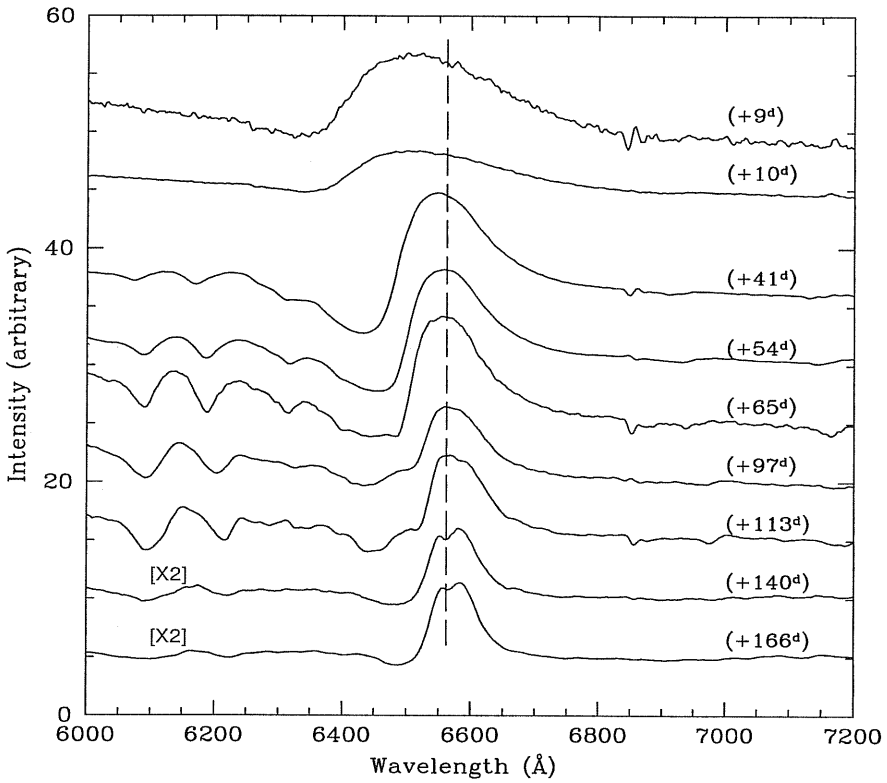

Figure 2.12: The evolution of Hα spectral region. The spectra are corrected for the host galaxy redshift and scaled arbitrary in intensity, some spectra are also multiplied by a shown factors for clarity. The rest wavelengths and days since explosion are also reported

.

with the model Hα computed assuming a spherical distribution of optical depth and net emission source functions. The residual shows excess in the blue and red, which conceivably reflects the overexcitation produced by ^{56}Ni jets. It is, of course, not a unique representation of the spherical model, but this one at least demonstrates this possibility. An alternative view on the fine structure in Hα of SN 1987A suggests that the blue bump, on the contrary, reflects underexcitation of hydrogen at some velocity in the atmosphere related to the deep recombination following the cooling wave (Chugai 1991a [15]). Recently this conjecture was confirmed by the non-steady state calculations of the hydrogen recombination in the atmosphere of SN 1987A with the inclusion of reactions with H^- and hydrogen molecules (Utrobin & Chugai 2002 [65]). This modelling also confirmed the dominant role of the ionization freeze-out effect in the population of the second hydrogen level and the Hα formation at the photospheric epoch (Chugai 1991b [16]). According to the latest computations the non-monotonic behaviour of the excitation in the atmosphere of SN 1987A (and SNe IIP in general) would be a natural outcome of the freeze-out effects, combined with the neutralization of H^+ in the ion-molecular reactions. Of course, only direct similar modelling for SN 1999em will give a conclusive answer concerning the plausibility of this mechanism for the blue bump. Figure 2.15(right) demonstrates, how the Sobolev optical depth in Hα would appear in order to reproduce the appropriate blue bump. Note, although the blue structure is fitted quite well, some excess in the red remains unaccounted for in the model and therefore indicates a real asymmetry of the hydrogen excitation.

In fact soon after, on day 113 the red excess became even more evident. It increases with time and on day 444 it is also detected in He I 10830 Å. On days 140 and 166 the Hα maximum shows significant deviation from a round-shaped form. The complicated structure with the dominant red peak apparently indicates the asymmetric distribution of the line-emitting gas in the central region $v < 1500$ km s^{-1}. The comparison of He I 10830 Å with Hα at the similar epoch (Figure 12.6) shows that the peak is redshifted by the same value as in Hα. We believe that this red bump at $\approx +400$ km s^{-1} is caused by the ^{56}Ni asymmetry. The He I line is narrower (in the red Pγ contributes). The blue width at half maximum (BWHM) is 2000 km s^{-1} for Hα and only 1000 km s^{-1} for He I 10830 Å. The He I 10830 Å line traces non-thermal excitation more closely than Hα, since for hydrogen additional ionization from the second level is more important than for He I. The width and position of the He I 10830 Å line thus indicates that the bulk of ^{56}Ni is distributed inside a sphere with velocity $v < 1500$ km s^{-1} and the ^{56}Ni zone is shifted to the far hemisphere by roughly 400 km s^{-1}.

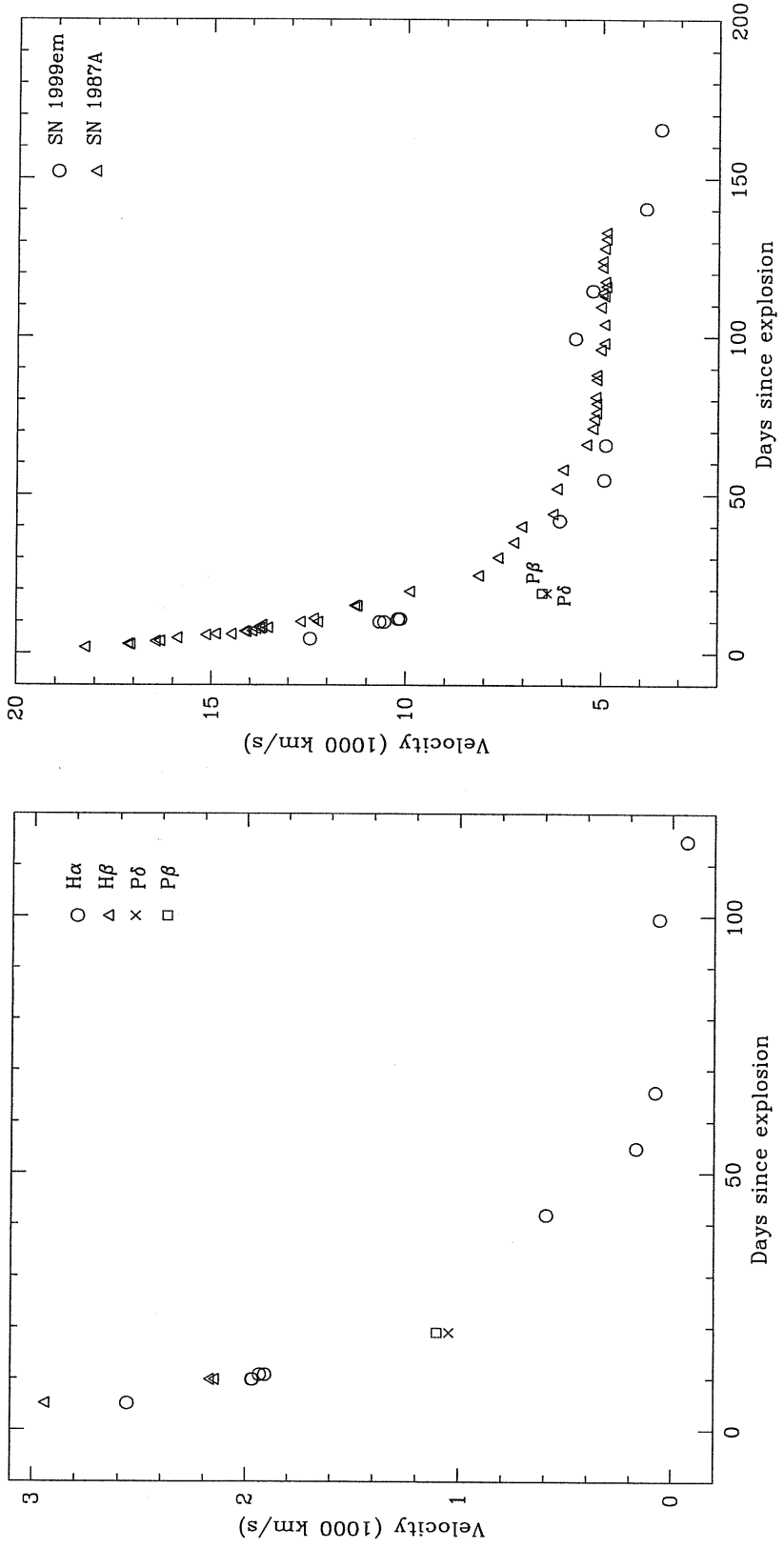

Figure 2.13: Left panel: the amount of the blueshift seen in the emission peaks of Hα and Hβ during the first phases. Line blending is a complication for Hβ. Right panel: the evolution of the expansion velocities, derived from the absorption minima in Hα profiles, for SN 1999em together with that of SN 1987A for comparison. For both panels the corresponding velocities of Pβ and Pδ from the $\sim +20$ d infrared spectrum are also shown.

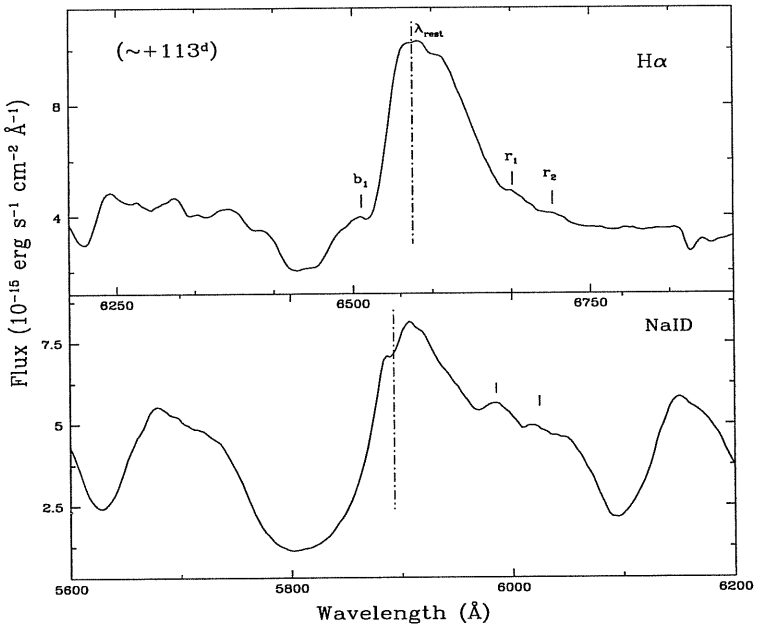

Figure 2.14: The Hα and Na I D line profiles at ~ +113 d after explosion. The rest wavelengths are also shown. The short bars in Na I D profile correspond to the derived velocities from the features seen in the Hα profile (see discussion in the text).

2.4 Evidence for dust formation around day 500

The temporal evolution of the [O I] profile can be an effective indicator of dust formation in the form of an observable blueshift in the emission peaks of the components (Danziger et al. 1991 [22]). It should be noted, that apart from the late time blueshift related to the dust formation, SN 1987A also showed an "early blueshift" in [O I] 6300 Å between day 200 and 300 that disapeared at the later epoch. We believe, the blueshift in [O I] 6300 Å observed in SN 1999em on day 312 and 391 and which vanished on day 465 is of the same origin as the early blueshift observed in SN 1987A and also that reported for SN 1988H (Turatto et al. 1993 [62]). Namely, it has nothing to do with the dust and probably is the result of the superposition of the blend of Fe II lines (multiplet 74). This latter is hinted at by the bump at 6250 Å attached to the blue wing of [O I] 6300 Å.

However between day 465 and 510 the [O I] 6300,6364 Å line and Hα demonstrate a pronounced evolution (Figure 2.17). The transformation in both profiles can be described as a flattening of the line accompanied by skewing towards the blue. The quality of the 642 d spectrum is not sufficient to confirm this effect, although the spectrum does not contradict the conclusion from the previous two spectra. The dramatic change of the line profile at the time scale of the order of 0.1 of the expansion time (or even faster) and a proximity of the age to the epoch of the dust formation in SN 1987A around day ~ 526 (Lucy et al. 1989 [43]) suggest that dust formation is the likely cause of this profile transformation. Note that the flattening of [O I] 6300 Å line profile in fact was

not observed in SN 1987A at the dust formation epoch. Instead the blueing of oxygen line in SN 1987A preserved the round-topped profile of the [O I] 6300 Å line which is consistent with the dust formation in the sphere with the expansion velocity of 1800 km s^{-1} and dust optical depth of the order of unity (Lucy et al. 1989 [43]).

Nevertheless, the flat-topped profile is expected, if the optical depth of the opaque core is very high. To emphasize the point we present the toy model (Figure 2.18), which suggests some smooth distribution of emissivity in the [O I] doublet lines (with the line ratio of 0.4, similar to SN 1987A at the same epoch) and the embedded opaque core. The model doublet in the absence of any absorption roughly represents the situation on day 465. Switching on the dust absorption in the dusty core with the boundary velocity of 800 km s^{-1} produces the effect, which markedly depends on the optical depth. For $\tau = 2$ the line shape and blue shift recalls what was seen in SN 1987A at the dust formation epoch after day 530, where the estimated optical depth of the core is $\tau_d \sim 1$ (Lucy et al. 1989 [43]). We see that the flat-topped [O I] doublet profile observed in SN 1999em on day 510 requires an optical depth of the dusty sphere $\tau_d \gg 10$, since in case of $\tau_d = 10$ the plateau has a noticeable inclination, which is absent in the case of $\tau_d = 50$. This illustration indicates that the dust formed between days 465 and 510 and the optical depth of the dusty core was enormous, $\tau_d \gg 10$. The blue end of the plateau in the [O I] 6300 Å line (Figure 2.17) indicates the velocity of the dusty sphere of about $v_d \approx 800 \pm 50$ km s^{-1}.

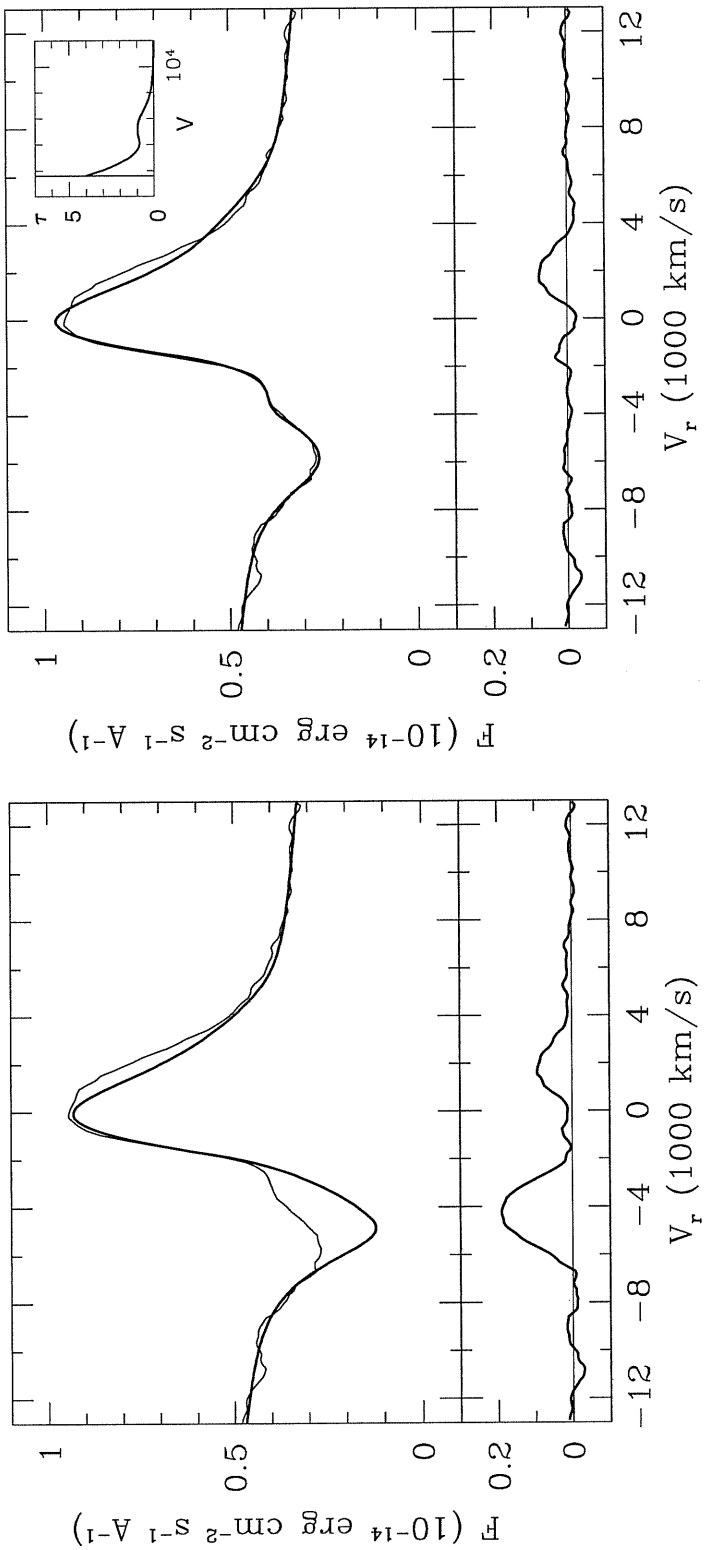

Figure 2.15: Left panel: the Hα on day 97. The overplotted (thick line) is a profile for a spherical model. The residual (bottom panel) shows two peaks, which can be interpreted as evidence for the presence of bipolar excitation regions in the atmosphere. Right panel: the Hα on day 97. The overplotted (thick line) is the profile for the spherically symmetric model with the non-monotonic behaviour of the optical depth shown in window (up right corner). The residual shows the excess in the red, which is indicative of overexcitation in the far hemisphere.

As in SN 1987A, for the Hα line the effect of the dust core is less apparent because of the more extended Hα-emitting zone and, primarily, because of the redward asymmetry of this line related with the ^{56}Ni asymmetry. Nevertheless, the blueward skewing in the spectrum on day 510 is seen in Hα also.

Even less apparent is the profile evolution of the [Fe II] 7155 Å line. The absence of the skewing towards the blue in this line on day 510 indicates that the unocculted fraction of asymmetric red component is strong enough to maintain the original redshift of this line seen on day 465. To illustrate this explanation we represent the profile of [Fe II] 7155 Å as a combination of the spherically-symmetric component and the component originating in the conic structure with the opening angle 2α and the angle between line of sight and the cone axis θ (Figure 2.19, upper panel). Adding to the model the dust core with $v_{\rm d} = 800$ km s^{-1} and $\tau_{\rm d} = 50$, we checked, if our choice for the asymmetrical component is tolerated by the 510 day spectrum of [Fe II] 7155 Å . The decomposition of the line profile into symmetric and asymmetric component is, of course, not unique, given the large noise in the 510 d line (the usual drawback for the inverse problem). However, we found that for small inclination angle, $\theta < 50°$, the skewing towards the blue in the model is unacceptably large. One of the acceptable possibilities found by trial and error procedure is shown in Figure 2.19(lower panel). In this case $\theta = 67°$ and $\alpha = 40°$. The line emissivity in the model cone is concentrated towards the cone axis and distributed along the radius with the broad maximum in the range $1000 - 3000$ km s^{-1}. In this modelling we followed a somewhat arbitrary but sensible requirement that the radial displacement of the maximum of the jet emissivity is minimal. The model with the dusty core obviously reproduces the major property of the profile on day 510, namely, the shift of the maximum towards the red. We thus conclude that the dust core implied by the [O I] doublet transformation is not in conflict with the [Fe II] 7155 Å line profile provided that the ^{56}Ni jet, responsible for the red asymmetric component, has relatively large inclination angle $\theta \geq 60°$. We do not insist on the uniqueness of the model of asymmetric distribution of emissivity of [Fe II] 7155 Å. Yet the one-sided asymmetry of emissivity implied by the profile evolution is strikingly consistent with the one-sided ^{56}Ni distribution suggested above by Hα and He I 10830 Å lines.

The manifestations of the dust formation in SN 1999em are different from those in SN 1987A in at least three respects. First, while in SN 1999em the [O I] 6300 Å line revealed the presence of the dust already on day 510, in the case of SN 1987A the blue shift in [O I] 6300 Å emerged only after day 526 (Danziger et al. 1989 [21]; Phillips & Williams 1991 [48]). A somewhat earlier emergence of the dust in SN 1999em is probably related to the lower amount of ^{56}Ni, which in its turn implies lower temperature at the given stage, so the condensation temperature was attained in SN 1999em earlier. Second, the velocity of the dust-forming zone is a factor two lower compared to the dusty core in SN 1987A (~ 1800 km s^{-1}) measured in the spectra around day 600 (Lucy et al. 1989 [43]). This difference possibly reflects both the smaller mass (and therefore velocity) of the metal-rich core of ejecta and smaller velocity of ^{56}Ni bubble, which presumably pressurizes the metal-rich zone thus producing dense clumps in which dust forms. The third is more clear cut: the optical depth of the dusty core in SN 1999em $\tau_{\rm d} \gg 10$ while in SN 1987A $\tau_{\rm d} \leq 1$ (Lucy et al. 1989 [44]). At first glance a factor two smaller radius of

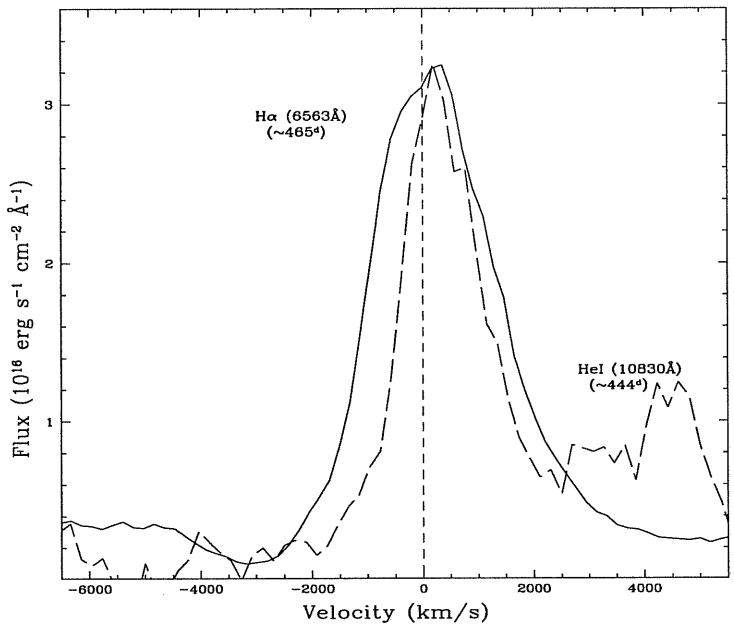

Figure 2.16: Hα and He I 10830 Å lines at the nebular epoch. Both lines show apparent redshift indicating the asymmetry of ^{56}Ni. The He I line blue width at half maximum is factor two lower, possibly indicating the actual width of the ^{56}Ni zone. Note that the He I 10830 Å maximum is shifted arbitrary to reach Hα maximum for comparison.

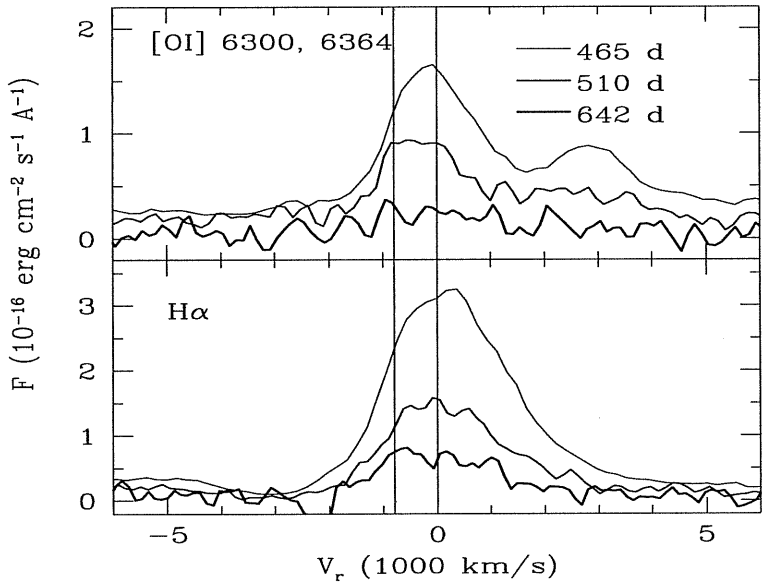

Figure 2.17: The oxygen doublet [O I] 6300, 6364 Å and Hα in the latest three epochs. The spectra on day 642 are multiplied by factor of six. The two vertical lines correspond to zero velocity and the approximate position of the blue edge of plateau in [O I] 6300 Å line. The spectra are not corrected for reddening.

the dust core in SN 1999em compared to SN 1987A is an explanation for this difference. Assuming a comparable amount of dust and the given factor of two smaller radius one gets a factor of four higher column density. However, this is still a small factor to explain at least a factor of 20 difference in the optical depth.

The explanation of the high optical depth derives from the model of the clumpy dust zone in SN 1987A proposed by Lucy et al. (1991)[44]. To account for the wavelength independent extinction the authors suggested that the dust is locked in very opaque clouds, so the effective optical depth of the dusty zone is actually the geometrical (occultation) optical depth produced by the cloud ensemble ($\tau_{\rm oc} = 3N/4\pi R_{\rm d}$, where N is the number of clouds, $R_{\rm d} = v_{\rm d}t$ is the radius of dusty core). Lucy et al. (1991)[44] estimate $\tau_{\rm oc} \approx 0.4$ for SN 1987A around day 625. To account for the high optical depth of the dusty core in SN 1999em, we must admit that the occultation optical depth is very high $\tau_{\rm oc} \gg 10$, i.e. the number of opaque cloudlets is substantially higher than in SN 1987A. We estimate the amount of dust required to produce the optical depth $\tau_{\rm d} = 50$ on day 510 as $\sim 10^{-4}\ M_{\odot}$, a quite moderate value. In fact, this number should be considered as a lower limit. An apparent blueward shift in the peak of Mg I] 4571 Å is apparent between days 465 and 510. Since the shift is similar in velocity to that observed in [O I] 6300 Å and clearly results from a depletion of flux on the red side, with the blue side remaining constant in velocity, it is consistent with our model for a very opaque core of dust with a large occultation optical depth.

The opaque dusty core must radiate as a black-body with the temperature determined by the absorbed luminosity and the radius. Modelling the Hα profile transformation we estimate that about 30% of the luminosity is intercepted by the dusty core on day 510. Given the bolometric luminosity at this epoch $L \approx 2 \times 10^{39}$ erg s^{-1} the luminosity of the dusty core must be then of $L_{\rm d} \approx 6 \times 10^{38}$ erg s^{-1}. The black-body temperature of the dusty core on day 510 was then ≈ 510 K with the maximum of the infrared spectrum at 6 μm. We are not aware of any IR observations of SN 1999em in M band at this epoch.

Since vibration-rotation bands of CO have been detected in the IR spectra of SN 1999em by Spyromilio et al. (2001)[58], one is entitled to conclude, as was done with SN 1987A, that the formation of molecules was a prelude to formation of dust. Moreover we expect dust condensation to cause a deficit in the optical radiation with respect to the case with no dust. Figure 2.20 displays an expanded version of the B, V and R late time light curves together with the least squares fits (the last point is excluded in the fit). It is clear that all the light curves display a deficit decline for day 510 compared with the linear trend shown by fitting the previous data as represented by the dashed line. The average deficit is close to 30 percent. This gives further support for dust formation after day 465. Such a deficit was also noted by Lucy et al. (1991)[44] at the time of dust formation in SN 1987A.

The fact that a fully opaque dusty core absorbs only a relatively small fraction ($\sim$ 30%) of the optical radiation is apparently related to the compactness of the dusty core and the large extent of the optical emitting zone. This is indicated by the fact, that the velocity of the dusty sphere is notably lower than the FWHM of Hα on day 465 (≈ 2700 km s^{-1}). A simple geometrical model to illustrate the situation is the dusty sphere with

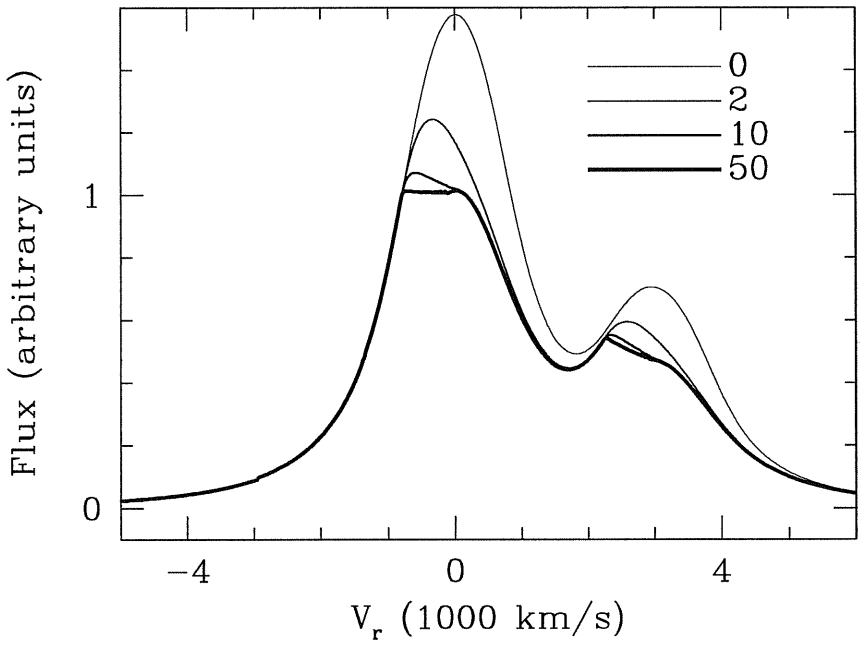

Figure 2.18: The effect of the opaque core on the [O I] doublet. Lines of different thickness correspond to different optical depths of the core, starting with $\tau = 0$ (thinnest line) through $\tau = 2$, $\tau = 10$, and $\tau = 50$ with progressively growing line thickness. Note, for $\tau = 10$ the plateau is still not settled and only for $\tau \gg 10$ the profile is flat-topped.

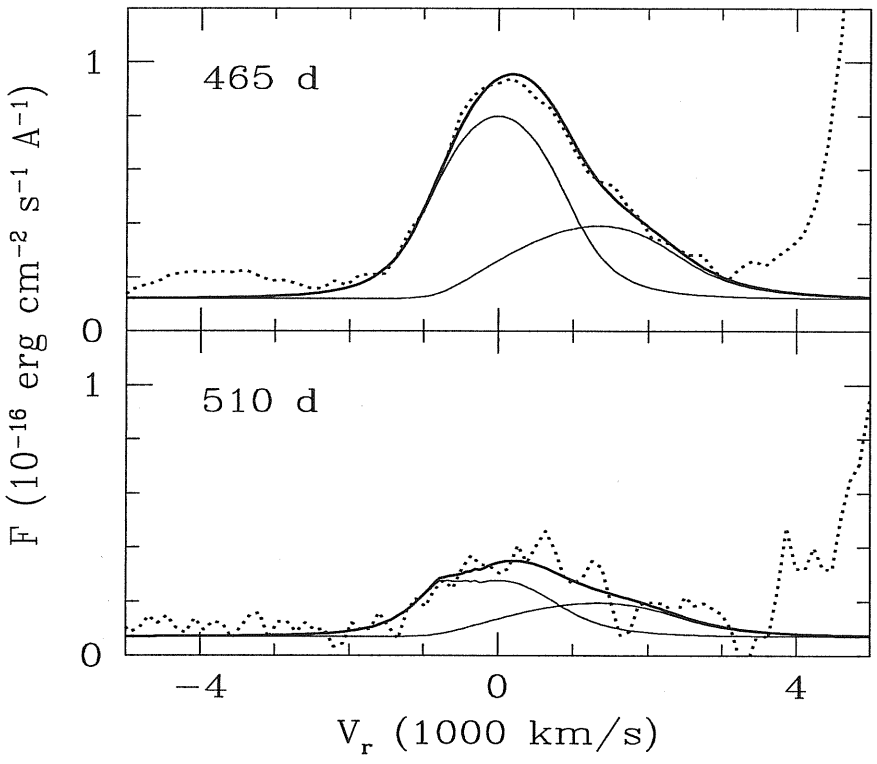

Figure 2.19: The effect of the opaque dusty core on the [Fe II] 7155 Å line. Top panel shows the model line profile model (*thick line*) overplotted on the observed profile on day 465 (*dotted line*). The model is a combination of the spherically-symmetric and asymmetric components (*thin lines*). The asymmetric component is modeled by the conic overexcitation zone in the far hemisphere. The lower panel shows a similar plot but on day 510 and with added opaque core velocity 800 km s^{-1} and $\tau = 50$ in the model. Note that the model flux on day 465 was multiplied by factor 0.5 to produce the adequate fit on day 510.

the velocity v_d embedded in the homogeneous extended emitting sphere (v_e). It is easy to show then that the absorbed energy fraction ~ 0.3 implies the ratio $v_d/v_e \sim 0.6$. Given $v_d \approx 800$ km s^{-1}, this leads to the effective velocity of the emitting sphere of $v_e \approx 1300$ km s^{-1}.

We may use a more physical model to directly constrain the extent of a ^{56}Ni zone (v_{Ni}) from the relative amount of absorbed light. Let the SN envelope be a homogeneous freely expanding sphere with the outer velocity v_0 determined by the ejecta mass M and kinetic energy E. We assume that ^{56}Ni is distributed homogeneously in the range $v < v_{Ni}$. We may then compute the bolometric luminosity (without infrared dust emission) treating the gamma-ray transfer in the absorption approximation with the conventional effective absorption coefficient $k = 0.03$ cm^2 g^{-1}. The positron deposition is assumed to be local. Simulations with and without dust using v_{Ni} as a tuning parameter permit us to find the extent of the ^{56}Ni zone from a condition that the dusty core with $v_d = 800$ km s^{-1} and $\tau_d = 50$ absorbs 30% of the light generated locally with the deposition rate. In the particular case of the ejecta mass of $M = 12\ M_\odot$, and two values of kinetic energy of $E = 10^{51}$ erg and $E = 5 \times 10^{50}$ erg we find that the required radius of the ^{56}Ni zone must be $v_{Ni} = 1100$ km s^{-1} and 1300 km s^{-1}, respectively. The parameter variation probably would not change the results markedly, although an asymmetry could slightly affect the situation. The resulting extent of the ^{56}Ni zone ($\sim 1100 - 1300$) km s^{-1} is quite sensible and consistent with our previous finding that ^{56}Ni lies inside the sphere of ~ 1500 km s^{-1}. Remarkably, the above simple geometrical analysis led to the extent of the emission region (1300 km s^{-1}) comparable to the extent of ^{56}Ni zone in the dense (low energy) model. This reflects a simple truth that a dense model is close to the situation of the local deposition, the approximation implicitly assumed in the simple geometrical model. We therefore conclude that the small partial blackout of the supernova light following the formation of an extremely opaque dusty core of SN 1999em stems from the fact that the dusty core is compact compared to the extended distribution of ^{56}Ni.

2.5 The photospheric temperature, explosion time and distance

At the early photospheric epoch the photosphere of SNe IIP is considered to approximate a black-body with a sharp boundary (Branch 1990 [10]). We made black-body fits to our spectra, after dereddening the fluxes in different bands with E(B − V)=0.1. The interstellar extinction laws of Cardelli et al. (1989) [12] were adopted. The derived temperatures are shown in Figure 2.20(upper panel), plotted as a function of time since explosion. We have used our Nov 3 spectrum to estimate the difference in temperature obtained by using a reddening of E(B − V)=0.1 and the smaller reddening used by Baron et al. (E(B − V)=0.05). That variation is then applied to the Baron et al. estimate for Oct 29 spectrum to give a revised higher temperature of T∼14300 K. In Figure 2.21(left lower panel), we plot the evolution of the difference in temperature between the case of no reddening correction (E(B − V)=0.0) and the one with E(B − V)=0.1. This behaviour

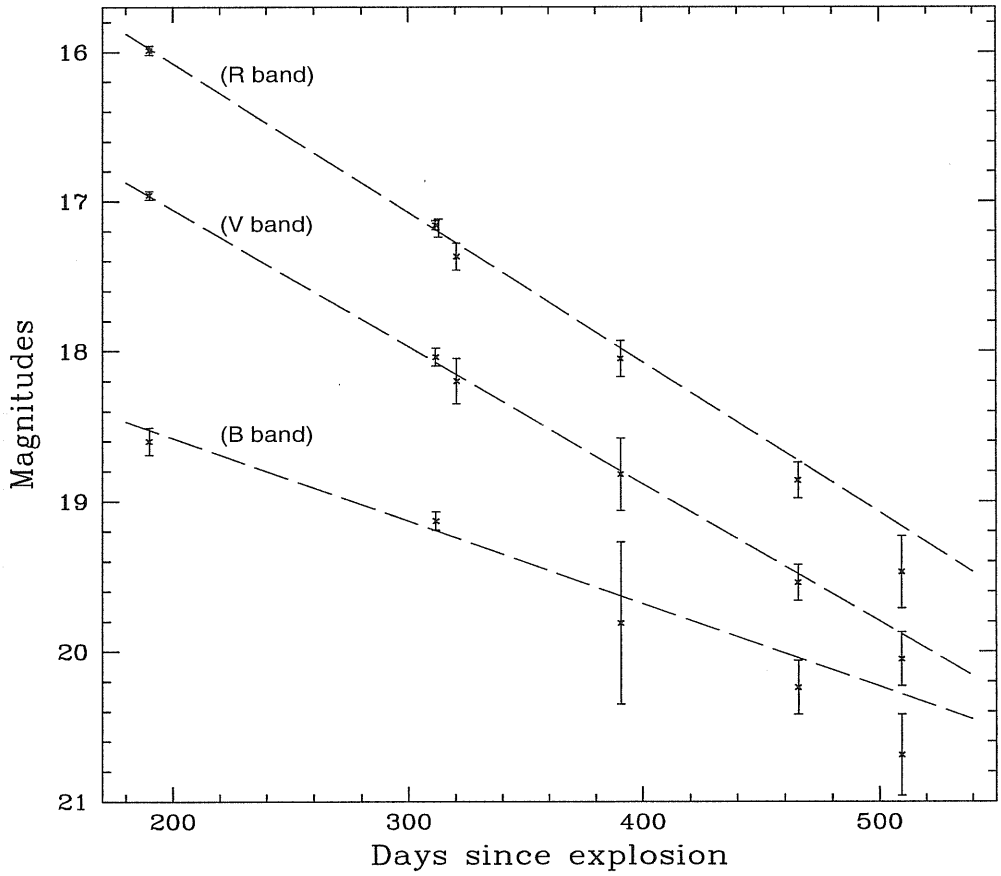

Figure 2.20: The late B,V and R light curves. The dashed lines represent the least squares fits of data weighted according to error estimates and excluding the last point at day 510. A deviation is seen in the last point of each colour, which supports the dust condensation scenario after day 465 as inferred from spectroscopy.

shows the effect of the reddening correction on the derived temperatures from black-body fitting. At early phases, close to the explosion time and when the object is very hot, the colours on the Rayleigh-Jeans tail are not sensitive to temperature and therefore small changes in colour produce large changes in temperature and as time progresses this difference decreases. Figure 2.21(left upper panel), on the other hand, confirms the strong initial cooling of the photosphere as the supernova ages followed by a relatively constant temperature starting at T$\sim$5500 K and dropping to T$\sim$4200 K.

We apply the expanding photosphere method (EPM) to our data in order to estimate the time of explosion of SN 1999em and its distance. More detailed studies concerning the use of this method in the case of SN 1999em were made by Hamuy et al. (2001)[32] and by Leonard et al. (2002) [39], who used broad band colours rather than spectrophotometry, and a larger data base. The EPM, also called Baade-Wesselink method, is based essentially on the assumptions that the SN IIP photosphere is spherical and emits as a dilute black-body, and that the expansion proceeds homologously ($v = r/t$). For small redshift ($z \ll 1$) the photospheric angular radius is

$$\theta = \frac{R}{D} = \sqrt{\frac{f_\lambda 10^{0.4A_\lambda}}{\xi_\lambda^2 \pi B_\lambda(T)}} \tag{2.2}$$

where $R = vt$ is the photospheric radius determined by the expansion time t and velocity at the photosphere v (here we assume that the presupernova is a point), D is the distance to the SN, f_λ is the apparent flux density, A_λ is the total reddening coefficient, $B_\lambda(T)$ is the Planck function evaluated at T, and ξ_λ is the dilution parameter to account for the fact that the SN does not radiate as a perfect black-body.

We adopt $A_V = 0.31$, f_λ at $\lambda = 5500$Å (from observations), $B_\lambda(T)$ using the temperatures of the black-body fitting of the spectra, and the parameter ξ according to temperature and wavelength dependence given by to Hamuy et al. (2001)[32].

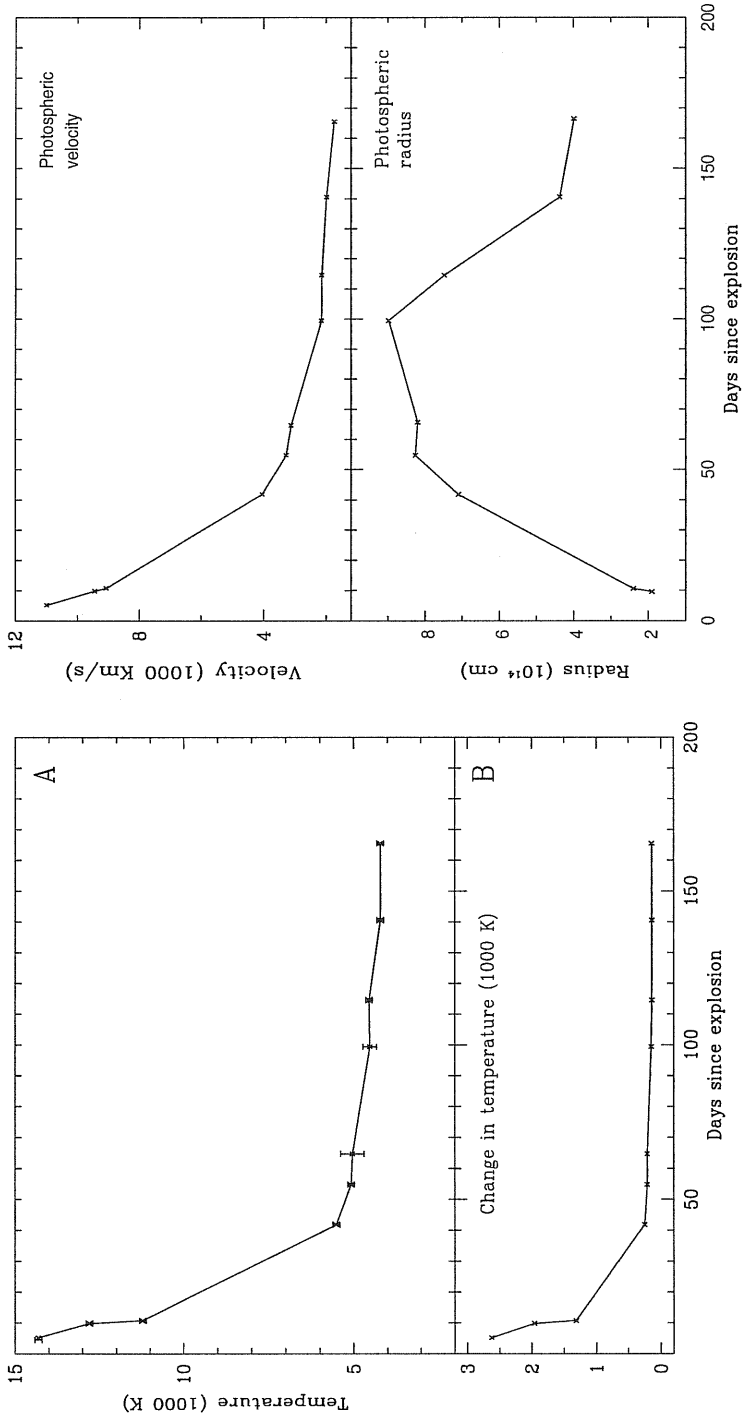

Figure 2.21: Left panel: the evolution in time of the derived temperatures from black-body fitting of the spectra (A), and the variation of the change in temperature from E(B − V)=0.0 to E(B − V)=0.1 (B). Right panel: the photospheric velocity and the photospheric radius evolution. This later is computed using the temperature and the bolometric luminosity (sections 2.2 & 2.5).

The expansion velocity v was measured from our spectra, using the absorption minima of weak lines such Hβ and Fe II lines at 5018 Å & 5169 Å, formed in material close to the photosphere (Eastman & Kirshner 1989 [23]). The velocity evolution is shown in Figure 2.21(right). This leaves two unknowns, t_0 and D, to determine. Results are reported in Table 2.3. Figure 2.22 shows a least squares fitting of our data. We found $t_0 \sim$ JD 2451476($\pm$1day) corresponding to 1999 October 24.5 and a distance of 7.83 $\pm$0.3 Mpc. These derived values agree well with results of the more detailed studies of the EPM for the case of SN 1999em (Hamuy et al. 2001 [32] and Leonard et al. 2002 [39]). Our use of the same values of ξ and the reddening as those used by Hamuy et al. links the two results. It is the use of different type of photometry and independantly determined velocities that strengthens the conclusions by both groups that the results are robust. Thus the case of SN 1999em provides a check of the consistency of the EPM since, from observations, it is already known that the supernova exploded between Oct 20.45 and the discovery date Oct 29 (Li 1999 [40]). In addition the derived distance is in excellent agreement with that derived from a study of the stellar component of NGC 1637 by Sohn and Davidge (1998)[56].

We compute as well the photospheric radius using the luminosity and the temperature for a given time. The results are shown in Figure 2.21(right), together with the photospheric velocity evolution.

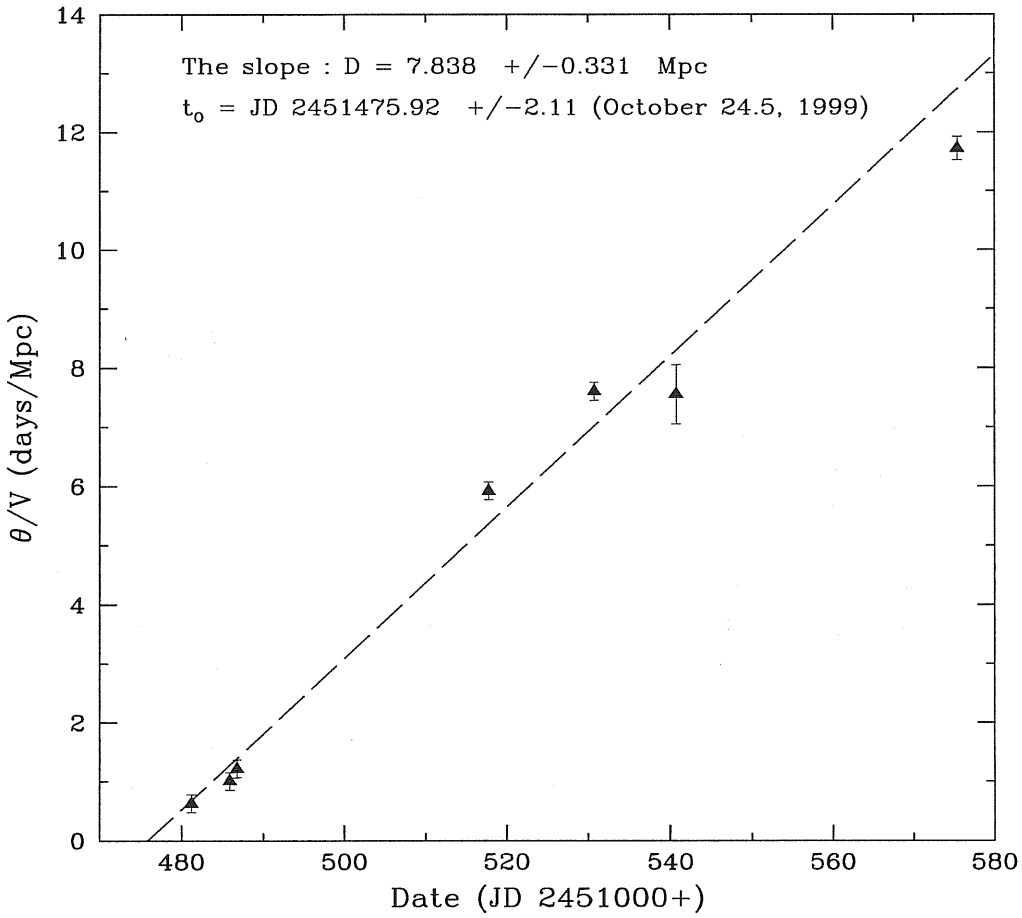

Figure 2.22: The derived EPM results from our data. Also shown the least squares fit and the estimated explosion time and the distance to the SN. The discovery time corresponds to JD 2451480.94.

Table 2.3: The EPM results for SN 1999em.

Date (JD 2451000+)	*Flux* (10^{-14}ergs/s/cm^2/Å in V)	T_{bb} (K)	V (km/s)	ξ	θ (10^{13}cm/Mpc)
481.2	1.101	14312	10990	0.45	6.034
485.863	1.398	12802	9440	0.424	8.278
486.767	1.385	11217	9072	0.42	9.685
517.795	1.228	5510	4050	0.65	20.707
530.755	1.184	5080	3280	0.75	21.578
540.7	1.152	5040	3120	0.8	20.361
575.42	0.874	4520	2150	0.88	21.772

The values of ξ are taken from Hamuy et al. (2001)[32].

Table 2.4: Decline rates for the second plateau feature.

Supernova	B band (mag)	V band (mag)	R band (mag)	I band (mag)
1997D	$\sim$ 0.33 in 221 d	$\sim$ 0.69 in 89 d	$\sim$ 0.57 in 79 d	$\sim$ 0.53 in 51 d
1991G	—	$\sim$ 0.3 in 30 d	$\sim$ 0.2 in 40 d	$\sim$ 0.15 in 40 d
1999em	$\sim$ 0.22 in 58 d	$\sim$ 0.5 in 58 d	$\sim$ 0.45 in 58 d	$\sim$ 0.54 in 58 d

The B-light curve of SN 1991G is not available in the work of Blanton et al. (1995)[9].

2.6 Progenitor star properties

The detailed observations of SN 1999em provide us with three important phenomenological parameters: the plateau duration ($t_{\rm p}$), absolute V magnitude at the plateau (M_V) and the velocity at the photosphere measured from weak absorption lines ($V_{\rm ph}$). These three parameters permit us to recover the explosion energy (E), ejecta mass (M) and presupernova radius (R) using the light curve models as originally proposed by Litvinova & Nadyozhin (1985)[41]. In this paper useful expressions are given, which are used to estimate SN parameters. Similar, but somewhat different expressions are given by Popov (1993)[50] based on the analytical model, which will also be used here. The input parameters of the model are the duration of the plateau phase ($t_{\rm p}$), a representative photospheric velocity at the beginning of the plateau phase ($V_{\rm ph}$) and its absolute V magnitude ($M_{\rm V}$). From observations of SN 1999em we find $V_{\rm ph} \approx 4050$ km s^{-1} using weak lines in the spectrum on day 41, $M_V \approx -15.76$ at the same epoch and the duration of the plateau $t_{\rm p} \approx 80$ days. According to the relations from Popov (1993)[50] we derive the following parameters for SN 1999em: ejecta mass $M \approx 11\ M_{\odot}$, explosion energy $E \approx 1.1 \times 10^{51}$ erg, presupernova radius $R \approx 120\ R_{\odot}$. Applying the expressions derived by Litvinova & Nadyozhin (1985)[41] using a grid of hydrodynamic models for type II SNe, we find: ejecta mass $M \approx 9.8\ M_{\odot}$, explosion energy $E \approx 0.5 \times 10^{51}$ erg, presupernova radius $R \approx 180\ R_{\odot}$. Both estimates are then consistent with a claim of a presupernova radius of $\sim 120 - 150\ R_{\odot}$, an ejecta mass of $10 - 11\ M_{\odot}$ and an explosion energy $\sim (0.5 - 1) \times 10^{51}$ erg. With approximately 1.5 $M_{\odot}$ enclosed in the neutron star and $0.5 - 1\ M_{\odot}$ lost by the wind, we thus obtain the $12 - 14\ M_{\odot}$ as a possible range for the main sequence mass of the progenitor. This is consistent with the values based upon oxygen mass estimate (section 2.2.1), and as well with the upper limit on the main-sequence mass using pre-supernova field images (Smartt et al. 2001 [55]).

The parameters derived using both sets of analytical expressions and the radius in particular ($\sim 120 - 150\ R_{\odot}$) suggest that the progenitor was a $G_0 - G_5$ supergiant (Cox 2000 [19]). If it were at the detection limit of $m_V = 23.2$ suggested by Smartt et al. (2002)[55] it would have had $M_V = -6.58$ and $M_{bol} = -6.42$ and an effective temperature of the order 5570 K. Using these parameters and the theoretical tracks of Maeder & Meynet (2001)[45] we conclude that the most probable mass would be $12\pm1\ M_{\odot}$. This conclusion is not significantly affected by uncertainties in rotational velocities and metallicity. These estimates provide one with the main parameters of the SN progenitor as a starting point for more detailed computations.

An interesting feature of the bolometric evolution of SN 1999em is the short duration of the peak before the fall to the plateau phase. In fact it has been shown that this early peak is very sensitive to the presupernova mass-loss history. Indeed Falk & Arnett (1977)[24] have demonstrated that a rapid rise and short duration peak ($\sim$ 1-2 days) is consistent with the absence of an extended dense circumstellar shell and hence a low mass loss rate immediately prior to the explosion. This is also in agreement with *Chandra* x-ray and radio observations of SN 1999em (Pooley et al. 2001 [49]).

Table 2.5: Parameters of some selected SNe.

Supernova	t_p (days)	E (10^{51}ergs)	R ($R_\odot$)	$M(^{56}\mathrm{Ni})$ ($M_\odot$)	M_{ms} ($M_\odot$)	Source
1999em	~ 80	$\sim 0.5-1$	120 - 150	~ 0.022	12 - 14	A
1987A	~ 40	~ 1.3	~ 40	0.075	~ 20	B
1997D	~ 50	0.1	85	0.002	8 - 12	C
1993J	$---$	1.6	$---$	0.078	12 - 16	D
1969L	~ 90	~ 1.7	~ 220	~ 0.07	~ 20	E

Sources:

A: The present work

B: Danziger et al. 1988 [20]; Woosley et al. 1989 [68]

C: Chugai & Utrobin 2000 [18]; (see Turatto et al. 1998 [63] for alternative model)

D: Utrobin 1996 [64]; Chugai & Utrobin 2000 [18]

E: Arnett 1996 [2]; Sollerman et al. 1998 [57]

2.7 Summary and conclusions

We have presented photometric and spectroscopic data for SN 1999em, from ~ 9 d until ~ 642 d after the explosion. The shape of the light curve ($t_p \sim 80$ days) as well as spectral features show that it is a type IIP supernova. The problem of reddening has been discussed and we conclude that an optimum choice is close to that determined by Hamuy et al. (2001)[32]. The analysis of late phase photometry, up to ~ 510 d, shows that the exponential tail decay rate is close to the one of the radioactive decay ^{56}Co to ^{56}Fe, indicating that this is the main source of energy powering the light curve.

A photometric comparison of SN 1999em with SN 1987A, especially in the later phases, provides constraints on the radioactive ^{56}Ni mass. We have constructed the "UBVRI" bolometric light curve, and comparing it with that of SN 1987A we obtain an estimate of the amount of ^{56}Ni produced by the explosion of 0.02 $M_\odot$, a smaller value than that derived for typical type IIP SNe such as SN 1969L and SN 1988A which have $M(^{56}\mathrm{Ni}) \sim 0.07\ M_\odot$.

We have noticed some flattening in the light curves, just after the steep decline from the plateau phase, and clearer for the blue bands. This behaviour is also seen in the light curves of two other objects, namely the peculiar SN IIP 1997D and the SN IIP 1991G. All three events have some common features, being type IIP and all having a lower ejected ^{56}Ni mass: a similar amount for both SN 1999em and SN 1991G,($\sim 0.02\ M_\odot$) while SN 1997D ejected an even lower mass ($\sim 0.002\ M_\odot$). In addition, the duration of this "second plateau" on the tail seems greater for SN 1997D than for SNe 1991G and 1999em. The decline rates and the observed duration of the flattening period are reported in Table 2.4. These measurements suggest that the "second plateau" feature is a common feature for this low ^{56}Ni mass type IIP supernovae, and that its duration is correlated with the amount of ejected ^{56}Ni. Further support for this possible correlation comes from the case of SN IIP 1999eu (Pastorello et al. in preparation) which shows a

very clear second plateau feature of duration $\sim$ 200 d (clear in V and B bands). Moreover it seems that this SN has a very low ejected ^{56}Ni mass similar to SN 1997D. Note that the prototype type IIP supernovae SN 1969L and 1988A do not show clear evidence of this behaviour. On the other hand SN 1969L and SN 1988A are known to produce an amount of ^{56}Ni similar to SN 1987A $\sim$ 0.07 $M_{\odot}$. Improved statistical samples and better sampled light curves are required in order to confirm or rule out this behaviour. Radiation diffusion effects, still important at the beginning of the radioactive tail, are a possible cause of this behaviour.

SN 1999em provided a test of the validity of the EPM since we have observational constraints on the explosion time and distance. In fact analysing the spectrophotometry, we derive an explosion time consistent with these constraints and in good agreement with what was found from more detailed broad band photometric studies of SN 1999em (Hamuy et al. 2001 [32]; Leonard et al. 2002 [39]).

We analysed the phenomenon of the fine structure of Hα at the photospheric epoch, which was reminiscent of the "Bochum event" in SN 1987A. Two possible explanations, a bi-polar jet proposed by Lucy (1988)[42] for SN 1987A and underexcitation of hydrogen combined with ^{56}Ni asymmetry, are discussed. This analysis does not permit one to discriminate between those models. Yet the one-sided ^{56}Ni ejection seems to find support in the small red shift of the He I 10830 Å profile and the larger red shift of the Hα line profile at the nebular epoch. We note that the He I 10830 Å line should be more sensitive to non-thermal excitation resulting from γ-ray deposition. These lines indicate that the ^{56}Ni distribution could be imagined to be a filled sphere with a velocity of $\sim$ 1500 km s^{-1} shifted to the far hemisphere by 400 km s^{-1}. A somewhat surprising coincidence is that in SN 1987A the ^{56}Ni distribution also shows one-sidedness with a shift to the far hemisphere.

Analysing the [O I] 6300,6364 Å line profile evolution we found a rapid change between days 465 and 510, which we interpret as an effect of the dust formation during this interval. Other support for dust formation comes from the deficit seen in optical radiation measured by late time photometry. It is the second SN IIP (after SN 1987A) where convincing evidence of dust formation exists. In SN 1987A and SN 1999em we detected the rapid ($\Delta t/t \sim 0.1$) transformation of profiles during the nebular epoch. The dust phenomenon in SN 1999em has some distinctive characteristics compared to SN 1987A. The dust condensation happened earlier (between days 465 and 510) than in SN 1987A (after day 526), which is probably explained, by the lower ^{56}Ni mass and, accordingly, lower temperature. The dust resides in the core with a velocity of $\approx$ 800 km s^{-1}, much lower than in SN 1987A. This greater confinement of dust in SN 1999em possibly results from the lower velocity creating a more confined metal-rich region where the condition for dust formation prevails. Another remarkable difference is the very large optical depth of the dusty zone ($\tau \gg 10$) compared to SN 1987A ($\tau \sim 0.5$, Lucy et al. 1991 [44]). We interpret this difference as an indication that in SN 1999em the dust is distributed more homogeneously (or the number of the opaque dusty clumps is notably greater) than in SN 1987A.

These facts show clearly the importance of studying more samples of SNe IIP (SNe

II in general), because of the diversity they provide in manifesting the same event (i.e. dust condensation) and thus the opportunity of understanding the physics behind such events.

We used relations by Litvinova & Nadyozhin (1985)[41] and Popov (1993)[50] to find SN parameters from observational characteristics. The estimated mass of the progenitor $M_{\rm ms} \approx 12 - 14\ M_{\odot}$ and presupernova radius ($120 - 150\ R_{\odot}$) are just consistent with the failure to detect a progenitor star with imaging of the pre-SN field. Moreover, our derived progenitor mass agrees with our finding that the oxygen mass in SN 1999em is about four times smaller compared to SN 1987A.

There is growing observational evidence of a significant decrease in the mass of Fe produced as the progenitor mass for type II SNe decreases when we include derivations for other objects. It is therefore encouraging to note that this behaviour is what is required to explain abundance patterns such as [O/Fe] and [Mg/Fe] in metal-poor halo stars modeled by Argast et al. (2001) [1].

The correlation of progenitor mass of SN IIP and core collapse SN in general with other parameters is vital for testing explosion models and the theory of stellar evolution. In Table 2.5, we present parameters of SN 1999em along with other SNe II. Note that the parameters reported in the table, except for SN 1999em, are not obtained directly by using the analytical models of Litvinova & Nadozhin (1985)[41] and Popov (1993)[50]. They are however the most reliably determined through modelling of obse[44]rvations.

Table 2.5 demonstrates that for type II SNe there begins to emerge a monotonic relation between progenitor mass on the one hand and both explosion energy and ^{56}Ni mass on the other. Although the uncertainties in these parameters remain, of necessity, large, it seems that in the progenitor mass range $10 - 13\ M_{\odot}$ there is also a steep decrease in both energy and ^{56}Ni mass. This suggests that these latter 2 parameters are not independent but physically linked. Results for other core collapse objects (type Ib,c) with higher progenitor masses tend to support this correlation even if the current scatter is unavoidably large. Future observations supported by modelling will surely elucidate this conclusion. It is clear from our analysis that high S/N spectra of SNe at late phases are an invaluable tool for understanding type II supernovae.

The fact that SN 1999em probably resulted from the explosion of a $G_0 - G_5$ supergiant also indicates, as did SN 1987A, that the evolutionary stage at which massive stars can explode is not yet well delineated.

Bibliography

[1] Argast D. et al. 2001 (Astro-ph/0107153)

[2] Arnett W.D. 1996, in Supernovae and nucleosynthesis, (Princeton University Press)

[3] Baldwin J.A. & Stone R.P.S., 1984, MNRAS, 206, 241

[4] Barbon R. et al. 1990, A&AS, 237, 79

[5] Barbon R. et al. 1995, A&AS, 110, 513

[6] Baron E. et al. 2000, ApJ, 545, 444

[7] Benetti S. et al. 2001, MNRAS 322, 361

[8] Bionta, R.M. et al. 1987, Phys. Rev. Lett. 58, 1494

[9] Blanton E.L. et al. 1995, AJ, 110.2868

[10] Branch D. 1990, in Supernovae, ed. Albert G.Petshek (New York: Springer-Verlag), P.30

[11] Cappellaro E. et al. 1995, A&A, 293, 723-732

[12] Cardelli J.A., Clayton G.C. and Mathis J.S. 1989, ApJ, 345, 245

[13] Chugai N.N. 1987, SvAL, 13, 282

[14] Chugai N.N. 1988, SvAL, 14, 334

[15] Chugai N.N. 1991a, SvAL, 17, 400

[16] Chugai N.N. 1991b, in Supernovae, ed. S. E. Woosely(New York: Springer), Eastman R.G., Kirshner R.P. 1989, ApJ, 286

[17] Chugai N.N. 1994, ApJ, 428, 17

[18] Chugai N.N., Utrobin V.P. 2000, A&A, 354, 557-566

[19] Cox A.N. 2000, in Allen's Astrophysical Quantities. Fourth edition

[20] Danziger I.J. et al. 1988, in SN 1987A in the Large Magellanic Cloud, eds. Kaplan M. & Michlitsianos A.G., Cambridge University Press, Cambridge p.37

[21] Danziger I.J., Bouchet P., Gouiffes C., Lucy L.B. 1989, IAUC 4746

[22] Danziger I.J., Lucy L.B., Bouchet P. & Gouiffes C. 1991, in Supernovae, ed. S. E. Woosely (New York: Springer), p.69

[23] Eastman R.G., Kirshner R.P. 1989, ApJ, 347, 771

[24] Falk S.W., Arnett W.D. 1977, ApJS, 33, 515

[25] Fox D.W. & Lewin W. 1999, IAUC 7318

[26] Filippenko A.V. 1988, in SN 1987A in the Large Magellanic Supernovae, ed. S. E. Woosely (New York:Springer), 69. Cloud, eds. Kaplan M. & Michlitsianos,A.G., Cambridge University; Press Cambridge p.106

[27] Filippenko A.V. 2001 (Astro-ph/0102485)

[28] Fransson C. et al. 1993, in Supernova and Supernova remnants, MCCRAY and WANG, Xian, China, Colloquium 145 p.211

[29] Green D. 1999, IAUC 7303

[30] Hamuy M. et al. 1992, PAPS, 104, 533

[31] Hamuy M. et al. 1994, PAPS, 106, 566

[32] Hamuy M. et al. 2001, ApJ, 558, 615

[33] Hanuschik R.W., Thimm G., Dachs J. 1988, MNRAS, 234, 41

[34] Hirata, K. et al. 1987 Phys. Rev. Lett. 58, 1490

[35] Jeffery D., Branch D. 1990, in Supernovae, ed Wheeler J.C., Piran T., Weinberg S. (World Scientific Publishing Co. Singapore) p.149

[36] Lacey C.K. et al. 1999, IAUC 7336

[37] Landolt A.U., 1992, AJ, 104, 340

[38] Leonard D.C. et al. 2000, ApJ, 553, 861

[39] Leonard D.C. et al. 2002, PASP, 114, 35

[40] Li W.D. 1999, IAUC 7294

[41] Litvinova I.Y. & Nadozhin D.K. 1985, SVAL, 11, 145

[42] Lucy L.B. 1988, in SN 1987A in the Large Magellanic Cloud, eds. Kaplan M. & Michlitsianos,A.G., Cambridge University Press

[43] Lucy L.B., Danziger,I.J., Gouiffes, G., Bouchet, P. 1989, In Structure and dynamics of the Interstellar Medium, ed. G. Tenorio-Tagle et al., IAU Colloquium No. 120 (Springer-Verlag)

[44] Lucy L.B., Danziger,I.J., Gouiffes, G., Bouchet, P. 1991, in Supernovae, ed. S. E. Woosely (New York: Springer), p.82

[45] Maeder A. and Meynet .G. 2001, A&A 373, 555-571

[46] Patat F., Barbon R., Cappellaro E. & Turatto M. 1994,A&A, 282, 731

[47] Phillips M.M., Heathcote S.R. 1989, PASP, 101, 137

[48] Phillips M.M., Williams R.E., 1991, in Supernovae, ed. S. E. Woosely (New York: Springer), p.36

[49] Pooley D. et al. 2001, AAS, 198, 8005

[50] Popov D.V. 1993, ApJ, 414, 712

[51] Ruiz-Lapuente P. et al. 1990, ApJ, 110, 782

[52] Safar J. et al. 1999, IAUC 7331

[53] Sartori M.J., De la resa R. 1990, RMxAA, 21, 450

[54] Schlegel D.J., Finkbeiner D.P. and Davis M. 1998, 500, 525

[55] Smartt S.J. et al. 2002, ApJ, 565, 1089

[56] Sohn Y.J. and Davidge T.J. 1998, AJ, 115:130-143

[57] Sollerman J. et al. 1998, AJ, 493, 933

[58] Spyromilio et al. 2001, A&A, 376,188

[59] Stone R.P.S. & Baldwine J.A., 1983, MNRAS, 204,237

[60] Suntzeff N.B. et al. 1988, AJ, 96, 1864

[61] Turatto M. et al. 1990, AJ, 100, 771

[62] Turatto M., Cappellaro E., Benetti S and Danziger I.J. 1993, MNRAS 265, 471

[63] Turatto M. et al. 1998, AJ, 498, L129-L133

[64] Utrobin V.P. 1996 , ApJ, 306, 219

[65] Utrobin V.P. and Chugai N.N. 2002, Astron. Lett. (in press)

[66] Xu. Y. et al. 1992, ApJ, 386, 182

[67] Yoshida S. & Kadota K. 2000, IAUC 7401

[68] Woosley S.E., Pinto P.A. & Hartmann D., 1989, ApJ, 346, 395

[69] Woosley S.E., Weaver T.A., 1995, ApJ, 101, 181

Chapter 3

SNe IIP: light curves and Hα luminosities as indicators of ^{56}Ni mass.

This work have been done in collaboration with I. J. Danziger and N. N. Chugai.

"Not only is the universe stranger than we imagine,
it is stranger than we can imagine."

Sir Arthur Eddington (1882 - 1944)

Abstract

The possibility is investigated that the Hα luminosity at the nebular epoch may be an additional indicator of ^{56}Ni mass in type II supernovae with plateau (SNe IIP), on the basis of available photometry and spectra. We first derive the ^{56}Ni mass from the M_V magnitude on the radioactive tail using a standard approach. A confirmation of the correlation between ^{56}Ni mass and plateau M_V magnitude found recently by Hamuy (2003)[22] is evident. There is strong evidence of a correlation between steepness of the V light curve slope at the inflection time and the ^{56}Ni mass. If confirmed, this relation may provide distance and extinction independent estimates of the amount of ^{56}Ni in SNe IIP. We then apply upgraded radioactive models of Hα luminosity at the nebular epoch and claim that it may be a good indicator of ^{56}Ni, if mass, energy and mixing properties vary moderately (within factor $\sim$ 1.4) among SNe IIP . This method of the ^{56}Ni mass determination from Hα luminosities yields results which are consistent with the photometric mass of ^{56}Ni mass to within 20%. This result also implies that the parameters of SNe IIP events (mass, energy and mixing properties) are rather similar among the majority of SNe IIP, except for rare cases of SN II intermediate between IIP and IIL (linear), of which SN 1970G is an example.

3.1 Introduction

Supernovae type II with a plateau in the light curve (SNe IIP) are thought to be a spectroscopically and photometrically homogeneous family of core collapse supernovae (Filippenko 2001 [19]). The light curve of SN IIP is characterized by two distinct phases; a plateau with a duration of $60-100$ days and a quasi-exponential tail at the later epochs. The plateau corresponds to the radiative cooling of the hot opaque envelope originally heated by the explosion (Grassberg et al. 1971 [20]). Variations of observational properties at the plateau phase are interpreted in terms of variation of ejecta mass, explosion energy, and radius of the progenitor (Litvinova & Nadyozhin 1985 [27]). The exponential tail is attributed to the instant reprocessing of the energy of radioactive decay of ^{56}Co (Weaver & Woosley 1980 [37]) and the luminosity at this stage is directly determined by the mass of ejected ^{56}Ni, a fact successfully exploited for SN 1987A (Catchpole et al. 1988 [10]).

The SN IIP phenomena are believed to originate from the explosion of red supergiant stars whose main sequence masses lie in the range $10-25$ $M_\odot$; precise boundary are still a subject of controversy, as well as the mechanism(s) of explosion. The study of optical properties of SNe IIP provides a means of recovering their major characteristics (mass, energy, ^{56}Ni mass, asymmetry) and eventually to impose constraints on the explosion models and pre-supernova parameters. The ^{56}Ni mass is one of the crucial parameters since it presumably depends on the presupernova structure and the explosion model (Aufderheide et al. 1991 [2]) and can be directly measured.

The straightforward way to measure ^{56}Ni mass in SNe IIP is based upon the physical argument that the early (120–300 d) bolometric luminosity on the radioactive tail should be equal to the luminosity of radioactive decay of ^{56}Co. This is because at this stage the loss of the internal energy to expansion (pdV work) is small, while the envelope is nearly opaque to gamma-rays. This method was successfully used for SN 1987A (Catchpole et al. 1988 [10]; Bouchet & Danziger 1993 [7]) with estimates 0.08 $M_\odot$ and 0.07 $M_\odot$, accordingly, and an average 0.075 $M_\odot$. The application of this method to other SNe IIP is, however, hampered by the lack of infrared observations longward of the I band. Note, the $UBVRI$ data account for about half of the luminosity at this age according to results for SN 1987A (Catchpole et al. 1988 [10]; Schmidt et al 1993 [33]). Therefore, for SNe IIP one uses the absolute flux in one band (e.g. V) or several bands in the optical, which, on being compared with the absolute flux of SN 1987A provides an estimate of ^{56}Ni mass. This method essentially assumes that the absolute flux in one or several optical bands is a constant fraction of the bolometric flux, i.e. the spectral energy distribution (SED) during the radioactive tail epoch is similar for all SNe IIP. Using this approach, Phillips et al. (1990)[29] claimed that similar B and V absolute magnitudes of SN 1987A, SN 1969L and SN 1983K on the radioactive tail implies similarity of their ejected ^{56}Ni masses. A similar conclusion was made by Patat et al. (1994)[28] from a study of a large sample of type II SNe. Schmidt et al. (1993)[33] slightly modified this method applying a procedure of reconstruction of the light curve using a bolometric correction determined from SN 1987A data. Using a constant bolometric correction does not necessarily improve the accuracy of the determination of ^{56}Ni mass compared with

the use of absolute magnitudes in one or several filters. Recently Hamuy (2003)[22] using this method recovered ^{56}Ni mass for an extensive sample of SNe IIP and pointed to an interesting correlation of ^{56}Ni mass with the luminosity (M_V) on the plateau.

Here we revisit the problem of ^{56}Ni mass in SNe IIP, pursuing two major goals. First, we independently determine the ^{56}Ni mass for a different sample using a unified approach to distance determination and present a new correlation between ^{56}Ni mass and light curve shape. The second major goal is to check the possibility of the use of Hα luminosity as a tracer of ^{56}Ni mass. This possibility is intriguing bearing in mind that in the case of high redshift SN IIP ($z \geq 0.05$) we face a problem of contribution of the host galaxy background, which will inhibit the confident estimation of the broad band magnitude at the radioactive tail phase. On the other hand, Hα is not affected by the stellar background and thus may be used as an indicator of the ejected amount of ^{56}Ni. Nevertheless incorrect substraction of any underlying H II region emission could hamper accuracy; identification of this narrow component in the blend would remove this problem.The use of Hα as an indicator of ^{56}Ni mass is prompted by early radioactive models which show an expected proportionality between Hα luminosity and the amount of ^{56}Ni (Chugai 1990 [11]). This has also been noted in connection with the comparison of light curve and Hα luminosities for SN 1999em and SN 1987A (Elmhamdi et al. 2003 [15]).

This chapter is organized as follows. We first select a sample of well observed SNe IIP with late photometry and spectra, and adopt appropriate distances and extinction (Sect. 3.2). We then apply the V light curve technique to estimate the ^{56}Ni mass for these supernovae and study correlations between the ^{56}Ni mass and light curve shape (Sect. 3.3). Then we use the late Hα luminosity to derive ^{56}Ni mass (Sect. 3.4). Both photometric and specroscopic ^{56}Ni mass are then compared and the implications are discussed (Sect. 3.5).

3.2 Sample, distance, extinction

Our basic sample consists of 9 SNe IIP, namely: SN 1987A, SN 1969L, SN 1988A, SN 1988H, SN 1990E, SN 1991G, SN 1992H, SN 1997D and SN 1999em, although throughout the work we will be invoking other objects (SN 1970G, SN 1995ad, SN 1995V, SN 1995W, SN 1999gi and SN 1999eu). The events are selected on the basis of published and unpublished photometric and spectroscopic observations at the plateau and later epochs. The sample parameters are presented in Table 3.1 together with the corresponding references to the literature from which the photometry has been taken. In what follows we adopt the standard reddening laws of Cardelli et al. (1989)[9]. For the problem of ^{56}Ni determination the total extinction and distance estimates are of principal importance. Galactic extinction is removed using the map of galactic dust extinction by Schlegel et al (1998)[31]. The host galaxy reddening is then estimated from the $B-V$ and $V-R$ colour excess compared to the intrinsic colour curves of SN 1987A. This approach is justified by the fact that at the late photospheric phase SNe IIP seem to follow colour evolution similar to SN 1987A (Schmidt et al. 1992 [32]). The use of the $B-V$ colour

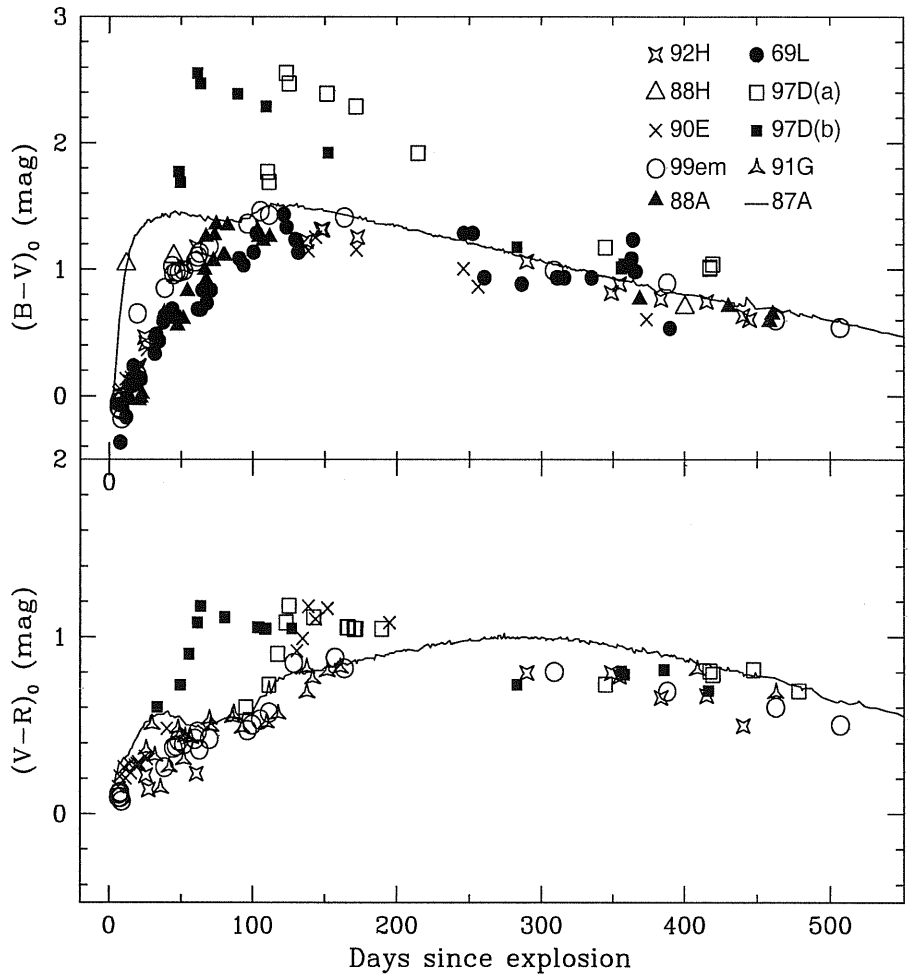

Figure 3.1: The $B-V$ (upper panel) and $V-R$ (lower panel) intrinsic colour evolution of the SNe sample. Both options for SN 1997D are shown (sect. 3.2). The used reddening is reported in Table 3.1 (fourth column).

Table 3.1: Parameters data of the SNe IIP sample

SN name	Parent galaxy	Distance (Mpc)	A_V^{tot}	M_V late slope mag $(100d)^{-1}$	References
1987A	LMC	0.05	0.6	0.976	1, 2
1999em	NGC 1637	8.8	0.31	0.97	3, 4, 5
1969L	NGC 1058	9.057	0.203	0.97	6, 7
1988A	NGC 4579	22.95	0.136	1.12	8, 9
1988H	NGC 5878	28.47	0.47	− − −	9
1990E	NGC 1035	16.18	1.2	0.86	11, 14
1991G	NGC 4088	14.11	0.065	1.11	10
1992H	NGC 5377	29.07	0.054	0.97	15
1997D	NGC 1536	16.84	0.07	0.87	12, 13, 16
1970G	NGC 5457	7.2	0.4	1.04	6, 17
1999gi	NGC 3184	10.91	0.65	− − −	18
1999eu	NGC 1097	− − −	− − −	− − −	19

REF:

1- Arnett 1996[1]; 2- Hirata et al. 1987[23]; 3- Baron et al. 2000[4]; 4- Elmhamdi et al. 2003[15];

5- Hamuy et al. 2001[21]; 6- Kirshner & Kwan 1975[24]; 7- Patat et al. 1994[28]; 8- Ruiz-lapuente et al. 1990[30];

9- Turatto et al. 1993[35]; 10- Blanton et al. 1995[8]; 11- Benetti et al. 1994[5]; 12- Turatto et al. 1998[36];

13- Benetti et al. 2001[6]; 14- Schmidt et al. 1993[33]; 15- Clocchiatti et al. 1996[13]; 16- Zampieri et al. 2002[40]

17- Barbon et al. 1973[3]; 18- Leonard et al. 2002[26]; 19- Pastorello et al. 2003

$*$ H_0=70 km $s^{-1}Mpc^{-1}$ is adopted.

alone to estimate the host galaxy reddening may present some problems, as in most cases it provides negative reddening. This point was noted also by Hamuy (2003)[22] who used the $V-I$ index for an independent estimate of extinction.

The recovered total visual reddening (A_V^{tot}) of our sample is listed in Table 3.1. Fig. 3.1, on the other hand, displays the intrinsic $B-V$ and $V-R$ colour evolution. Note that for the case of SN 1997D, both colours show a large excess by the end of the photospheric phase. The small (case b; Turatto et al. 1998 [36]) and large (case a; Zampieri et al. 2002 [40]) age scenarios are displayed. This high reddening seems unlikely since the presence of interstellar lines was not reported in the early spectra as one may expect in a case with such high reddening (Turatto et al. 1998 [36]). The very red colour at the end of the photospheric phase is seen in other objects with a very low ejected ^{56}Ni mass (e.g. SN 1999eu; Pastorello et al. 2003, in preparation). An explanation of this peculiarity may be related to the fast cooling from the plateau phase to reach the faint radioactive tail, and/or possibly relates to the nature and structure of the progenitor star. Interestingly, the late nebular intrinsic $B-V$ colours of the complete sample seem to be very similar to that of SN 1987A, both in slope and magnitude. The convergence to the same fate at later phases is also confirmed for the faint object SN 1997D and as well as for the underluminous SN 1999eu (Pastorello et al. 2003). Although studying the spectral energy distribution (SED) of SNe IIP is beyond the scope of the present work, the fact of a small scatter ($\sim \pm 0.3$ mag) in the sample around the SN 1987A intrinsic $(B-V)_0$ colour indicates the similarity in the SED for SNe IIP on the radioactive tail. The distance of D = 50 kpc is used for SN 1987A, while for the other SNe we adopt distances derived from the recession velocity of the host galaxy corrected for Local Group infall onto the Virgo Cluster as reported in the "LEDA[1]" extragalactic database. The Hubble constant H_0=70 km s^{-1}Mpc^{-1} is adopted. The computed distances are reported in third column of Table 3.1. We note here that a possibly more accurate value of the distance to SN 1999em, 7.8 Mpc, comes from stellar studies of the parent galaxy NGC 1637 (Sohn & Davidge 1998 [34]).

3.3 ^{56}Ni mass from V light curve

The luminosity of SN IIP on the radioactive tail is controlled by the radioactive decay (^{56}Co$\rightarrow^{56}$Fe) and if the trapping of gamma rays is efficient, the decline rates of the light curves of SNe II should converge to the exponential life-time of ^{56}Co (i.e. 111.26 days or 0.976 mag per 100 d). The radioactive tails in SN IIP all show similar decay rates, especially in the V band (Patat et al. 1994 [28]). This fact provides a solid basis for using the V light curve for the recovery of the ejected ^{56}Ni mass (Phillips et al. 1990 [29]; Schmidt et al. 1993 [33]). In Fig. 3.2 we display the absolute V light curves of the SNe sample together with that of SN 1987A. The computed late time decline slopes (150 – 400 days since explosion) are reported as well in Table 3.1 (fifth column). Their mean value is $< \gamma^V > \simeq 0.99$ (± 0.13), consistent with the radioactive decay of ^{56}Co

[1]available online at http://leda.univ-lyon1.fr/cgi-bin/single.pl

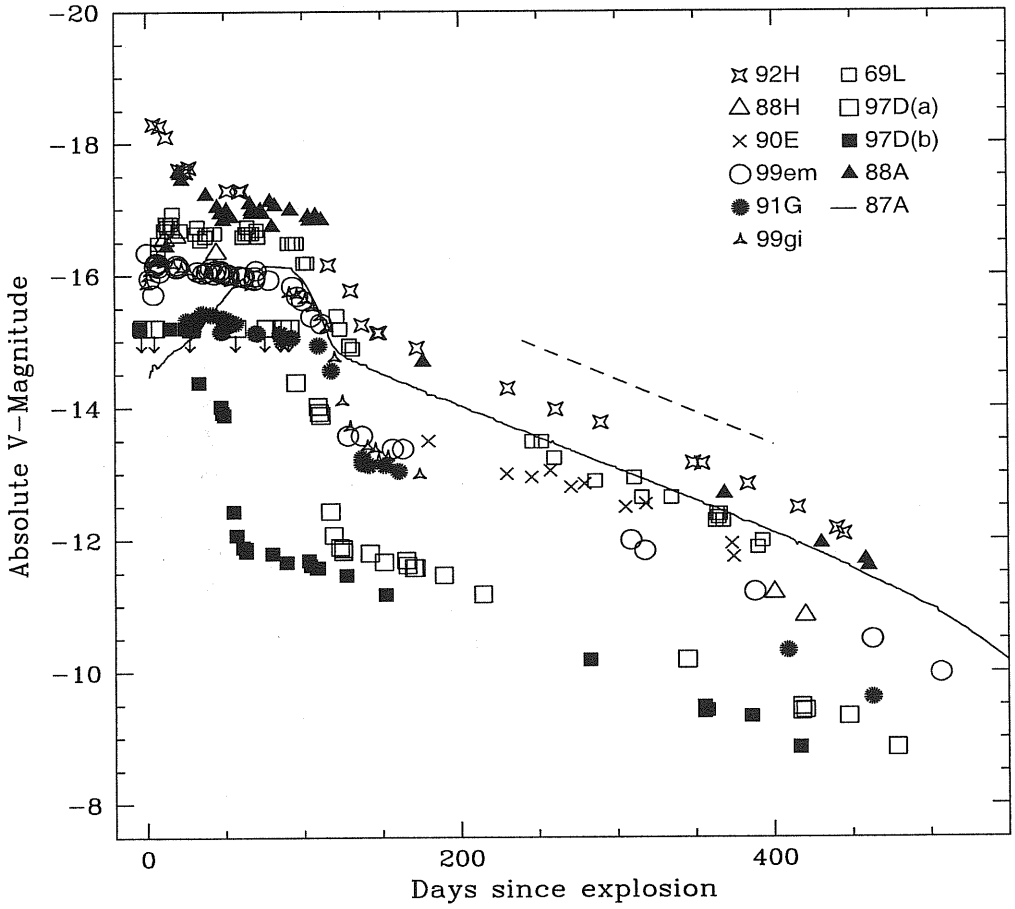

Figure 3.2: The absolute V-magnitude evolution of the SNe sample. The used parameters are reported in Table 3.1. Both possibilities for SN 1997D are plotted. The dashed line shows the slope for ^{56}Co decay.

Table 3.2: ^{56}Ni mass estimates from photometry

SN name	$M_{\rm Ni}(V)$ ($M_\odot$)	t_i (days)
1987A	0.075	107 ($\pm$2)
1969L	0.067 ($\pm$0.002)	110 ($\pm$4)
1988A	0.088 ($\pm$0.003)	134 ($\pm$4)
1988H	0.033 ($\pm$0.004)	$- - -$
1990E	0.043 ($\pm$0.0024)	$- - -$
1991G	0.021 ($\pm$0.0032)	122 ($\pm$5)
1992H	0.123 ($\pm$0.002)	112 ($\pm$5)
1997D(a)	0.0065 ($\pm$0.0003)	112 ($\pm$5)
1997D(b)	0.0036 ($\pm$0.0002)	112 ($\pm$5)
1999em	0.027 ($\pm$0.002)	112 ($\pm$4)
1970G	0.051 ($\pm$0.003)	94 ($\pm$4)
1999gi	0.0246 ($\pm$0.0007)	120 ($\pm$3)
1999eu	0.0028*	110 ($\pm$4)

* From Pastorello et al. 2003 (In preparation)

and consequent trapping of the gamma-rays.

The ^{56}Ni mass is estimated from absolute M_V magnitudes between $120-400$ d using the SN 1987A tail as a template. Results produced by the least squares fit are reported in Table 3.2. Both possible cases for SN 1997D are reported (more details concerning this event are discussed in sect. 3.2). These values show a significant range of the ejected ^{56}Ni masses, from 0.0028 $M_\odot$ and 0.0036 $M_\odot$ for subluminous SN 1999eu and SN 1997D(case b) respectively to 0.123 $M_\odot$ for SN 1992H with the average value $\approx$ 0.05 $M_\odot$. Our values differ somewhat from those determined recently by Hamuy (2003)[22] for objects in common. The differences stem primarily from the different distances adopted here. As noted earlier the methodology followed by Hamuy is based upon the conversion of V magnitude into a bolometric luminosity through an assumed constant bolometric correction, while we are adopting SN 1987A luminosities as a template at late epochs.

With our values of the ^{56}Ni masses it is instructive to check that the correlation between plateau M_V magnitude and the amount of ^{56}Ni found by Hamuy (2003)[22] is preserved. We have modified the definition of the plateau M_V magnitude compared to Hamuy (2003)[22] in order to avoid any uncertainty in the explosion time. Therefore, we use the inflection time during transition from plateau to the radioactive tail as a zero point. The inflection time t_i is defined as the moment when the first derivative at the transition phase $S = -dM_V/dt$ (we dub it "steepness") is maximal. To calculate S we use the following procedure. The V band flux in the transition period from plateau and radioactive tail is approximated by a sum of plateau and radioactive terms:

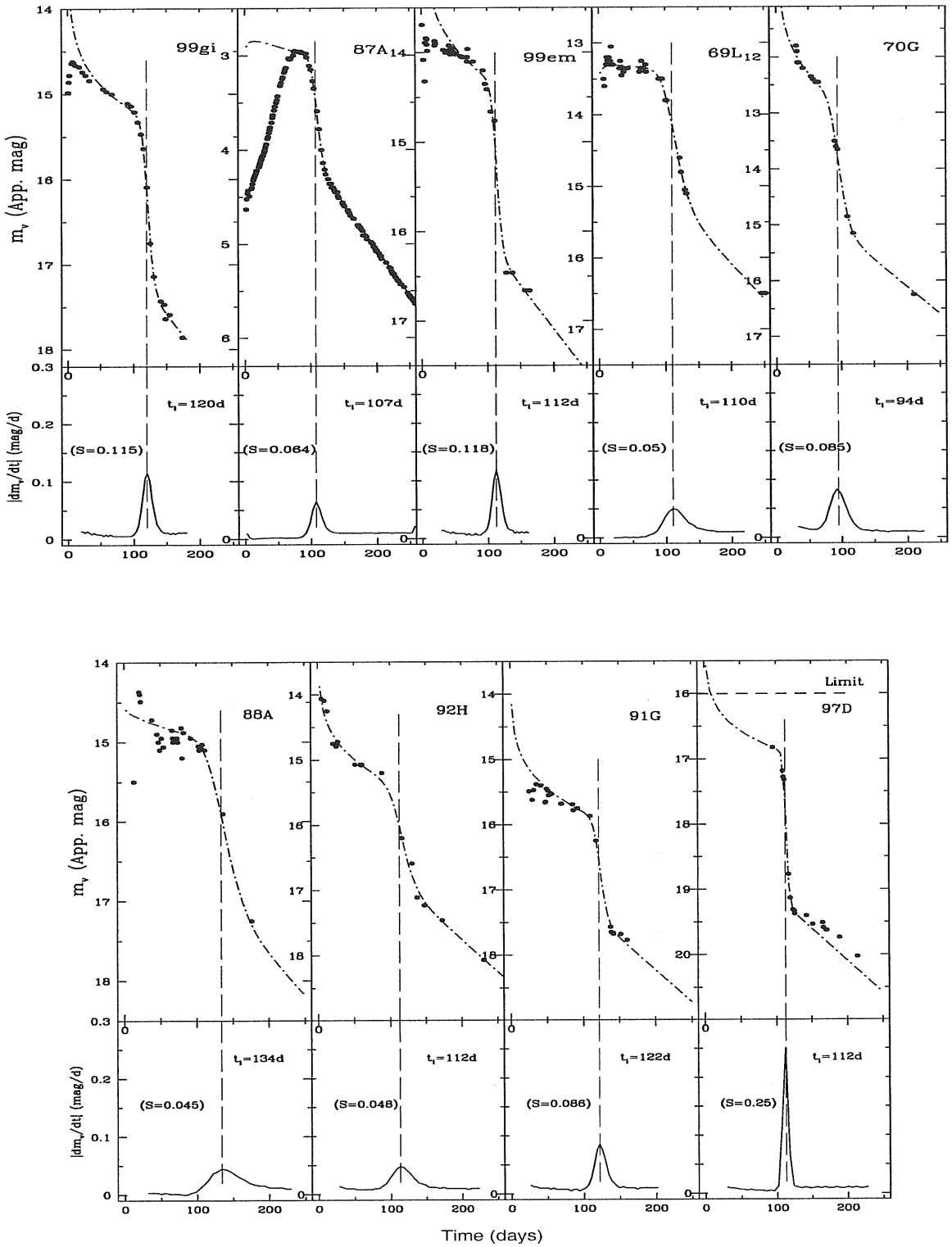

Figure 3.3: Determination of the steepness and moment of inflection. For each SN of the sample: upper panel displays the V light curve (dotted points) together with the best fit (dashed curve) while lower panel shows the steepness S (see text). The inflection point t_i shown by dashed line corresponds to the maximum of S. SN 1999eu is not shown because the data is not yet published.

$$F = A\frac{(t/t_0)^p}{1+(t/t_0)^q} + B\exp(-t/111.26), \tag{3.1}$$

where A, B, t_0, p and q are parameters derived by the χ^2 minimization technique in the sensitive interval $t_i \pm 50$ days. The behaviour of S and determination of t_i is demonstrated for each SN in Fig. 3.3. The derived t_i are reported in Table 3.2 (third column) with the corresponding errors while the computed S values and their errors are presented in Fig. 3.5. The errors in S and t_i are estimated according to the best fit (shown in Fig. 3.3) and as well by introducing test points for events with poor data especially at the transition phase (from plateau to radioactive decay). With the determined inflection time t_i we choose the epoch $t_i - 35$ days as a reference for the M_V on the plateau.

Fig. 3.4 (upper panel) demonstrates the correlation between photometric ^{56}Ni mass and the absolute magnitude $M_V(t_i - 35)$ for the sample of SNe IIP with measurable S and t_i values. This plot shows small scatter around a linear trend and thus supports the correlation found by Hamuy (2003)[22]. In our case, and assuming case "a" (Zampieri et al. 2002 [40]) for SN 1997D, the linear correlation is described by the equation:

$$\log M(^{56}\mathrm{Ni}) = -0.438 M_V(t_i - 35) - 8.46. \tag{3.2}$$

Therefore this result suggests a direct correlation between V magnitudes (absolute or apparent) of plateau and radioactive tail. In fact Fig. 3.4 (lower panel) demonstrates the correlation between M_V magnitudes at plateau (on $t_i - 35$ day) and tail (on $t_i + 35$ day).This is therefore a direct form of the correlation shown in the upper panel.

The sample we explore reveals another interesting correlation. Fig. 3.5 demonstrates that the steepness S anticorrelates with ^{56}Ni mass: the lower is the ^{56}Ni mass the larger is S, i.e. the steeper is the transition from plateau to the tail. We note however, that an accurate determination of S necessitates a V light curve with a reasonably high density of observational points at the end of the plateau phase and the beginning of the radioactive tail. Indeed SNe 1990E and 1988H are not studied here because of the paucity of their light curve data. The best linear fit (Fig. 3.5) reads:

$$\log M(^{56}\mathrm{Ni}) = -6.2295\, S - 0.8147 \tag{3.3}$$

The interpretation of this correlation requires hydrodynamical modeling with different amounts of ^{56}Ni and degrees of mixing. In the case of unmixed ^{56}Ni one does not expect a notable dependence of the steepness on the amount of ^{56}Ni. This is readily seen from the modeling SNe IIP light curves by Eastman et al. (1994)[14]. For the same amount of ^{56}Ni the mixing results in a decreased steepness because of an increase of radiative diffusion (Eastman et al. (1994)[14]). Unfortunately, in the cited paper the authors did not model cases of variable ^{56}Ni mass with similar degrees of mixing, so the question of the physics behind the above correlation, remains open. At this stage, we may only suggest that somehow the increase of the ^{56}Ni mass in SNe IIP ejecta favours the larger contribution of radiative diffusion at the end of the plateau and, therefore, a less steep transition from plateau to the radioactive tail. It may well be that the increase of the

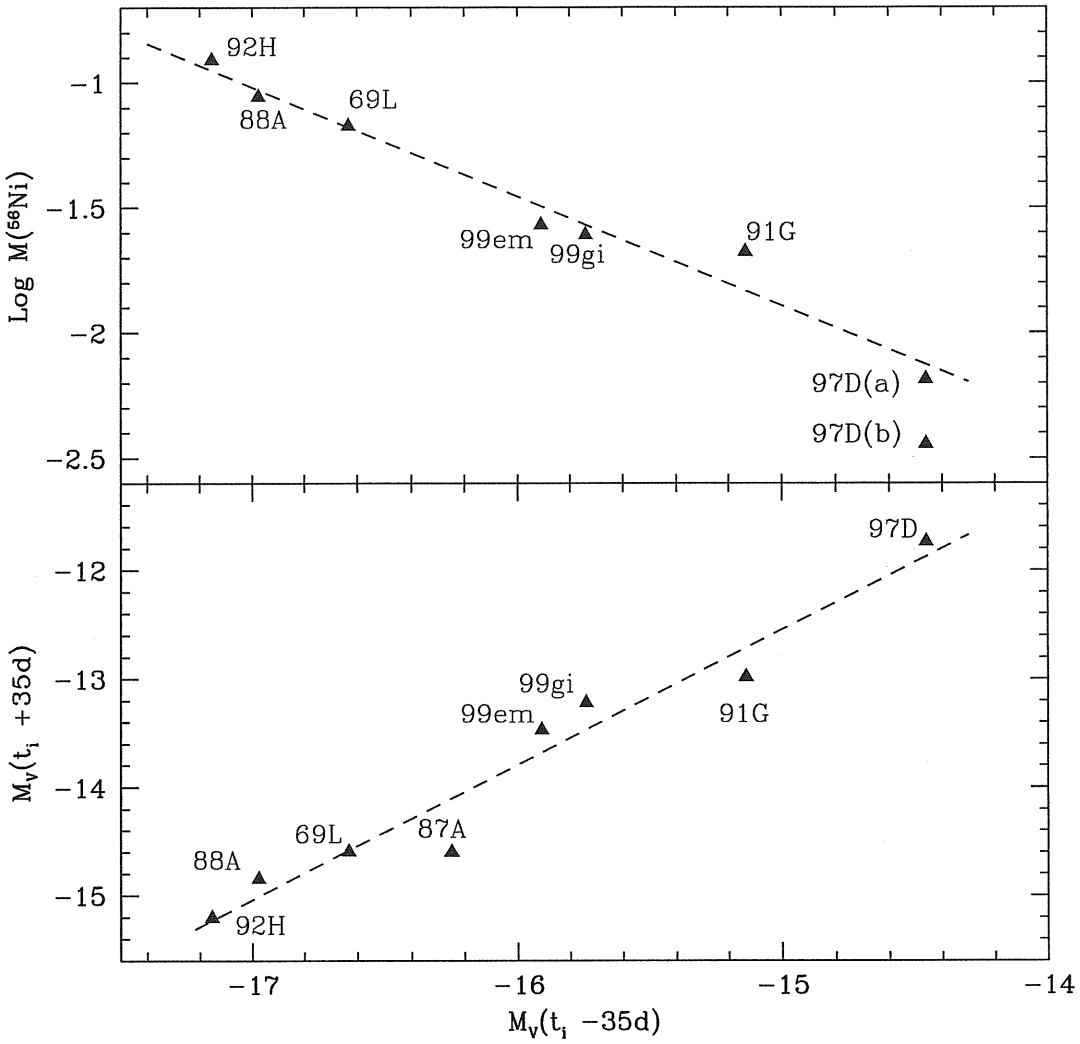

Figure 3.4: The correlation between M_V magnitudes of plateau and of radioactive tail. Upper panel shows the correlation between M_V at the moment $(t_i - 35d)$ and ^{56}Ni mass derived from the tail magnitudes; case "a" of SN 1997D is adopted for the fit. Lower panel shows directly the correlation of plateau magnitude $M_V(t_i - 35d)$ and tail magnitude $M_V(t_i + 35d)$.

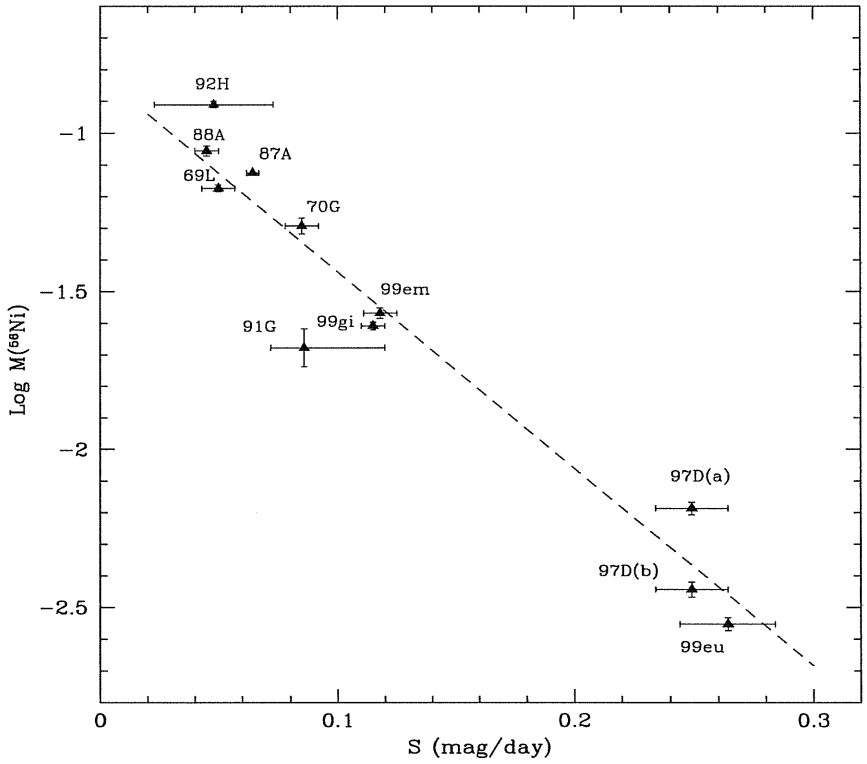

Figure 3.5: The correlation between ^{56}Ni mass and steepness S. Case "a" of SN 1997D is adopted for the linear fit (dashed line).

^{56}Ni mass is accompanied by the growth of the degree of mixing degree which favours a less steep decline as demonstrated in Fig. 10 and Fig. 12 of Eastman et al. (1994)[14].

Interestingly, if the correlation between steepness and ^{56}Ni mass is confirmed, this will provide us with an exciting possibility of probing ^{56}Ni mass in SNe IIP from the light curve shape in a manner independent of the distance and extinction.

3.4 ^{56}Ni mass from Hα luminosity

The Hα luminosity of SNe IIP at late epochs reflects the total ionization in the weakly ionized gas caused by radioactive decay of ^{56}Co and, therefore, to a first approximation is proportional to the overall deposition rate and hence to the ^{56}Ni mass (Chugai 1990 [11]; Xu et al. 1992 [39]; Kozma & Fransson 1992 [25]) unless effects due to higher densities become important. This suggests that the Hα luminosity resulting from gamma-ray trapping may provide a quantitative measure of the ^{56}Ni mass in SNe IIP. The accurate measurements on SN 1987A provide a control. To explore deviations from the simple proportionality we use an upgraded radioactive model of the Hα luminosity.

3.4.1 Model of Hα luminosity

Some brief comments about the modified model of Hα luminosity powered by the radioactive decay are in order. The primary purpose of the modification of the previous version (Chugai 1990 [11]) is to specify better the early nebular phase. This was done by the implementation of macroscopic mixing, collisional and radiative de-excitation effects. The supernova envelope is mimicked by two zones. The inner zone with the radius $r_{\rm mix} = v_{\rm mix}t$ is a mixing core with a total mass fraction $f_{\rm mix}$, which is divided between metals together with He-rich matter (we dub this mixture "metals" with the mass fraction of $f_{\rm m}$) and H-rich matter with the mass fraction $1 - f_{\rm mix}$. The outer zone consists of hydrogen-rich matter. All the ^{56}Ni resides in the mixing core and has a generally clumpy distribution. This is mimicked by ^{56}Ni clumps in cocoons of metals with the total area of cocoons being $4\pi r_{\rm mix}^2 f_{\rm s}$. Here $f_{\rm s}$ is a mixing parameter, which is unity if all metals reside in the spherical layer with the inner spherical cavity occupied by ^{56}Ni. We adopt $f_{\rm s} = 2$ which corresponds to moderate mixing. The escape probability for gamma-rays through the metal layer is $\exp(-\tau_{\rm m})$, where $\tau_{\rm m}$ is the optical depth of the metal layer, while the absorption probability in the mixing zone is described by the expression $\tau_1/(1+\tau_1)$, where τ_1 is the optical depth of the inner zone. In the mixing core gamma-rays have a finite probability of being absorbed by H-rich material, which is proportional to $1 - f_{\rm mix}$. The absorption probability for the outer hydrogen layer with the optical depth τ_2 is defined as $p_2 = 1 - \exp(-\tau_2)$.

The energy deposited in the hydrogen is shared between ionization, excitation and thermal energy with corresponding branching ratios (Kozma & Fransson 1992 [25]; Xu et al. 1992 [39]). The ionization of hydrogen is calculated in the approximation of three levels plus continuum. The photoionization from the second level by two-photon and continuum radiation was calculated assuming the continuum luminosity is equal to the deposited luminosity while the spectrum is assumed to be dilute black-body with the temperature $T_{\rm c}$. The electron temperature was set to be 5000 K. Effects of radiation transfer in Balmer and Paschen continua are treated in the escape probability approximation (Chugai 1990 [11]).

Table 3.3: Parameters of the Hα evolutionary models

Parameter	Unit	Standard	a	a1	b	b1	b2	c	d	e	f	f1
M	$M_\odot$	14	10	7	14	14	14	14	14	14	14	14
E	10^{51}	1	1	1	1	1	1	1.5	1	1	1	1
$M_{\rm Ni}$	$M_\odot$	0.075	0.075	0.075	0.0375	0.00375	0.15	0.075	0.075	0.075	0.075	0.075
$f_{\rm mix}$		0.4	0.4	0.4	0.4	0.4	0.4	0.4	0.4	0.1	0.4	0.4
$f_{\rm met}$		0.2	0.2	0.2	0.2	0.2	0.2	0.2	0.2	0.2	0.3	0.6
$T_{\rm c}$	K	7000	7000	7000	7000	7000	7000	7000	5000	7000	7000	7000

The sensitivity of the radioactive model to parameter variations (Table 3.3) is demonstrated in Fig. 3.6. Each panel shows the effect of a single parameter variation compared to a standard model, which is in fact the optimal model for the Hα luminosity of SN 1987A. The saturation at the early epoch is a new feature compared to the previous model and this is related to several factors: gamma-ray trapping in the inner zone, collisional de-excitation of the third level and Hα absorption in the Paschen continuum, especially in the mixing zone. In Fig. 3.6a we present models with lower mass (10 and 7 $M_\odot$) compared to the standard 14 $M_\odot$. A lower mass results in a high rate of the luminosity decay owing to a lower optical depth for gamma-rays. For moderate mass variation (factor ≤ 1.4) the Hα luminosity in the range $200-300$ d shows less than 10% deviation from the standard case. With the rest of parameters fixed the Hα luminosity is proportional to the ^{56}Ni mass (Fig. 3.6b) at the nebular epoch $t > 200$ days. This property reflects the simple truth that to a good approximation the total ionization rate of hydrogen in the envelope is proportional to the total radiactive decay rate, i.e. ^{56}Ni mass. The proportionality, however, breaks down for $t < 200$ days because of saturation effects related to Hα collisional de-excitation and continuum absorption, which become important at early epoch. The effect of factor 1.5 higher kinetic energy is similar to the effect of factor ~ 1.2 lower mass (Fig. 3.6c), in accordance with the dependence of optical depth on both parameters $\tau_\gamma \propto M^2/E$. A lower continuum temperature (Fig. 3.6d) results in a lower luminosity, especially, at the early epoch ($t < 200$ d) since the ionization (and therefore recombination) rate becomes lower. A lower mixing core fraction (Fig. 3.6e) results in the higher Hα luminosity since the total deposition in the outer H-rich matter increases. The higher metal fraction in the mixing core (Fig. 3.6f), on the contrary, suppresses the late time Hα luminosity consistent with the decreased deposition into mixed hydrogen material. However, this effect is small if the variation of this parameter is within a factor 1.5.

The modeling shows that if ejecta parameters vary less than a factor 1.4 compared to those of SN 1987A, the Hα luminosity is then proportional to the ^{56}Ni mass (to within 10% accuracy) at the late time nebular phase $200-400$ days. In this age range using the SN 1987A model as a template we may estimate the ^{56}Ni mass in other SNe IIP from the ratio of Hα luminosity to that of SN 1987A. It is worth noting here that despite the large possible variation of the main sequence mass for SNe IIP, presumably say $10-25$ $M_\odot$, the range in mass of the ejecta may actually be smaller since mass loss increases rapidly with the mass.

3.4.2 Results of ^{56}Ni mass determination

The spectra utilized in this section are based on data in the Asiago/ESO SN Catalogue. Additional spectra were kindly provided by R. Stathakis. A sample of the spectra is shown in Fig. 3.7 together with some line identifications. The available spectra of our sample were corrected for reddening effects and the recovered integrated Hα line fluxes are then translated to luminosities using adopted distances. In a straightforward approach we use the Hα luminosity of SN 1987A as a template to recover the ^{56}Ni mass from the Hα luminosity of SNe IIP assuming proportionality between the ^{56}Ni mass and

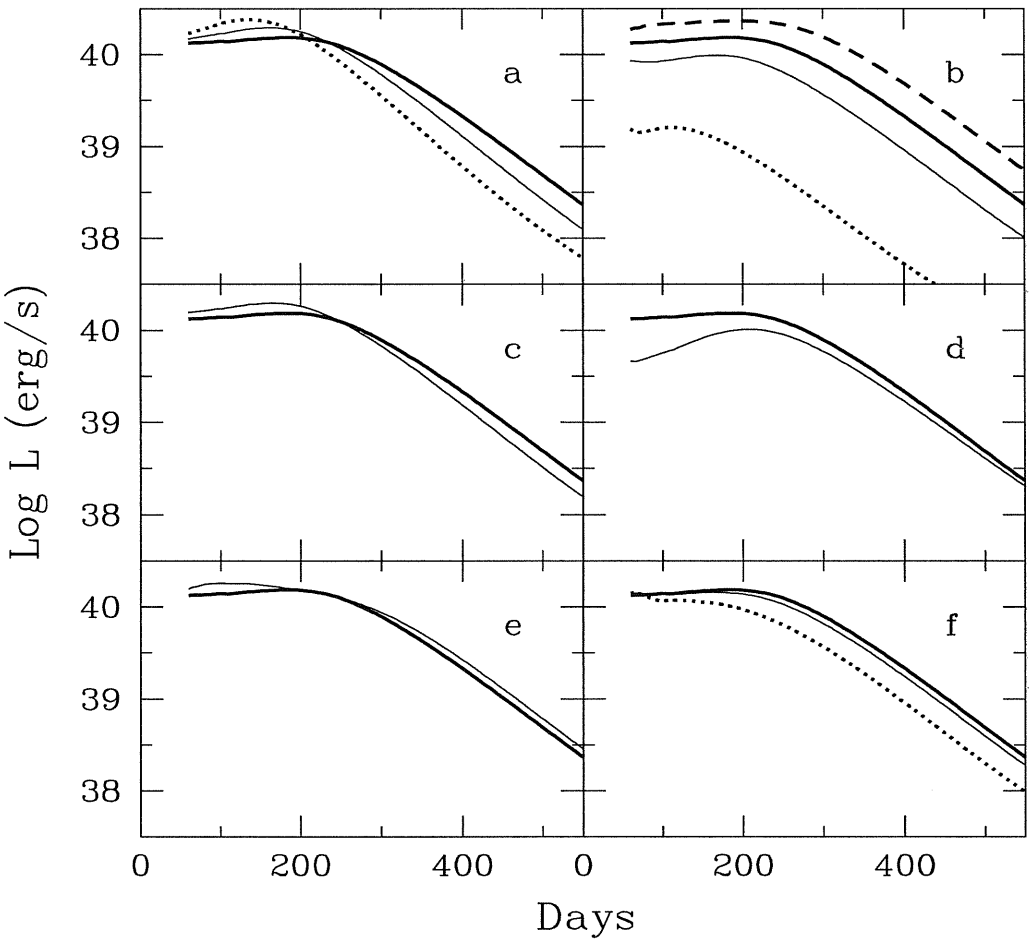

Figure 3.6: The Hα luminosity in the radioactive model. The *thick line* shows the standard model, while *thin line* curves show models *a, b, c, d, e, f.* Dotted lines in panels a, b and f correspond to models *a1, b1* and *f1* respectively. Additional model is shown in panel b (model *b2, dashed line*). Details of model parameters are presented in Table 3.3.

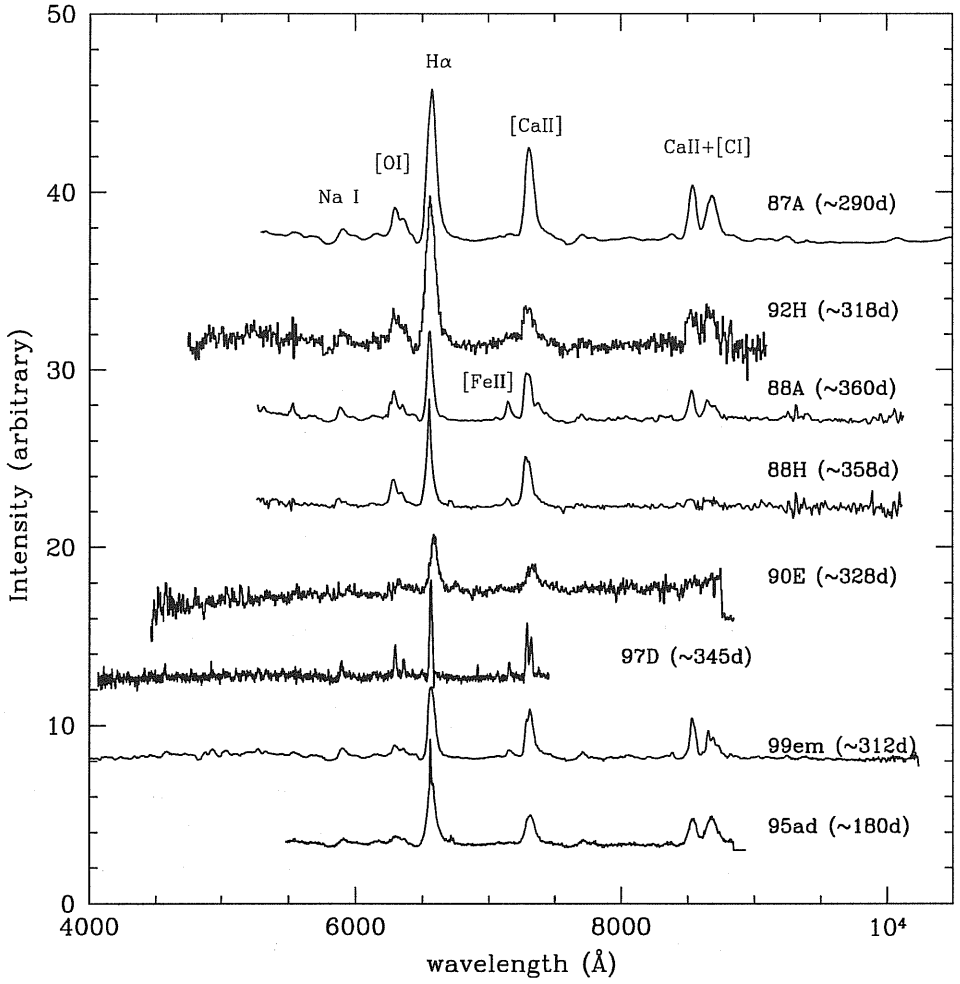

Figure 3.7: Sample of late time spectra of SNe IIP with the corresponding time since explosion. The spectra have been corrected for the recession velocities of their host galaxies. Some line identifications are also indicated.

the Hα luminosity in the range between 200 – 400 days. The resulting values of ^{56}Ni mass are given in Table 3.4 in the second column.

Another approach has been to fit the Hα light curves with the model of luminosity evolution. All the other parameters, except for ^{56}Ni mass, are assumed to be the same as in the standard model for SN 1987A unless additional information indicates essentially different parameters. The plateau of SN 1970G is very brief ($t_p \approx 60$ d) which indicates a lower ejecta mass than that of a typical SN IIP. We adopt 8 $M_\odot$ as the most appropriate value for SN 1970G ejecta taking into account both the light curve and the rate of the Hα flux decay. The results are plotted for 9 SNe in Fig. 3.8. Recovered values of ^{56}Ni mass are given in Table 3.4 (third column). Note that the straightforward approach based upon the use of the Hα light curve of SN 1987A (second column of Table 3.4) and

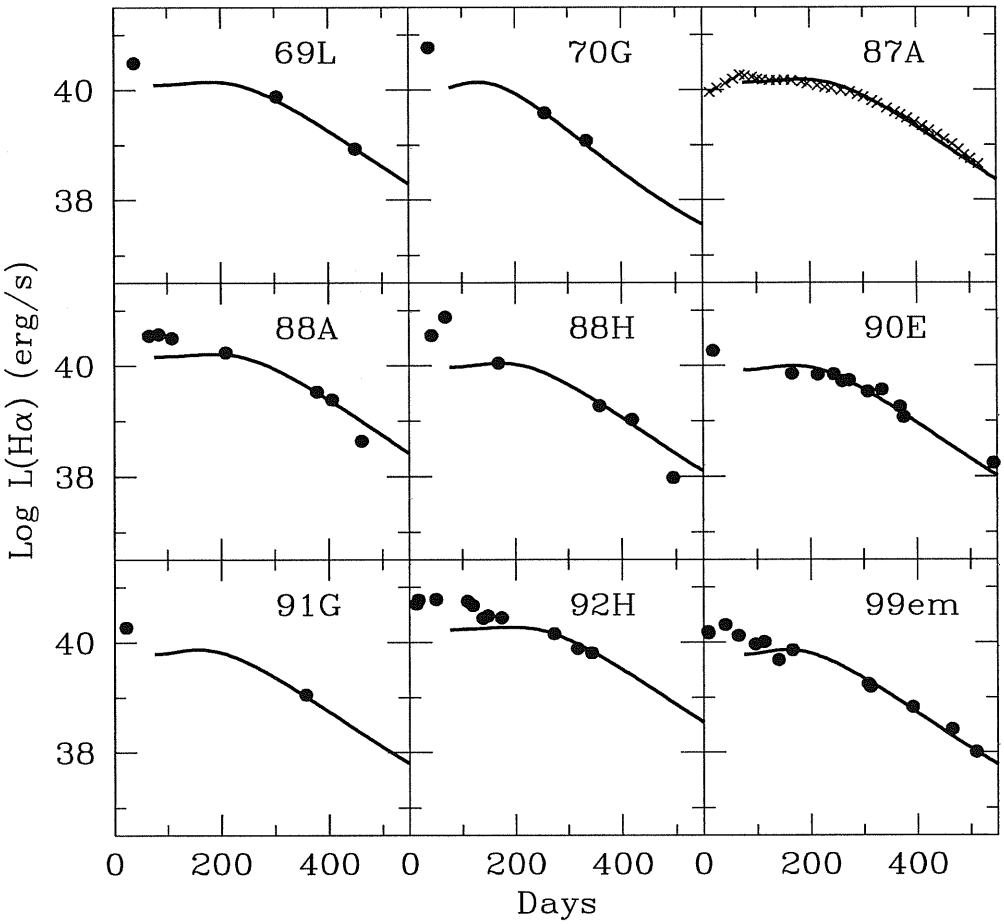

Figure 3.8: The Hα luminosity evolution in different SN IIP. Models (*solid lines*) are overplotted on the observational data *dots* (sect. 3.2).

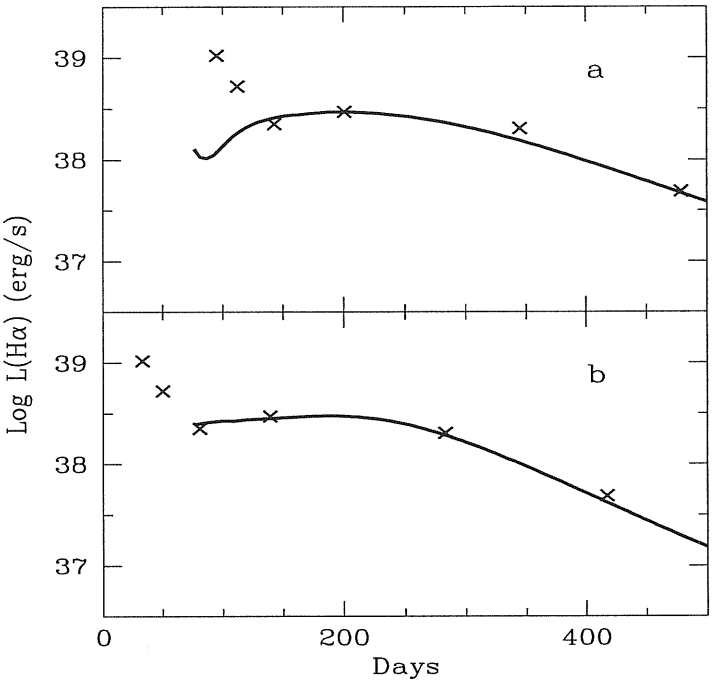

Figure 3.9: Modeling Hα luminosity for SN 1997D. The upper panel shows the large age option, while lower panel shows the small age option. Model results (*solid lines*) are overplotted on observational dots.

the application of model fitting produce quite similar values with a maximal difference, apart from SN 1970G(SNP/L) and SN 1997D(treated bellow), of ~13% for SN 1988H.

This deviation may be adopted as an uncertainty of the ^{56}Ni mass determination from the accurate data. Given the uncertainty of the observed value of the Hα luminosity (at least 10%) we are therefore able to derive a ^{56}Ni mass from Hα with an uncertainty of about 25%. The subluminous SN 1997D is a special case. Originally, the age of the supernova at discovery has been estimated to be $t_d = 50$ days (Turatto et al. 1998 [36]), while Zampieri et al. (2002)[40] argue for an age almost twice as large $t_d \approx 95$ days. We consider both large and small age options. In the large age case we adopt $M = 18$ M$_\odot$, $E = 9 \times 10^{50}$ erg (Zampieri et al. 2002 [40]), while in the small age option we adopt $M = 6$ M$_\odot$ and $E = 1 \times 10^{50}$ erg (Chugai & Utrobin 2000 [12]). A reasonable fit in the first case (Fig. 3.9a) is found for the ^{56}Ni mass of 0.011 M$_\odot$ with a mixed core fraction $f_{mix} = 0.05$, which corresponds to the mixing core having 0.9 M$_\odot$ and a core metal fraction $f_m = 0.99$, i.e. with the metal core practically devoid of hydrogen. The model also requires a low continuum temperature in the ultraviolet $T_c = 4500$ K. For the small age choice the fit (Fig. 3.9b) corresponds to $M(^{56}\text{Ni}) = 0.0024$ M$_\odot$. In this case $f_{mix} = 0.05$, $f_m = 0.3$ (a significant amount of mixed hydrogen) and $T_c = 5500$ K.

The ^{56}Ni mass derived from the Hα luminosity adopting SN 1987A as template, $M_{\rm Ni}$(Hα), is plotted in Fig. 3.10 versus photometric ^{56}Ni mass, $M_{\rm Ni}(V)$, derived from the tail M_V magnitude (Table 3.2). Both sets of values agree within 20% . This consistency supports the proposition that the Hα luminosity may be a good indicator of ^{56}Ni mass in SNe IIP unless we are dealing with extreme cases such as SN 1970G (SNP/L) or underluminous cases such as SN 1997D.

3.4.3 Application of Hα to ^{56}Ni diagnostics

In the absence of the late time photometry but with available spectra of SNe IIP at the nebular epoch we may use the Hα luminosity to estimate ^{56}Ni mass ejected by supernova provided the explosion time is known. We demonstrate this approach to SN 1995ad, SN 1995V and SN 1995W (all type IIP) for which late photometric data are not available. Distances are computed using the corrected recession velocities (reported in "LEDA" data base assuming H_0 =70 km s^{-1}Mpc^{-1}).

SN 1995ad: This SN was discovered on Sep. 28.8 UT in NGC 2139 by R. Evans (IAUC 6239 [17]). Its Sep. 29.3 UT spectrum, obtained by S. Benetti, displays a hot continuum with temperature $T_{bb} \sim$ 13000 K and a broad Hα emission ($FWHM$ =11000 km s^{-1}). These characteristics combined with the fact that nothing was seen at the position of the SN in the Aug. 25 image (IAUC 6239 [17]) provide constraints on the explosion time. The assumed distance and reddening are respectively D = 23.52 Mpc and A_V = 0.112 mag (NED; Schlegel et al. 1998 [31]) while the galaxy inclination is 40.9°. The spectrum we use here is taken 1996 March. 24, about 180 days since explosion. The derived Hα luminosity, $\sim 1.06 \times 10^{40}$ erg s^{-1}, is then compared to that of SN 1987A at a similar epoch to recover an ejected mass $\approx 0.056 \odot M_\odot$.

SN 1995V: discovered in NGC 1087 by R. Evans (IAUC 6197 [16]). The galaxy inclination is 33.2°. The adopted distance and reddening are, accordingly, D = 20.61 Mpc and A_V = 1.37 mag, while the explosion time is assumed to be 1995 July. 25 (Fassia et al. 1998 [18]). The available late spectrum was taken around day 409 since explosion. Comparing the recovered Hα luminosity, $\sim 1.33 \times 10^{39}$ erg s^{-1}, with that of SN 1987A leads to the estimate of $M(^{56}\mathrm{Ni}) \approx 0.046$ M$_\odot$.

SN 1995W: discovered on Aug. 5.65 UT in NGC 7650 by A. Williams and R. Martin (IAUC 6206 [38]). The spectrum taken on Aug 17.29 UT displayed features of SN IIP around one month (IAUC 6206 [38]). The distance is D = 44.81 Mpc, and the reddening is A_V = 0.044 mag (NED; Schlegel et al. 1998 [31]) and the host galaxy inclination is 47.4°. The late spectrum was taken around day 300 (1996 May. 12). The Hα luminosity, $\sim 4.79 \times 10^{39}$ erg s^{-1}, when compared to that of SN 1987A at similar epoch yields an amount of ^{56}Ni mass of $M(^{56}\mathrm{Ni}) \approx 0.048$ M$_\odot$.

Note that the adopted reddening values for SN 1995ad and SN 1995W do not include the host galaxy reddening. For these events the inclination of their host galaxies may provide further indication of uncertainty in the extinction since large extinctions might be expected for highly inclined galaxies if the SN occurred towards the far side. Although

Table 3.4: Recovered mass of ^{56}Ni using SN 1987A as template (second column), and from late time L(Hα) modeling "$M^m_{\rm Ni}(H\alpha)$".

SN name	$M_{\rm Ni}$(Hα) ($M_\odot$)	$M^m_{\rm Ni}$(Hα) ($M_\odot$)
1969L	0.068(±0.004)	0.065
1970G	0.029(±0.011)	0.035
1988A	0.085(±0.004)	0.083
1988H	0.039(±0.005)	0.045
1990E	0.04(±0.003)	0.038
1991G	0.022(±0.0005)	0.025
1992H	0.106(±0.008)	0.105
1997D(a)	0.0028(±0.0006)	0.011
1997D(b)	0.0018(±0.0004)	0.0024
1999em	0.022(±0.003)	0.024

no sign of high extinction from interstellar lines was reported in early spectra of these two objects, the derived amounts of $M(^{56}\mathrm{Ni})$ might be taken as lower limits bearing in mind the significant inclination of their host galaxies.

3.5 Discussion and conclusion

The primary goal of this work was to demonstrate that the Hα luminosity at the nebular epoch may be an indicator of the ^{56}Ni mass in SNe IIP ejecta. To explore this idea we selected a sample of well observed SNe IIP, and using V magnitudes on the radioactive tail we derived in a standard way the photometric mass of ^{56}Ni mass. With our sample we confirmed using a slightly different approach the correlation between ^{56}Ni mass and absolute magnitude M_V of the plateau reported recently by Hamuy (2003)[22]. We then applied a two-zone model of the Hα luminosity in SN IIP to explore the sensitivity of the Hα behaviour to variation of model parameters. We found that if mass, energy and mixing conditions do not vary strongly among SNe IIP (less than factor 1.4) then with an accuracy better than 10% Hα luminosity is proportional to ^{56}Ni mass during the 200 – 400 days after explosion. Hα luminosities were then used to derive ^{56}Ni masses. This was done employing two approaches: first, using the Hα light curve in SN 1987A as template and, second, applying the model computations. Both approaches agree within 15% unless we are dealing with extreme cases such as SN 1970G (type IIP/L) and underluminous SN 1997D. In both these cases we should possess additional information about ejecta mass and energy to derive the ^{56}Ni mass from Hα. The ^{56}Ni mass values derived from the photometry and Hα luminosity agree within 20%, which thus gives us confidence that Hα is a good indicator of the amount of ^{56}Ni in SNe IIP. Simultaneously, this consistency suggests that parameters of SNe IIP (mass, energy and mixing) are not very different. In fact this is consistent with the uniformity of plateau luminosities and

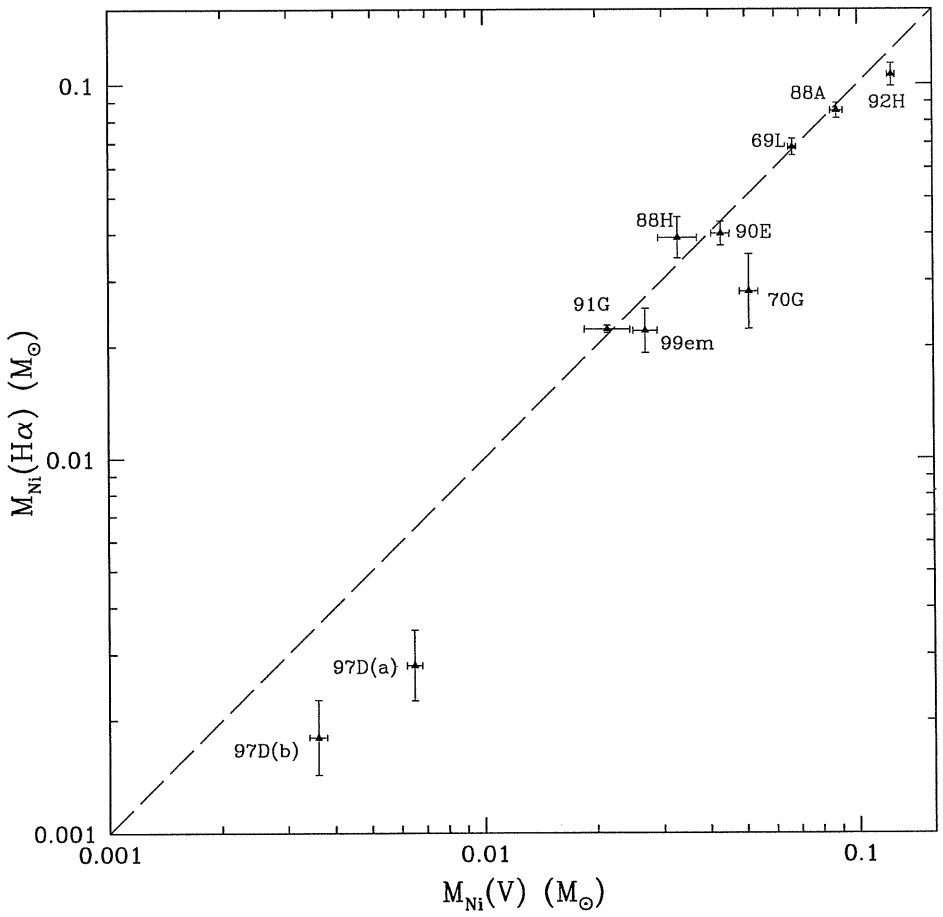

Figure 3.10: The correlation between the ^{56}Ni mass derived from the Hα luminosity, $M_{\rm Ni}$(Hα), and that derived from the tail M_V magnitude, $M_{\rm Ni}(V)$. The dashed line has a slope of unity. Clear deviation is seen for SN 1970G(SNP/L) and for both scenarios of the faint event SN 1997D.

plateau lengths of SNe IIP.

We applied the method of ^{56}Ni mass estimation from Hα for three SNe IIP (SN 1995ad, SN 1995V and SN 1995W) without photometry at the nebular phase and derived ^{56}Ni masses of $\approx$ 0.056 $M_\odot$, 0.046 $M_\odot$, 0.048 $M_\odot$, quite reasonable values, although they could be underestimates, since the host galaxy extinction (for SN 1995ad & 1995W) has not been taken into account. Nevertheless, this is a good demonstration of the possibility of the method. Generally, the approach based upon Hα may be indispensable in cases, when the photometry at the nebular epoch is absent, or when there is a problem with subtraction of stellar background (SN IIP in the bulge, or in high redshift galaxies).

An interesting by-product of the analysis of the SNe IIP sample is the demonstrated correlation between ^{56}Ni mass and the steepness parameter (S) introduced to measure the light curve decay rate at the inflection point. The correlation is such that the steeper

the decline at the inflection point the lower is the ^{56}Ni mass. Thus radiative diffusion times and ^{56}Ni masses are linked. How an increased radioactive energy input leads to a higher effective opacity will require elaboration by hydrodynamical modeling. This correlation, if confirmed, will provide us with a distance and extinction independent way to determine the amount of ejected ^{56}Ni.

Finally we note that in Fig. 3.10 the clustering of the points around two values of ^{56}Ni mass viz. 0.005 and 0.05 $M_\odot$ may result from poor statistical sampling. On the other hand it may be a hint that a mechanism such as fall-back is an important one in the evolution of the low-mass group.

Bibliography

[1] Arnett W. D. 1996, in "Supernovae and nucleosynthesis", (Princeton University Press)

[2] Aufderheide M. B., Baron E. & Thielemann F. K. 1991, ApJ, 370, 630

[3] Barbon R., Ciatti F. & Rosino L. 1973, A&A, 29, 57

[4] Baron E., Branch D, Hauschildt P. et al. 2000, ApJ, 545, 444

[5] Benetti S., Cappellaro E., Turatto M. et al. 1994, A&A, 285, 147

[6] Benetti S., Turatto M., Balberg S. et al. 2001, MNRAS 322, 361

[7] Bouchet P. & Danziger I. J. 1993, A&A, 273, 451

[8] Blanton E. L., Schmidt B. P., Kirshner R. P. et al. 1995, AJ, 110, 2868

[9] Cardelli J. A., Clayton G. C. & Mathis J. S. 1989, ApJ, 345, 245

[10] Catchpole R. M., Whitelock P. A., Feast M. W. et al. 1988, MNRAS, 231, 75

[11] Chugai N. N. 1990, SvAL, 16, 457

[12] Chugai N. N. & Utrobin V. P. 2000, A&A, 354, 557

[13] Clocchiatti A., Benetti S., Wheeler J. C. et al. 1996, AJ, 111, 1286

[14] Eastman R. G. et al. 1994, ApJ, 430, 300

[15] Elmhamdi A., Danziger I. J., Chugai N. N. et al. 2003, MNRAS, 338, 939

[16] Evans R. O., Jarman J., Cragg T. et al. 1995, *IAUC* 6197

[17] Evans R., Benetti S. & Grupe D. 1995, *IAUC* 6239

[18] Fassia A., Meikle W. P. S. Geballe T. R. et al. 1998, MNRAS, 299, 150

[19] Filippenko A. V. 2001, in "Young Supernova Remnants", ed. S. S. Holt (New York: American Institute of Physics)

[20] Grassberg E. K., Imshennik V. S. and Nadyozhin D. K. 1971, Astrophys. Space Sci, 10, 28

[21] Hamuy M., Pinto P. A., Maza J. et al. 2001, ApJ, 558, 615

[22] Hamuy M. 2003, ApJ, 582, 905

[23] Hirata K., Kajita T., Koshiba M. et al. 1987, Phys. Rev. Lett. 58, 1490

[24] Kirshner R. P. & Kwan J. 1975, ApJ, 197, 412

[25] Kozma C. & Fransson C. 1992, ApJ, 390, 602

[26] Leonard D. C., Filippenko A. V., Li W. et al. 2002, AJ, 124, 2490

[27] Litvinova I. Y & Nadyozhin D. K. 1985, SvAL, 11, 145

[28] Patat F., Barbon R., Cappellaro E. & Turatto M. 1994, A&A, 282, 731

[29] Phillips M. M., Hamuy M., Maza J. et al. 1990, PASP, 102, 299

[30] Ruiz-Lapuente P., Canal R., Kidger M., Lopez R. et al. 1990, ApJ, 100, 782

[31] Schlegel D. J., Finkbeiner D. P. & Davis M. 1998, 500, 525

[32] Schmidt B. P., Kirshner R. P. & Eastman R. G. 1992, ApJ, 395, 366

[33] Schmidt B. P., Kirshner R. P., Schild R. et al. 1993, ApJ, 105, 2236

[34] Sohn Y. J. & Davidge T. J. 1998, AJ, 115, 143

[35] Turatto M., Cappellaro E., Benetti S. & Danziger I. J. 1993, MNRAS, 265, 471

[36] Turatto M., Mazzali P. A., Young T. R. et al. 1998, AJ, 498, L129-L133

[37] Weaver T. A. & Woosley S. E. 1980, Ann. N.Y. Acad. Sci, 336, 335

[38] Williams A., Martin R., Greenhill J. et al. 1995, *IAUC* 6206

[39] Xu Y., McCray R., Oliva E. & Randich S. 1992, ApJ, 386, 181

[40] Zampieri L. et al. 2002, MNRAS; in press

Chapter 4

SN Ib 1990I: Clumping and Dust in the Ejecta?

This work have been done in collaboration with I. J. Danziger.

"Equipped with his five senses, man explores the universe around him and calls the adventure Science!.""

Edwin Hubble (1889 - 1953)

Abstract

Photometry and spectra of the type Ib SN 1990I are presented and analysed, covering about 400 days of evolution. The presence of optical helium lines is shown. SN 1990I seems to show higher velocities compared to a sample of type Ib events. The nebular emission lines display a high degree of asymmetry and the presence of fine structures, suggestive of non-spherical clumping in the ejecta of SN 1990I. Using the [O I] 6300,64 Å flux, we estimate a lower limit on the oxygen mass to fall in the range $(0.7 - 1.35)$ $M_{\odot}$. The oxygen mass requires a filling factor as small as $\sim 10^{-2}$ on day 254, indicating a highly clumpy distribution of the oxygen material. The [Ca II]/[O I] flux ratio evolution reflects the low ejecta mass of SN 1990I with respect to type II SN 1987A. A blueshift of the order 600 km s^{-1} is reported in the [O I] 6300,64 Å after day 254. The [Ca II] 7307.5 Å emission profile appears blueshifted as well at late epochs. We recover the quasi-bolometric "*BVRI*" light curve of SN 1990I. The constructed bolometric light curve shows a change of slope at late phases, with an *e*-folding time of 60 ±2 d in the [50 : 200] d time interval, considerably faster than the one of ^{56}Co decay (i.e. 111.3 d), suggesting the γ-rays escape with lower deposition, owing to the low mass nature of the ejecta. After day 200, an *e*-folding time $\simeq$47 ±2.8 d is measured. While the light curves of SNe 1990I and 1993J are similar in the [30 : 100] d time range, they tend to behave differently after day 200. A simplified γ-ray deposition model is applied after adding a contribution of about 35% to the computed pseudo-bolometric light curves to account for near-IR luminosities to estimate the ejecta and ^{56}Ni masses ($M(^{56}Ni) = 0.11$ $M_{\odot}$ and $M_{ej} = 3.7$ $M_{\odot}$). The deficit in luminosity is estimated to be about 50% around day 308. The observed spectral blueshift combined with the dramatic and sudden drop in the pseudo-bolometric light curve and $(B - V)$ colour is interpreted to be a consequence of dust condensation in the ejecta of SN 1990I around day 250.

4.1 Introduction

One of the interesting tasks in supernovae (SNe) research for the last few years has been the study of hydrogen deficient events, namely type Ib (helium-rich) and type Ic (helium-poor) events (Wheeler & Harkness. 1990 [56]). The particular interest addressed in these two subclasses comes from the fact that they are the least understood among supernovae varieties, on the level of their observational properties, progenitors and therefore the physics of the explosion (Nomoto et al. 1990 [33]; Baron. 1992 [2]). The possible connection of the strongly energetic ones with Gamma-ray bursts (GRBs) with the emergence of hypernovae (Woosley et al. 1999 [58]; Nomoto et al. 2000 [34]) makes them exciting events. In addition, the appearance of the transition events such SNe 1993J and 1987K suggests a physical connection between type Ib/c and type II objects; thus one needs to understand the differences as well as the similarities among them.

Type Ib and Ic SNe are classified on the basis of their spectra. These events are hydrogen deficient at maximum light. They lack also the deep Si II absorption near 6150 Å characterizing type Ia events. SNe Ic are spectroscopically similar to SNe Ib at late epochs where the spectra are dominated by oxygen and calcium emission lines, whereas at early phases SNe Ic do not show the He I lines (Wheeler & Harkness. 1990 [56]).

Different models have been suggested to explain the main observational properties of SNe Ib/c. The most accepted scenario is related to the mechanism of the hydrogen rich SNe II, namely core collapse in massive stars. There are many reasons for thinking that the core collapse events are favoured in the progenitors of type Ib/c SNe :

⋆ They are associated with population I stars, and are observed to occur in spiral galaxies ongoing star formation occurs.

⋆ The association with H II regions.

⋆ The presence of strong oxygen emission lines.

⋆ The discovery of transition events (e.g. SNe 1987K and 1993J), whose spectral properties changed from type II to type Ib/c as they aged.

⋆ The detection of such events in the radio (e.g. radio emission in SN 1983N and SN 1984L), suggests interaction with circumstellar material.

Here we present and analyse the photometry and spectral evolution of SN 1990I. The chapter is organized as follows. We describe first the spectral behaviour of SN 1990I during both the photospheric and nebular phases. The nebular emission lines are analysed. We use the [O I] 6300,64 Å luminosities to estimate the ejected mass of oxygen (Sect. 4.2.1). Then we study the light curves and colour evolution of SN 1990I. The photometry is compared to a selected sample of type Ib/c, IIb events (Sect. 4.2.2). We then describe a simple model of γ-ray deposition from radioactive decay used to fit the bolometric evolution of SN 1990I, providing ^{56}Ni and ejecta mass estimates (Sect. 4.3).

4.2 Observations

SN 1990I was discovered by Pizarro et al. (IAUC 5003 [37]) in NGC 4650A. Initially it was classified as type Ia on the basis of an early spectrum taken by Sivan and Marseille on April 30 (IAUC 5003 [37]). Based on three early spectra (May 18, June 7 and June 8) taken with the Cerro Tololo 1.5-m telescope, SN 1990I has been re-classified as a type Ib by Phillips (IAUC 5032 [36]).

We present spectra and photometry covering about $\sim$ 400 d of evolution. The data are collected from ESO-KP (Key Project) database.

4.2.1 Spectroscopic evolution

The spectroscopic evolution of SN 1990I, covering both the photospheric and nebular phases (from $\sim$ 18 d to $\sim$ 375 d), are illustrated in Figure 4.1. The corresponding days since explosion for each spectrum are also reported . The spectra have been corrected for the recession velocity (cz = 2902 km s^{-1}) of the parent galaxy NGC 4650A.

The early spectrum ($\sim$ 18 d) displays a blue continuum with broad P-Cygni profiles, indicating both high velocities and temperature. The He I 5876 Å is unambiguously recognized with a velocity of the order $\sim$ 13400 km s^{-1}, as measured from the absorption minimum, clearly high compared to the similar epoch SNe Ib typical velocity ($\sim$ 10000 km s^{-1}; Branch et al. 2002 [5], hereafter B02). For the 29 d spectrum, V$\sim$ 12500 km s^{-1} is measured, and this is used to infer the possible location of the various He I lines, namely 4471 Å, 5015 Å, 6678 Å and 7065 Å. Figure 4.2 demonstrates the evidence of the prominent optical He I lines in the ejecta of SN 1990I. The relative strengths of the He I lines are such that strong departures from LTE are apparent as suggested by Wheeler et al. (1987)[55] for other Type Ib SNe. Lucy (1991)[29] has shown that these strong departures from LTE result from excitation by non-thermal electrons originating from radioactive decay of ^{56}Co dispersed throughout the envelope. It must be kept in mind, nevertheless, that since the Fe II lines, especially 4924 Å, 5018 Åand 5169 Å, affect mainly the spectra shortward 5300 Å, the absorption features are subject to line blending in that portion of the spectra. In addition the He I 4471 Å line may be affected by the Mg II 4481 Å.

The photospheric velocity, as inferred from Fe II 5169 Å line, appears to be greater with respect to values derived from the SNe Ib sample in the B02 work. From the 29 d spectrum we measured $V_{phot} \sim$ 9000 km s^{-1}. At comparable phase B02 provided $V_{phot} \sim$ 6500 km s^{-1}. If we use the derived velocity as an indicator of the epoch, and hence try to fit the B02 sample data (their Figures 22 and 23), one estimates the epoch to be around maximum. This seems unlikely, taking into account the shape and nature of the spectrum. Therefore the high velocity nature of SN 1990I ejecta seems unavoidable.

The Ca II near-IR triplet, displaying broad P-Cygni profiles, is the strongest emission feature at red wavelengths at this phase. The Ca II H & K is also identified. Although features in the blue part of the spectrum are hardly discernible because of the noise,

we remark in the 38 d spectrum a weak absorption feature centered at $\sim$ 3890 Å. This feature has been a subject of discussion for early spectra of SN Ib 1999dn, and has been attributed to Ni II 4067 Å in order to fit the 3930 Å absorption (Deng et al. 2000 [14]; their Sep. 14 spectrum). Furthermore, this best fit at 3930 Å with Ni II 4067 Å , for the case of SN 1999dn, leads the authors to believe it is early evidence of ^{56}Ni mixing.

In Figure 4.2 two absorption features near 6050 Å and 6250 Å are marked (long-dashed lines). These features are both present in the three early spectra, while the 6250 Å feature is no more seen in the 60 d spectrum. Deng et al. (2000)[14], through spectrum synthesis of SN 1999dn around maximum, have argued for evidence of both C II and Hα, attributing the feature around 6300 Å to the blend of the two lines, and uniquely due to C II later on. Benetti et al. (2002)[3], on the other hand, have included Ne I lines to fit early spectra of SN 1991D, providing improvement in fitting both absorption features, similar to the ones marked by long dashed lines in Fig. 4.2.

Whether hydrogen is present or not in type Ib/c events is an important issue, since it is directly related to the nature of the progenitor stars and their evolution (Filippenko. 1997 [18]). Interestingly, SN 1990I allows one to follow spectroscopically features in the 6000 – 6500 Å region. The possible identification of the feature around 6250 Å as Hα, points to the presence of a thin hydrogen layer above the helium layer with high velocity, which disappears or is overwhelmed by C II 6580 Å as Hα optical depth decreases as a consequence of the envelope expansion (Deng et al. 2000 [14]). In fact, if correctly identified, we measure from the 29 d spectrum an Hα velocity as high as $\sim$ 15000 km s^{-1}, a higher one compared to He I 5876 Å($\sim$ 12500 km s^{-1}). Note that since SN 1990I is very similar to SN 1991D with respect to the presence and the shape of the two absorption features one might expect Ne I lines to provide good fit (Benetti et al. 2002 [3]), while the presence of Hα still remains a possible interpretation. Detailed synthetic spectra are needed to test both possibilities.

The absorption near 7500 Å is attributed to O I 7774 Å line in type Ib SNe, nevertheless in some cases the introduction of the blend with Mg II 7890 Å is needed to fit synthetic spectra (e.g. SN 1999dn, Deng et al. 2000 [14]).

As the supernova evolves in time the features display a shift towards the red part of the spectrum. This shift is caused by the retreat of the photosphere into the slower moving layers.

The last three spectra in Figure 4.1(A) present evidence of [O I] 6300,64 Å and [Ca II] 7291,7324 Å emission, suggesting the onset of the nebular phase. Figure 4.1(B), on the other hand, displays the real nebular phase spectra. As illustrated, the 254 d spectrum, displays a strong [O I] 6300,64 Å emission line, which is quite broad. The other prominent features are Na I D 5893 Å doublet and the broad Mg I] 4571 Å line. Additional nebular lines are difficult to discern. Regrettably, the 254 d spectrum does not extend redward 7000 Å, whereas the 315 d spectrum does. In fact, although the spectra are noisy, the [O I], [Ca II], Na I and Mg I] emission lines are still stronger compared to the continuum, and as time goes on they tend to shrink with respect to the continuum. This continuum may come from stars very close to the SN. In fact the presence of narrow Hα emission in at least five photospheric and either Hα emission or absorption in three of the nebular

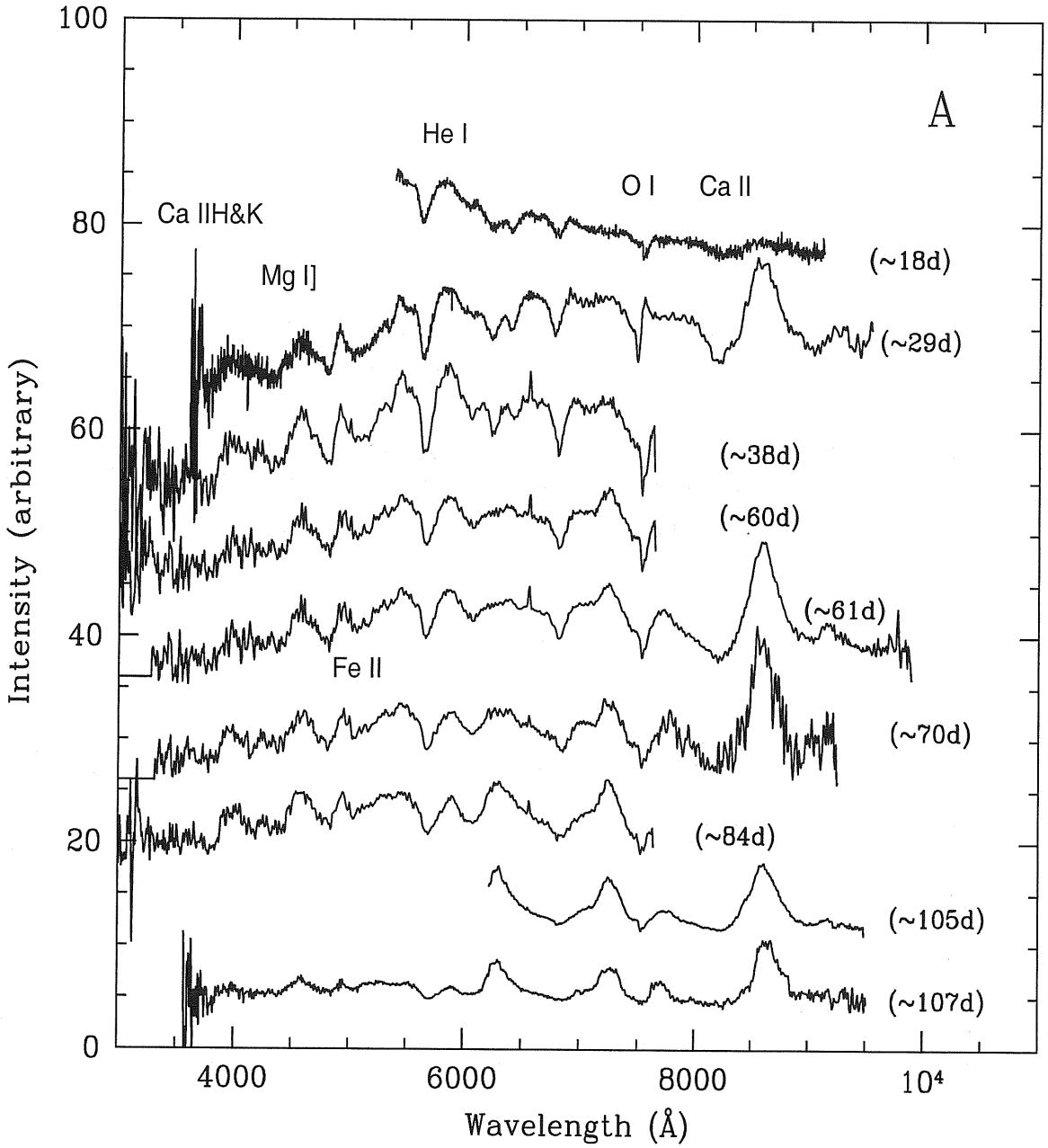
A
He I
O I
Ca II
Ca IIH&K
Mg I]
Fe II
(~18d)
(~29d)
(~38d)
(~60d)
(~61d)
(~70d)
(~84d)
(~105d)
(~107d)
Intensity (arbitrary)
Wavelength (Å)
0
20
40
60
80
100
4000
6000
8000
10⁴

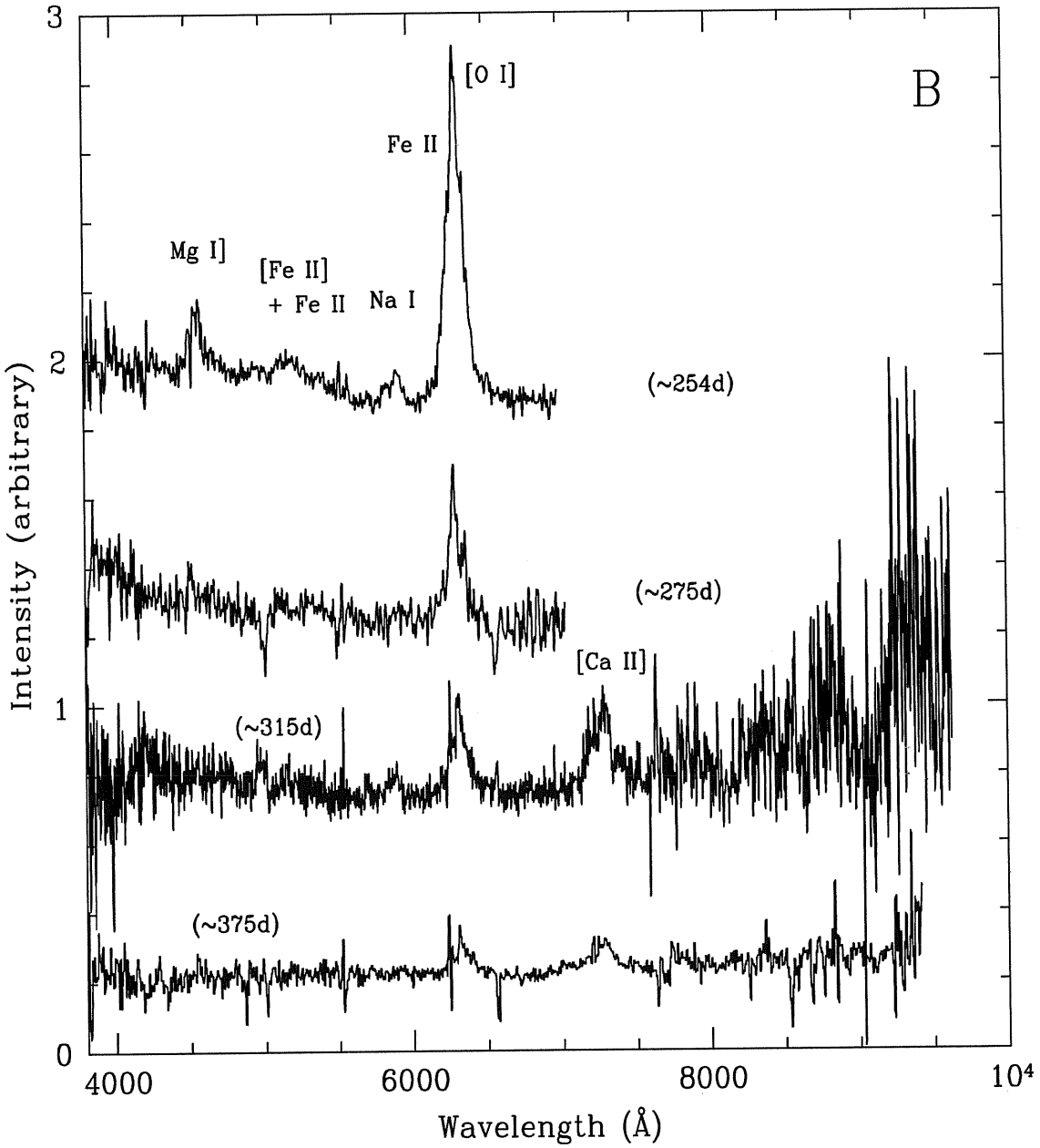

Figure 4.1: Spectral evolution of SN 1990I during the photospheric phase (A), and during the nebular phase (B). Days since explosion are shown. All the spectra have been corrected for the recession velocity of the host galaxy and scaled arbitrary for clarity. The strongest features are also reported.

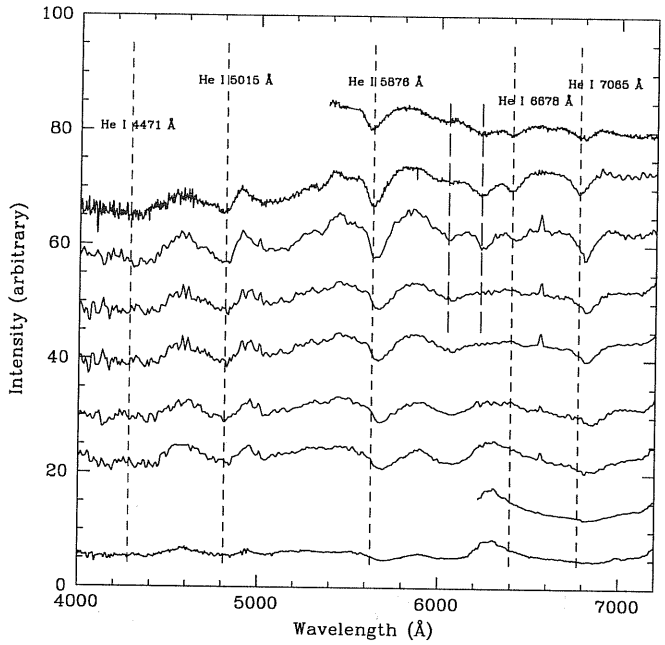

Figure 4.2: Possible location of He I lines in the photospheric phase of SN 1990I (short-dashed lines). The absorption features near 6050 Å and 6250 Å are marked (long-dashed lines; Section 4.2)

spectra suggests the presence of an H II region inadequately subtracted. The narrow Hα feature ($EW \simeq 3.8$ Å on day 38) is located at the rest wavelength of the host galaxy and is seen to not broaden with time, which reflects its association with H II region rather than with the SN.

Interestingly, at this phase, the [Ca II] and [O I] fluxes seem to be comparable. This is of interest since it is related to the nature of the progenitor star. Fransson & Chevalier (1987 [20], 1989 [21]) have shown that the forbidden emission line ratio [Ca II]/[O I] is weakly dependent on density and temperature of the emitting zone, and is expected to show an almost constant evolution at late epochs. Furthermore the ratio seems to be very sensitive to the core mass and hence to the main-sequence one. The ratio increases with decreasing main-sequence mass. In Figure 4.3 we show the evolution of the computed ratio in SN 1990I together with SNe 1985F(Ib), 1998bw(Ic), 1993J(IIb), 1996N(Ib) and 1987A(II). The plot indicates the lower mass nature of SN 1990I with respect to SN 1987A, and a clear similarity to the other events. It is note worthy, however, that in type Ib/c SNe there is no hydrogen rich Ca II emitting zone as is the case of type II events (de Kool et al. 1998 [13]). We note as well that the values reported for SN 1990I may be even lower if we correct for the depletion behaviour blueward of the [O I] emission (see next section).

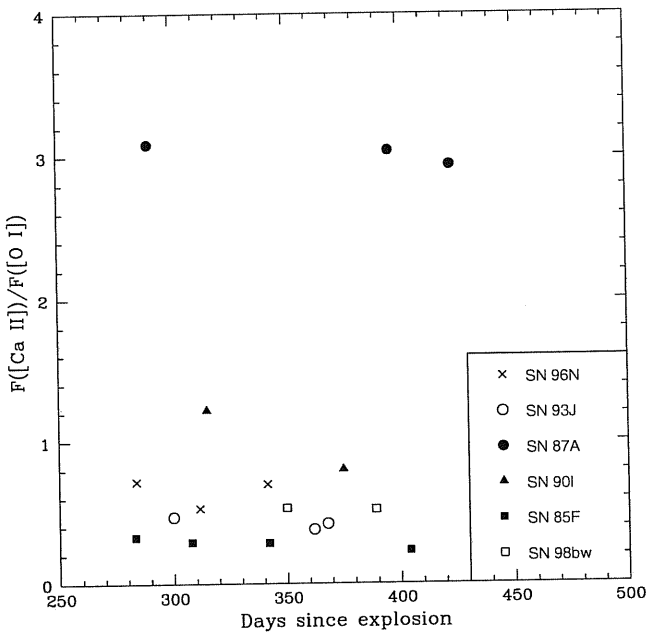

Figure 4.3: The time evolution of the ratio $F([CaII])/F([OI])$ of SN 1990I together with that of a sample of SNe. The difference between SN 1987A and the remaining SNe is clear. This indicates the high ejecta mass of SN 1987A (type II) with respect to the other events (type Ib/c).

Nebular emission line profiles

In Figure 4 we show, in velocity space, the late evolution of the most prominent nebular lines, namely Mg I] 4571 Å, [O I] 6300,64 Å, [Ca II] 7307.5 Å and O I 7774 Å.

At 107 d the flat topped nature of the [O I], [Ca II] and O I emission lines is indicative of shell structure. An approximate position of the blue edge of plateau in [O I] line is at 2600 km s^{-1}. The [O I] line on day 254 is still peaked at zero velocity, whereas on day 275 it appears blueshifted by $\sim$ 600 km s^{-1}. Unfortunately, the spectra in this transition phase, from +254 d to +275 d, do not show [Ca II] and O I profiles in order to check whether there is any dependence of the shift on wavelengths. The Mg I] 4571 Å , at that phase, is noisy which makes any conclusion about the blueshift behaviour doubtful although a hint of that fact is seen in the 275 d spectrum compared to the 254 d one. This behaviour was also seen in SN 1993J, and was interpreted as an indication of large scale asymmetries and clumpy distribution of the ejecta (Spyromilio. 1994 [47]). The [Ca II] 7307.5 Å line has a blue shift the magnitude of which seems to decrease from day 107 to day 375. Since this interval embraces the epoch of dust formation near day 250 (Section 4.2.2) and spectral observations are so sparse it is not possible to disentangle two possible competing effects. This scarcity of data also inhibits a more detailed discussion of the blueshift seen in the O I 7774 Å line at day 107. The strength of the O I 7774 Å feature, on the other hand, arising as it does from high levels in an envelope that

should be relatively cool, could indicate non-thermal electron excitation analogous to what has been proposed for the He I lines at an earlier phase.

Similar blueshifts affecting several lines have been reported for SN 1996N by Sollerman et al. (1998)[43] and extensively discussed there. Similar effects have also been reported for SNe 1987A, 1999em and 1988A. Various hypothesis have been reviewed without firm conclusions being drawn although large scale asymmetries are favoured. In spite of their reported lack of temporal evolution of the blueshifts in SN 1996N, evolution was evident in SN 1987A and seems evident in our sparse observations of [O I] 6300,64 Å prior to dust formation. We consider a decrease in line optical depth, possibly combined with different excitation conditions for different lines, as the most promising explanation.

On the other hand, we note the presence of fine structures superimposed clearly on the profiles of O I 7774 Å (107 d spectrum), [Ca II] 7307.5 Å (107 d and 305 d) and Ca II 8662 Å. In Figure 4.5 two structures on the top of [Ca II] 7307.5 Å and Ca II 8662 Å are marked. The bumps have comparable velocities (-800 and 500 km s^{-1}) in both lines. Similar bumps have been reported in the 1993J spectrum around day 174 on the top of [O I] 6300,64 Å and O I 5577 Å lines, and have been attributed to asymmetry, whereas the lack of similarity in line profiles of permitted and forbidden transitions of the same element is a result of spatially different excitation conditions (Spyromilio. 1994 [47]). In the longer wavelength lines fringing in the CCD could complicate and confuse a clearer interpretation.

The situation of SN 1990I may be more complicated in view of further information from the photometric evolution (Section 4.2.2), where the coexistence of both large scale asymmetries and dust condensation at later epochs (after day 254) is more probable. In fact a second blueing effect was reported in SN 1987A spectra, after $\sim$ 500 d, where the emission line profiles of Mg I] 4571 Å , [O I] 6300,64 Å and [C I] 9824,9850 Å became asymmetric with peak emission blueshifted by about $500-600$ km s^{-1}, and was attributed to extinction by dust within the metal-rich ejecta (Danziger et al. 1989 IAUC 4746 [11], Lucy et al. 1989 [28]). An analysis of SN 1999em data has indicated a similar conclusion about dust formation around day 500 (Elmhamdi et al. 2003 [15]).

The [O I] 6300 Å profile in the last two spectra displays a depletion of emission in the $[-2500 : 0]$ km s^{-1} region. In Figure 4.6 we present, at three different phases of evolution, the [O I] 6300 Å profile of SN 1990I compared to SNe 1993J and 1998bw. We shift arbitrarily the peaks to match each other for the clarity of the comparison. there are some points of interest on this figure. First, SN 1990I shows broad profile with respect to SN 1993J, and is similar to that of SN 1998bw confirming the high velocity nature of the ejecta. Second, the depletion feature is well seen in the bottom box, showing under-luminosity in the $[-2500 : 0]$ km s^{-1} region and pointing to different excitation conditions compared to that in the other two objects. Again a clumping of the radioactive material in the oxygen shell with velocities belonging to $[-2500 : 0]$ km s^{-1} zone is a possible explanation. Finally, the presence of this depletion structure in the 315 d and 375 d [O I] profiles prevents us from checking whether the blueshift seen in the 275 d [O I] emission increases or not with time.

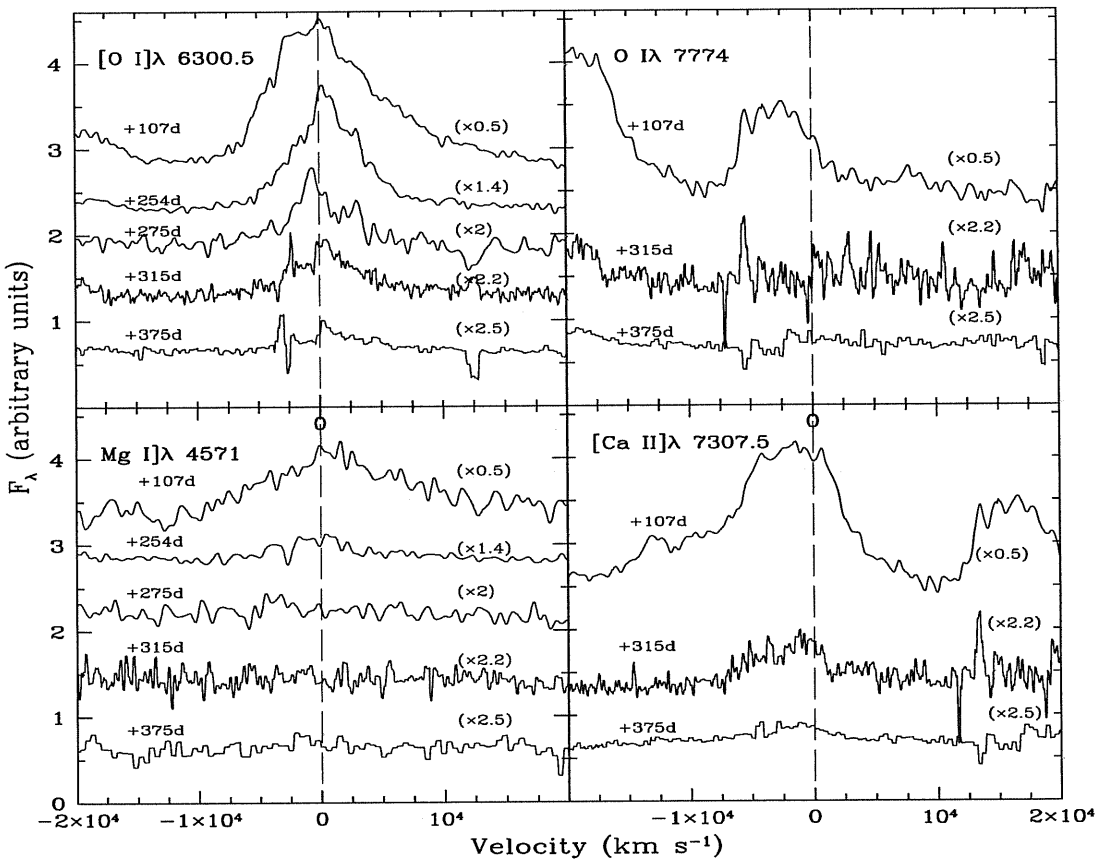

Figure 4.4: The time evolution, in velocity space, of the most prominent nebular lines: Mg I] 4571 Å, [O I] 6300,64 Å, [Ca II] 7307.5 Å and O I 7774 Å. Shown as well are the coefficient by which the spectra have been multiplied for clarity. Rest wavelengths are marked by vertical long-dashed lines.

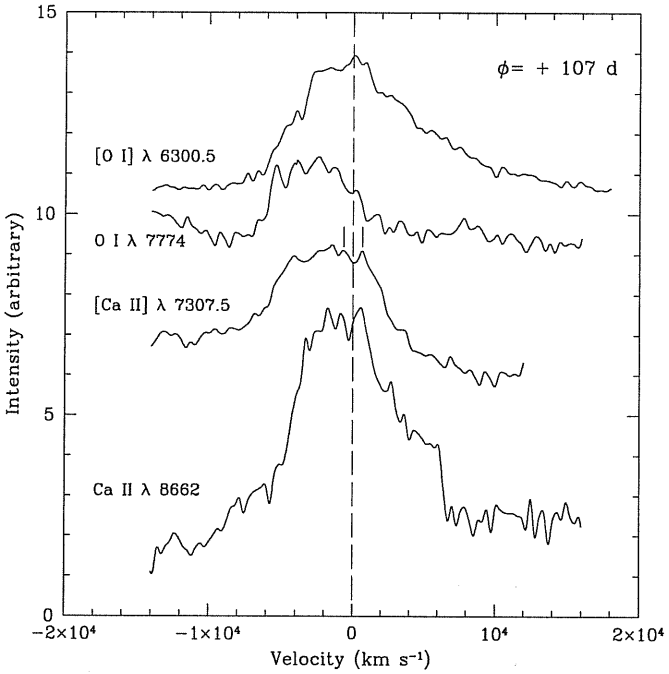

Figure 4.5: the strongest lines, in velocity space, of the 107 d spectrum. The features are clearly asymmetric and flat topped, with the presence of fine structures. Two bumps with similar velocities in the [Ca II] 7307.5 Å and Ca II IR-triplet lines are marked.

Oxygen mass

Estimating the oxygen mass is important as it can be indicative of the core mass and hence related to the nature of the progenitor star. The [O I] 6300,64 Å doublet line emission is known to be the primary coolant in the ejecta of Ib/c events, at least at late epochs, in view of the absence of hydrogen in this class of objects as opposed to type II events (Uomoto 1986 [54]; Fransson 1987 [19]). In principle, the mass of ejected oxygen can be recovered using the [O I] 6300,64 Å flux. Uomoto (1986)[54] has shown that the oxygen mass, in $M_\odot$, is given by:

$$M_{Ox} = 10^8 \times D^2 \times F([\text{O I}]) \times \exp(2.28/T_4) \qquad (4.1)$$

where D is the the distance to the supernova (in Mpc), F is the [O I] integrated flux (in ergs s^{-1} cm^{-2}) and T_4 is the temperature of the oxygen-emitting gas (in 10^4 K). Equation 4.1 holds for the high density limit ($N_e \geq 10^6$ cm^{-3}) where the density is above the critical density for the [O I] line ($\sim 7 \times 10^5$ cm^{-3}). This condition, on the other hand, is clearly achieved in the ejecta of type Ib/c SNe. In fact a rough estimate of the mass density can be computed at day 254. We have attempted to fit the [O I] 6300,64 Å feature with 2 Gaussians, fixing the wavelength separation of the doublet and with both having the same velocity width. It is not possible to obtain a particularly good overall fit since one is left with either a residual in the blue wing of [O I] 6300 Å for

narrower lines, or little evidence of the [O I] 6364 Å feature for broader lines. Thus a one-component Gaussian fit may not represent the real situation where clumping is present. On the other hand by assuming that there is a contribution from an Fe II 6239 Å emission, and allowing its velocity width to be a free parameter we obtain the fit shown in Fig. 4.7. The $FWHM$ for the [O I] lines is $\sim$ 60 Å while for the Fe II 6239 Å line we obtain $\sim$ 46.8 Å. We also show residuals which might represent the effects of clumping in the [O I] emitting region. This fit has the advantage that the velocity width for the Fe II feature is less than that for [O I] as might be expected. We adopt the velocity widths for [O I] determined in this way but note that similar values would be obtained if we accepted the best fit of the [O I] doublet alone around the peak emission of both components of the doublet. Furthermore, we notice in Fig. 4.7 that the largest negative residual seen shortward of 6300 Å may correspond to the more prominent depletion at later times. This would support the idea that the depletion is a real effect.

Using then the derived $FWHM$ of the [O I] line at 254 d ($\sim$ 2860 km s^{-1}), and adopting the ejecta mass of M_{ej} = 3.7 M$_\odot$ (Sect. 4.3.2) we derive a value of $N_e \sim 1.16 \times 10^7$ cm^{-3}. We have assumed abundance fractions of He, O and heavier elements in the following proportions: 0.1, 0.22 and 0.68, respectively. We also assume that half of the He and O and all of the other elements are singly ionized. Since we assume matter uniformly distributed this should be a lower limit for regions where clumping occurs.

An accurate estimate of the density is based on the relative strengths of the [O I] doublet components (Leibundgut et al. 1991 [26]; Spyromilio & Pinto. 1991 [46]). The authors of both papers have computed the variation of the line doublet ratio as function of the density at a given time and found it insensitive to the adopted temperature, especially at late epochs. From the 254 d [O I] line profile fit we measure a relative intensity $I(6300)/I(6364) \simeq 1.69$, similar to that of SN 1987A at similar phase ($\sim$ 1.45 at 250 d). The uncertainty in the temperature leads to the following range $2.3 \times 10^9 \leq N_e \leq 4 \times 10^9$ according to Fig. 4.6 of Leibundgut et al. (1991)[26]. The large difference (a factor of about 100) between this density estimate and the one from the simple approach using the volume calculated from the [O I] velocity and M$_{ej}$ indicates, indeed, that the oxygen material fills the volume at day 254 in a clumpy way rather than homogeneously. This high density would favour the presence of Fe II features mentioned previously and identified in Figure 4.1.

Equation 4.1 implies time-dependence because of the variation of F([O I]) and the temperature. Schlegel & Kirshner (1989)[40], when estimating the oxygen masses ejected by SNe Ib 1984L and 1985F using this method, have adopted a constant temperature T_4=0.4 at the nebular phase. The assumption of a constant temperature at different late phases provides different oxygen masses as one may expect, since earlier nebular epochs are hotter compared to latter ones. Worth noting is the exponential dependence of the oxygen mass on temperature.

A method for estimating temperature at a given time is based on the [O I] 5577 Å to [O I] 6300,64 Å flux ratio. This comes from the assumption that the O I lines are formed mainly by collisional excitation, and the ratio is given by the following expression (Houck & Fransson 1996 [24]):

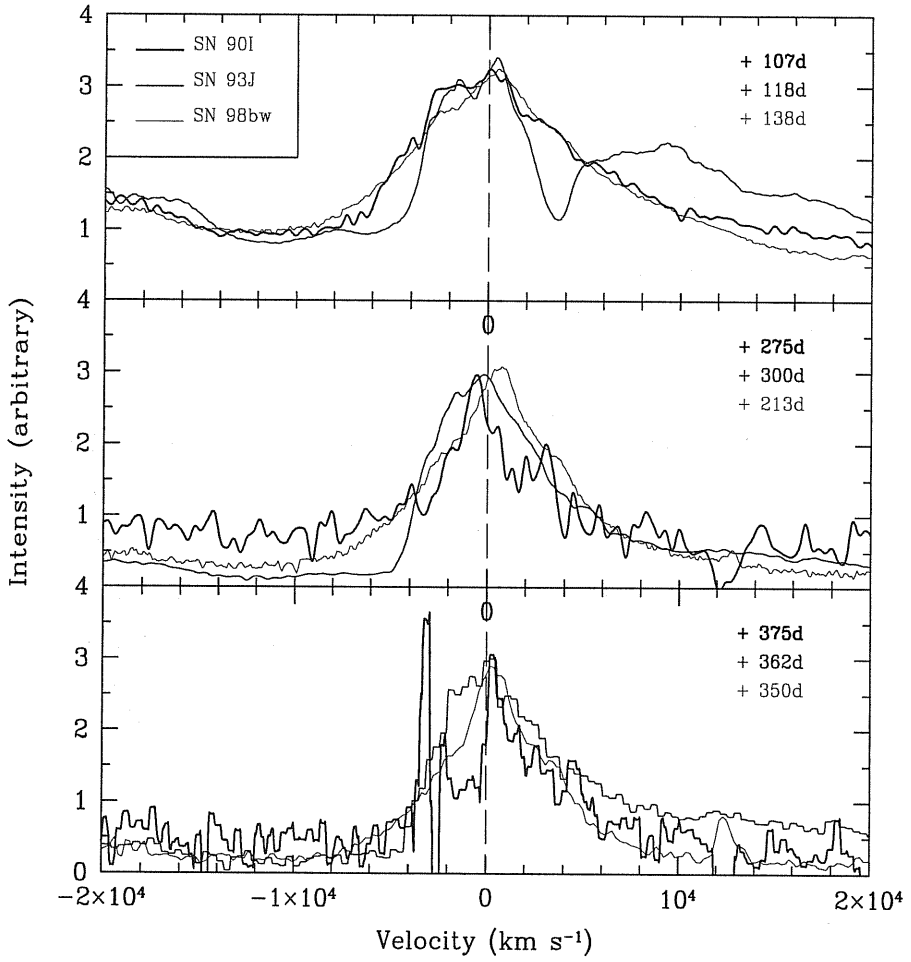

Figure 4.6: The [O I]6300,64 Å line profile of SN 1990I in three different epochs of evolution. Comparison with SNe 1993J and SN 1998bw is made, indicating the high velocity nature of SN 1990I and the presence of a "*depletion*" structure in the blue edge of the emission profile (lower panel).

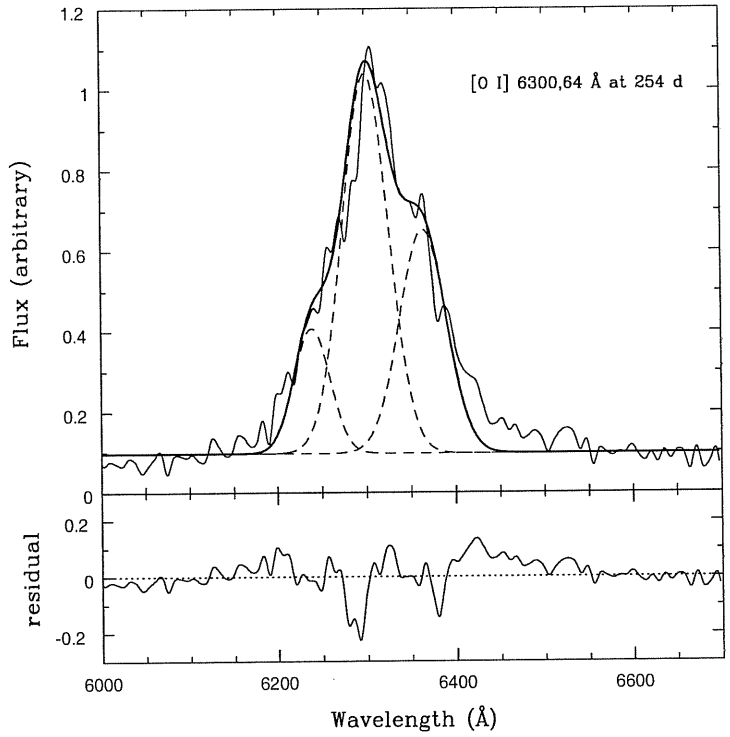

Figure 4.7: Fit to the 254 d [O I] 6300,64 Å line profile of SN 1990I. Shown in thick line is the sum of the three Gaussians for [O I] 6300 Å , [O I] 6364 Å and Fe II 6239 Å (dashed lines; see text). The residuals are displayed in the lower panel.

$$\frac{F(6300)}{F(5577)} = 0.03\beta_{6300} \times [1 + 1.44 T_3^{-0.034} (\frac{10^8}{N_e})] \times \exp(25.83/T_3) \qquad (4.2)$$

where T_3 is the temperature of the oxygen-emitting gas (in 10^3 K), β_{6300} is the [O I] 6300 Å Sobolev escape probability ($\simeq 1$) and N_e is the electron density.

After correcting the SN 1990I late spectra for reddening and calibrating them with photometry (when needed), we compute the fluxes. Because of line blending, mainly with Fe II lines, the [O I] 5577 Å flux measurements are less precise, especially for the last three spectra. We use the 254 d spectrum because it is less noisy and does not show the depletion feature seen later in the blue side of the [O I] 6300,64 Å emission profile. A lower limit on the ratio (left hand term in Eq. 4.2) can be estimated using an upper limit on the [O I] 5577 Å flux by integrating over the same velocity interval of the [O I] 6300,64 Å profile. When using the density range estimated on the basis of the [O I] 6300,64 Å doublet ratio we derive temperatures of the order 3200 – 3500 K. We obtain then 0.7 – 1.35 $M_\odot$ as oxygen mass. Here we note that since we are adopting an upper limit on the [O I] 5577 Å flux, the recovered oxygen mass is a lower limit. The very weak [O I] 5577 Å feature in the last three spectra is an indication of low temperatures in

Table 4.1: The estimated ejected oxygen mass.

SN name	SN type	M_{Ox} ($M_\odot$)	References
1987A	II	1.5-2	1, 2
1984L	Ib	$\sim 0.3^\star$	3
1985F	Ib	$\sim 0.3^\star$	3
1987M	Ic	$0.4^\star$	4
1990I	Ib	$0.4\text{-}1.35^\star$	this work
1993J	IIb	~ 0.5	5
1996N	Ib	$0.1\text{-}0.3^\star$	6

Refs:

1- Fransson et al. 1993[22]; 2- Chugai 1994[8]; 3- Schlegel & Kirshner 1989[40];

4- Filippenko et al. 1990[17]; 5- Houck & Fransson 1996[24]; 6- Sollerman et al. 1998[43].

$\star$ Estimated adopting the same method (i.e. using Eq. 4.1)

the oxygen-emitting zone. Indeed, although the determination of oxygen mass following this method suffers from several uncertainties, it seems that SN 1990I has reached lower temperatures earlier and has a higher oxygen mass compared to typical Ib/c SNe. In Table 4.1 we report the amount of ejected oxygen mass for a selected sample of type Ib/c SNe. The table includes as well data of SN II 1987A and SN IIb 1993J. One should note however that adopting a different method, Tutukov & Chugai (1992)[53] have argued for an amount of ~ 0.8 $M_\odot$ as total ejected oxygen mass[1] (neutral and ionized) for type Ib SN 1984L, and concluded that a typical value of ~ 1 $M_\odot$ should be ejected as well by SNe Ib 1983N and 1985F.

The somewhat higher oxygen mass and lower temperature with respect to other SNe Ib/c may be related to other observational peculiarities in SN 1990I. First the higher expansion velocity (i.e. faster cooling), and second the possible dust condensation at a time as early as ~250 d (to be discussed photometrically later).

4.2.2 Photometric evolution

In Figures 4.8, we present the B, V, R and I light curves of SN 1990I. Based on the shape of the light curves during the first $\sim$ 30 days of evolution and bearing in mind that the typical rise time of type Ib/c SNe is about $15 - 20$ days to reach maximum light, we estimate the explosion time to be April 11, 1990 (JD 47992), in accord with the reported first spectrum properties (i.e. broad P-Cygni profiles superimposed on a blue continuum). This date is taken as reference time in this work.

SN 1990I suffers high galactic extinction, $A_V^{gal} = 0.374$ mag, according to maps of the galactic dust distribution by Schlegel, Finkbeiner & Davis.(1998)[41]. This corresponds

[1] 0.2 $M_\odot$ neutral and 0.6 $M_\odot$ as ionized-oxygen mass.

to a colour excess about $E(B-V) = 0.12$, where the standard reddening laws of Cardelli et al. (1989)[7] have been used. In addition we note the presence of a very narrow NaI D interstellar absorption feature in the 29 d spectrum, with an equivalent width (EW) ~0.26 Å, and hence we can derive the reddening in the host galaxy. Using correlations relating EW(Na I D) to the reddening within the parent galaxy from the literature we obtain $E(B-V) \sim 0.06$ (Barbon et al. 1990 [1]) and $E(B-V) \sim 0.034$ (Benetti et al., in preparation). Therefore, in what follows, we adopt $A_V = 0.4$ mag as an estimate of the total extinction.

After the fast fall from maximum light (γ_V ~5.6 mag (100 d)$^{-1}$), SN 1990I settles onto a linear decline with a rate in the V band γ_V ~1.92 mag (100 d)$^{-1}$ up to about 230 days since explosion (dotted line in Fig. 4.8). The ^{56}Co to ^{56}Fe decay slope, 0.98 mag (100 d)$^{-1}$, corresponding to full γ-ray trapping is also shown. Except for rare cases where the late slope approaches the full trapping rate (e.g. SN Ib 1984L; Schlegel & Kirshner 1989 [40]), the steeper decline rate of about 1.9 mag (100 d)$^{-1}$ is common for type Ib/c SNe at late epochs (e.g. SN Ib 1983N, SN Ic 1983V, SN Ic 1994I and SN IIb 1993J, Clocchiatti & Wheeler 1997 [10]; SN Ib 1996N, Sollerman et al. 1998 [43]). This rapid decline, on the other hand, is indicative of significant γ-ray escape resulting from the low mass ejecta in this class of object.

Interestingly, however, SN 1990I shows an even steeper decline starting at about day 230 with a V-band decline rate γ_V ~2.7 mag (100 d)$^{-1}$. In addition, while the R and I light curves confirm this behaviour, the B light curve tends to flatten. The least-squares fit to the light curves at the three different phases of evolution are reported in Table 4.2. At early phase, the B light curve declines faster compared to the other bands, whereas for the two following phases it exhibits a lower decline rates. The V band, on the other hand, is the faster fading band during the following two phases. We compute as well the third to second phase decline slope ratio for each band. Results are shown in Table 4.2. The change in slope behaviour at late phases is seen also in other events, namely SN 1993J, SN 1998bw and SN 1996N with different occurrence times. SN 1996N, between 184 d and 312 d, seems to have similar V, R and I decline rates as SN 1993J (Sollerman et al. 1998 [43]). The last photometric point of SN 1996N (around day 342) is clearly deviating from the linear trend of the previous data, indicating the occurrence of a phase with steeper decline after day 312. In Table 4.2 we present the SN 1996N third to second decline rate ratios using the available photometric data from Sollerman et al. (1998)[43]. Interesting points can be read out from Table 4.2. A comparison of ratio values demonstrates the peculiar behaviour of SN 1990I with an increasing ratio towards the red bands, indicating some kind of dependence of the defined ratio on wavelength. Although there is a paucity of SN 1996N data, it is similar to SN 1990I in having a "*greater than one*" ratio, whereas SNe 1993J and 1998bw tend to flatten. Furthermore, SN 1993J has an opposite behaviour with respect to SN 1990I, in the sense that its B light curve declines more rapidly in the third phase while the V, R and I light curves flatten. The opposite holds for SN 1990I.

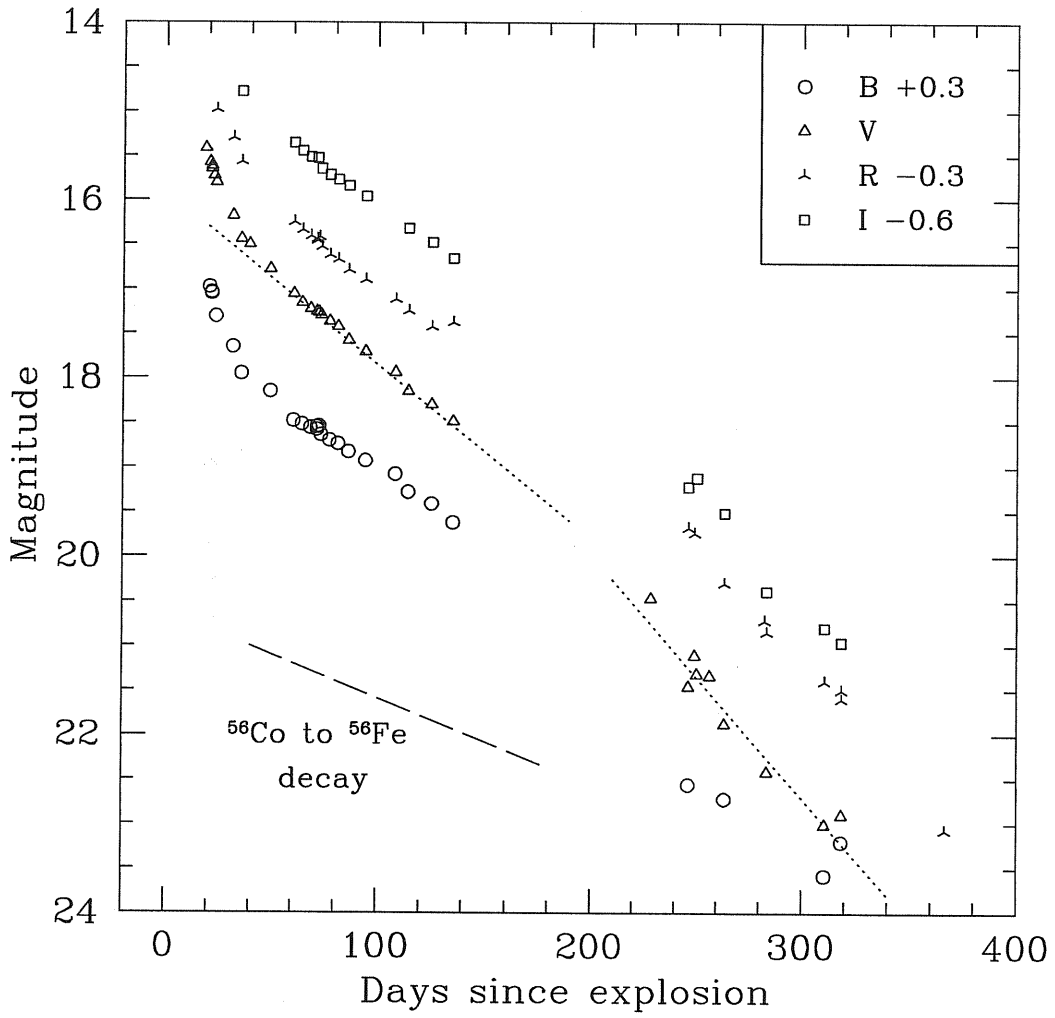

Figure 4.8: B, V, R, and I light curves of SN 1990I. The light curves have been shifted by the reported amounts. Also shown are the fits to the V-light curve tail (dotted lines) and as well the ^{56}Co to ^{56}Fe decay slope.

Table 4.2: Decline rates of SN 1990I. Data for events with two slopes at late times are also reported (see text for discussion).

Phase range (days)	γ_B mag $(100\ \mathrm{d})^{-1}$	γ_V mag $(100\ \mathrm{d})^{-1}$	γ_R mag $(100\ \mathrm{d})^{-1}$	γ_I mag $(100\ \mathrm{d})^{-1}$
[16 : 40]	6.2	5.6	4.78	– – –
[50 : 150]	1.53	1.92	1.77	1.7
[200 : 340]	1.2	2.7	2.6	2.6
The third to second phase decline slopes ratio :				
$\gamma_{[200:340]}/\gamma_{[50:150]}$(90I)	0.79	1.4	1.467	1.53
$\gamma_{[150:350]}/\gamma_{[45:150]}$(93J)	1.47	0.82	0.62	0.75
$\gamma_{[310:490]}/\gamma_{[40:330]}$(98bw)	0.86	0.56	0.78	0.745
$\gamma_{[t\geq 312]}/\gamma_{[t\leq 312]}$(96N)	– – –	$\sim$1.6	$\sim$1.4	– – –

In Figure 4.9 the absolute V light curve of SN 1990I is compared with other type Ib/c core collapse events. Table 4.3 summarizes the main parameters adopted for the selected sample. The figure reveals a strong similarity between SN 1990I and 1993J, from maximum to about day 230, with SN 1990I about 0.2 mag brighter. For SN 1990I a heliocentric velocity corrected for the Local Group infall onto the Virgo Cluster is 2751 km s^{-1} (as reported in the LEDA database) translates into $\mu \sim 32.97$. The maximum brightness is, on the other hand, quit comparable to those of SNe 1987M and 1994I and intermediate between the bright SNe 1999bw and 1991D and the faint SN 1983I. Moreover SNe 1990I, 1993J, 1991D and 1998bw decline from maximum with a similar rate to reach the exponential decay and indicate similar peak-to-tail contrast, whereas SNe 1983I, 1987M and 1994I display narrower peak widths and greater peak-to-tail contrast. The sample we are studying, although small, shows a correlation between the peak width and the peak-to-tail contrast. SN 1984L seems to be the extreme case of the sample, with the smaller peak-to-tail contrast and a possibly broader peak. The decline rate from maximum and the peak-to-tail contrast are computed and shown in Table 4.3 for events with well sampled early data. Interestingly, the events with steeper decline rates (i.e. narrow widths) and greater peak-to-tail contrast are classified as type Ic SNe, while the remaining events are type Ib. This is not surprising since the width and the way the light curve declines from maximum during this early phase of evolution are related to the progenitor star properties, namely the mass, radius, energy and the degree of mixing. These parameters, especially the ejected mass, controls the time the trapped decay energy takes to diffuse through the envelope (Ensman & Woosley 1988 [16]). In fact, for smaller mass the maximum is reached earlier because of larger radioactive heating and higher expansion velocity. The smaller the ratio "M_{ej}/E" and the closer the ^{56}Ni to the surface the faster the light curve declines (Shigeyama et al. 1990 [42]). One scenario for SNe Ic shows, indeed, that they originate from slightly smaller masses compared to type Ib objects (Yamaoka & Nomoto. 1991 [59]).

As discussed before, and except for SN 1984L, all the SNe of the sample decay, on the exponential tail, faster than ^{56}Co (short-dashed line in Figure 4.9). If we assume the V light curves trace approximately the bolometric ones, they all reflect smaller ejecta masses allowing greater $\gamma-$ray escape. After 230 d, SN 1990I deviates clearly from its previous slope and the deviation from the SN 1993J tail increases with time, approaching even the SN 1996N light curve. In fact, while around day 225 the SN 1990I light curve coincides with SN 1993J tail a deviation about 1.3 mag is measured around day 310.

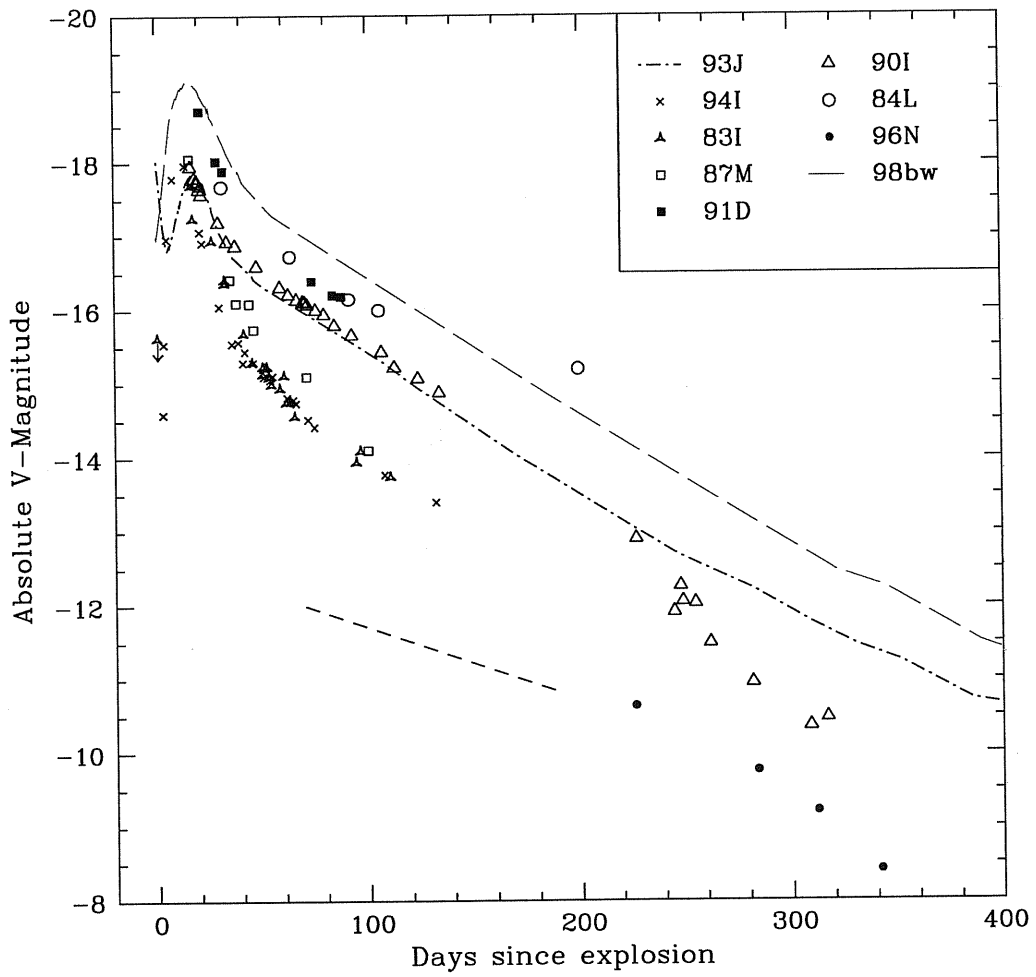

Figure 4.9: Comparison of the V absolute light curve of SN 1990I with those of other Ib/c events. The ^{56}Co to ^{56}Fe decay slope is shown (short-dashed line). The used parameters are reported in Table 4.3.

Table 4.3: Main parameters of the SNe sample.

SN name	SN type	Host galaxy	Distance (Mpc)	A_V (mag)	$\gamma_V^{\ddagger}$ (mag (100 d)$^{-1}$)	Max-to-tail contrast (mag)	References
1990I	Ib	NGC 4650	39.3*	0.4	∼5.7	∼1.05	this work
1983I	Ic	NGC 4051	13.17*	0.043	∼8.4	∼2.2	1, 2
1984L	Ib	NGC 0991	20.44*	0.0	– – –	– – –	3, 4, 5
1987M	Ic	NGC 2715	22.7*	1.3	– – –	– – –	6
1991D	Ib	PGC 84044	178.52*	0.186	– – –	– – –	7
1993J	IIb	M81	3.64	0.93	∼7	∼1.23	8
1994I	Ic	NGC 5194	8.32	1.4	∼11	∼2.42	9
1996N	Ib	NGC 1398	22	0.0	– – –	– – –	10
1998bw	Ic-Hypernova	ESO 184-G82	35.16*	0.2	∼6	∼1.64	11, 12, 13, 14

Refs:

1- Tsvetkov 1985[50]; 2- Tsvetkov 1988[52]; 3- Meikle et al. 1984[31]; 4- Buta 1984[6]; 5- Tsvetkov 1987[51];

6- Filippenko et al. 1990[17]; 7- Benetti et al. 2002[3]; 8- Lewis et al. 1994[27]; 9- Richmond et al. 1996[39];

10- Sollerman et al. 1998[43]; 11- Galama et al. 1998[23]; 12- McKenzie & Schaefer 1999[30]; 13- Patat et al. 2001 [35]; 14- Sollerman et al. 2000[44].

⋆ Estimated using "LEDA" database and adopting $H_0 = 70\ km\ s^{-1} Mpc^{-1}$.

‡ Early decline rate from maximum.

We note the rapid change seen in the $B-V$ colour evolution. Figure 4.10 reports the $B-V$ intrinsic colour of SN 1990I together with that of other type Ib/c events for comparison. $(B-V)_0$ of SN IIb 1993J is also shown (dashed line). The comparison indicates that SN 1990I follows a similar evolutionary trend as the other SNe, displaying a rapid reddening during the first 40 days, reflecting the cooling due to the envelope expansion. After a short duration peak it turns to the blue with a slope in the [40 : 120] days time range of about 0.43 mag $(100\ \mathrm{d})^{-1}$, similar to SNe 1984L, 1987M and 1991D, although it is about 0.2 mag bluer. At this epoch, SN 1993J exhibits a faster decline ($\sim$ 0.92 mag $(100\ \mathrm{d})^{-1}$). The colour peak, around day 40, corresponds to the beginning of the exponential radioactive tail in the V-absolute light curves (Fig. 4.9). Then in Fig. 4.10, the SNe settle on an almost *"plateau"* phase of long duration, well sampled for SNe 1993J and 1990I. Unfortunately, late observations of SNe 1987M and 1991D are not available, however late phase data of SNe 1984L and 1985F may indicate the presence of a plateau phase.

Again, the SN 1990I intrinsic $(B-V)$ colour displays a dramatic fall after day 245. It decreases by $\sim$0.8 mag in about 75 days. The time of this rapid and steep decline reflects the occurrence of the previously seen deviation in the V-absolute light curve. These facts point to the presence of a phenomenon able to cause a deficit in the optical light curves and also to cause the line profiles to be blueshifted in a short time ($\Delta t/t \sim 0.1$; Section 4.2.1). This rapid transformation of profiles during the nebular epoch has also been reported in SNe 1987A and 1999em, and when combined with a sudden increase in the decay rate of the optical light curves, it has been interpreted as an indication of dust formation. We believe that this the case for SN 1990I also. In fact, bearing in mind that dust condensation is expected to correlate with the cooling of the ejecta, we interpret the formation of dust earlier in SN 1990I compared to SNe 1987A ($\sim$530 d) and SN 1999em ($\sim$500 d) to be due to lower ejecta mass and rapid cooling for this event. It might also result from the higher metallicity content in the envelope of SN 1990I. SN 1987A shows a slight wiggle around day 550 in the optical colour evolution $(B-V)$ (Suntzeff & Bouchet 1991 [48]), that was interpreted as a blueing associated with dust formation, but was not so dramatic as demonstrated by SN 1990I. Such a blueing effect at the time of dust formation has been suggested by Lucy et al. (1989)[28] to result from increased albedo of the dust at shorter wavelengths.

4.3 Physical parameters estimate

In this section we construct the bolometric light curve of SN 1990I, and adopt a very simple model for radioactive powering. A reasonable fit to the data, especially during the initial part of the radioactive tail after the steep decline from the maximum brightness, provides quantitative insights on the basic parameters responsible for the bolometric light curve shape, namely the ejecta and ^{56}Ni masses.

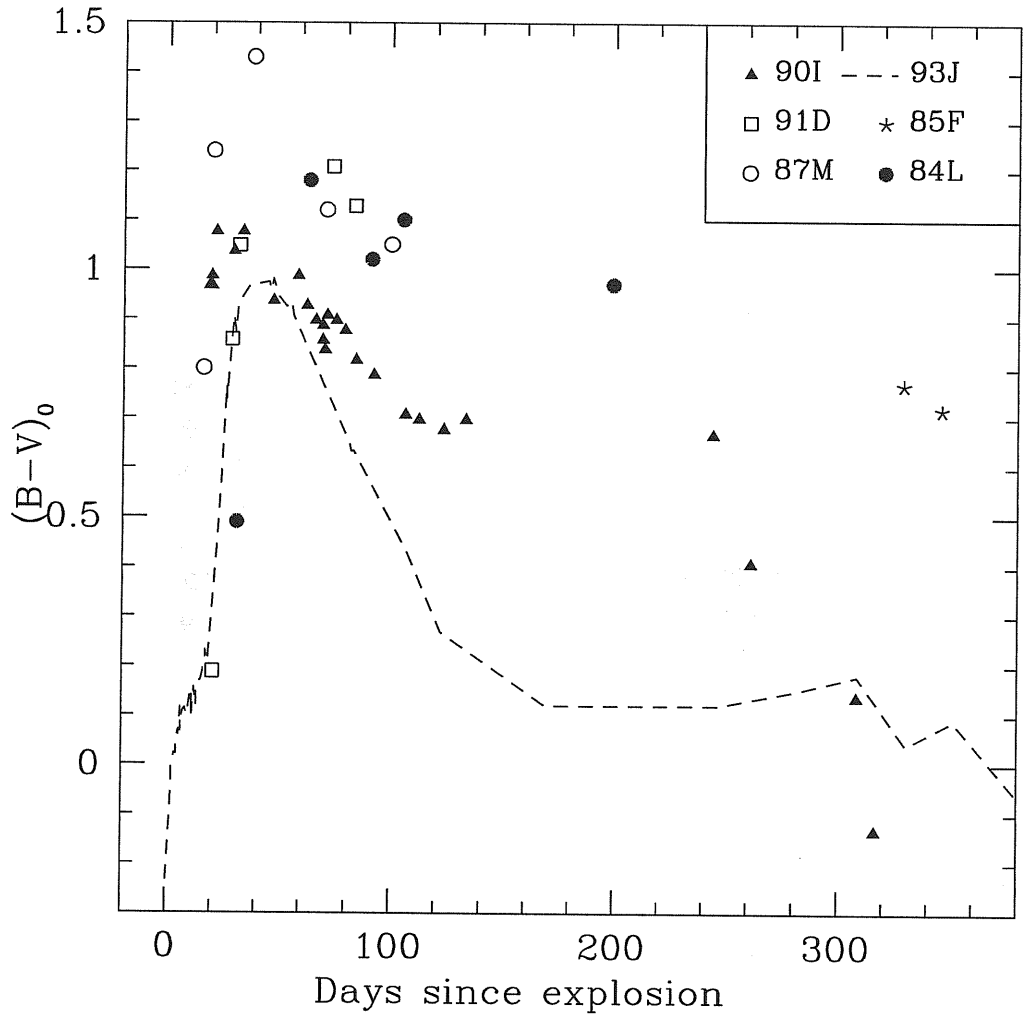

Figure 4.10: The evolution of the $B-V$ intrinsic colour of SN 1990I, compared to those of other Ib/c events. Adopted reddening for each event is reported in Table 4.3.

4.3.1 Bolometric light curve

In Figure 4.11 we present the "bolometric" light curve of SN 1990I together with that of SN 1993J ($UBVRI$; Richmond et al. 1994[38], 1996[39]) for comparison. The luminosities were computed by integrating the fluxes using the available photometric data bands. The conversion of the magnitudes to fluxes was carried out assuming the calibrations of Bessell (1979)[4]. The adopted parameters, i.e. distance and reddening, are reported in Table 4.3. The derived luminosities, however, should be corrected for the near-IR (JHK) fluxes. To account for this contribution, in the case of SN 1998bw, a fraction of 42% at day 370 was estimated to be added to the L_{BVRI} (Sollerman et al. 2002 [45]), whereas Patat et al. (2001)[35] have derived a fraction of about 35% on day 65.4. A fraction of about 50%, on the other hand, has been estimated around day 440 for SN IIP 1999em (Elmhamdi et al. 2003 [15]). Though not precise, in view of the possible increasing importance of the near-IR fraction with time (e.g. SN 1998bw; Sollerman et al. 2002 [45]), here we simply adopt 35% as a constant percentage contribution of the near-IR fluxes. The bolometric light curves of SN 1990I and 1993J shown in Figure 4.11 have been indeed scaled up to account for this constant contribution.

The constructed bolometric light curve of SN 1990I can be divided into three phases. *First phase* (the initial 40 days): although the rising part is not covered, the slow drop from the maximum compared to SN 1993J is confirmed. We note the similarity starting around day 30 with SN 1993J, not only in the decline rate but as well in the computed luminosity. Around day 20 SN 1990I was ~0.15 dex fainter. *Second phase* (the [50 : 200] days time interval): the light curve settles on the exponential decay tail, with a match with SN 1993J at least until day 100, whereas around day 130 SN 1990I seems to be $\sim$ 0.06 dex brighter. At this epoch, an e-folding time of 60 $\pm$2 days is measured, considerably faster than the one of ^{56}Co decay (i.e. 111.3 d), suggesting the γ-rays escape with decreased deposition, owing to the low mass nature of the ejecta. *Third phase* (after day 200): at this phase both SNe (1990I & 1993J) tend to behave differently. While SN 1993J flatten (e-folding time $\simeq$85 $\pm$2 d), SN 1990I shows the dramatic fall seen in the VRI broadband photometry (e-folding time $\simeq$47 $\pm$2.8 d).

The observed late time flattening in SN 1993J (and also in SN 1998bw) can be explained as due to the interaction of the ejecta with the circumstellar material (Sollerman et al. 2002 [45]), although for SN 1998bw Chugai (2000)[9] has found good agreement with observations adopting complete ^{56}Ni mixing and a higher matter density in the central part of the envelope. On the other hand, the sudden drop in luminosity after day 200 combined with spectral features in the case of SN 1990I point to dust condensation.

4.3.2 Simple γ-ray deposition model

The principal goal of the simple light curve modeling is to fit the bolometric behaviour starting at the transition phase (i.e. the early part of the radioactive decay tail) up to about 100 d. In the time range of interest, the contributions from radioactive elements other than ^{56}Ni and ^{56}Co are not taken into account, for the simple reason that the more

long-lived elements, like ^{57}Co, shown to be important at late phases (Woosley et al. 1989 [57]) are not sufficiently abundant to affect the light curves at day 100 (Danziger et al. 1991 [12]).

The model describes the luminosity evolution in an homologously expanding spherical ejecta with a point source γ-ray deposition from ^{56}Ni$\rightarrow^{56}$Co$\rightarrow^{56}$Fe. It is based on the simple approach adopted by Swartz & Wheeler (1991)[49] and Clocchiatti & Wheeler (1997)[10] when studying, respectively, the late time light curve of SN 1984L and type Ib/c SNe representative light curves. In fact, assuming free expansion of the ejecta ($v(r,t) = r/t$), a power law density distribution ($\rho(r,t) \propto r^{-n}(t)$) and a purely absorptive opacity (κ_γ) being constant throughout the ejecta, the equations for the mass, kinetic energy and γ-ray optical depth can be solved, giving rise to an expression for the total γ-ray optical depth relating the main physical parameters (Clocchiatti & Wheeler 1997 [10]):

$$\tau_\gamma = C\kappa_\gamma \times M_{ej}^2/E \times t^{-2} \tag{4.3}$$

where t refers to time since explosion and C is a constant depending on the density function. For a power index $n = 7$ we have $C \simeq 0.053$, adopted in our calculations. A typical value for the opacity, $\kappa_\gamma = 0.033\text{cm}^2\ \text{g}^{-1}$, is also assumed (Woosley et al. 1989 [57]).

Within this simplified picture, the emergent γ-ray luminosity, at a given time t, reads:

$$L(t) = L_0(t) \times [1 - exp(-\tau_\gamma(t))] \tag{4.4}$$

where $L_0(t)$ is the total γ-ray luminosity from radioactive decay.

In order to estimate L_0 at a given time, a compilation of the radioactive decay energy based on the properties of the ^{56}Ni$\rightarrow^{56}$Co$\rightarrow^{56}$Fe decay is needed. For this purpose, we adopt the main parameters presented by Jeffery (1999)[25] and Nadyozhin (1994)[32]. In this scheme the total released energy via γ-photons per ^{56}Ni decay is calculated to be 1.73 Mev, while the mean photon plus positron kinetic energy per ^{56}Co decay is computed to be 3.74 Mev. The positron fraction in energy is only about 3.5% of the total energy per ^{56}Co decay, while the neutrinos are assumed to escape the ejecta without any energy contribution (Jeffery 1999)[25].

Finally, we compute the total rate of radioactive energy production at a given time and combine it with equations 4.3 and 4.4, thus providing a general description of the simple radioactive decay energy deposition model in a spherical geometry. The model, although simple, might be a good indicator for ^{56}Ni and ejecta mass estimates, especially at the transition phase (i.e. in the [40 : 100] days time range).

Figure 4.11 displays the best fit of SN 1990I bolometric light curve (dotted line). Adopting, in fact, an energy $E(10^{51}\text{ergs}) = 1$, our best model fit indicates the following values: $M(^{56}Ni) = 0.11\ \text{M}_\odot$ and $M_{ej} = 3.7\ \text{M}_\odot$. The window in the figure displays the evolution of the fraction of the γ-ray luminosity deposited into the envelope corresponding to the best fit. Of course the model fit does not account for the late drop in luminosity, however it reproduces well the initial part of the radioactive tail. SNe 1990I and 1993J, in this context, seem to have similar ^{56}Ni ejected mass, whereas in view of

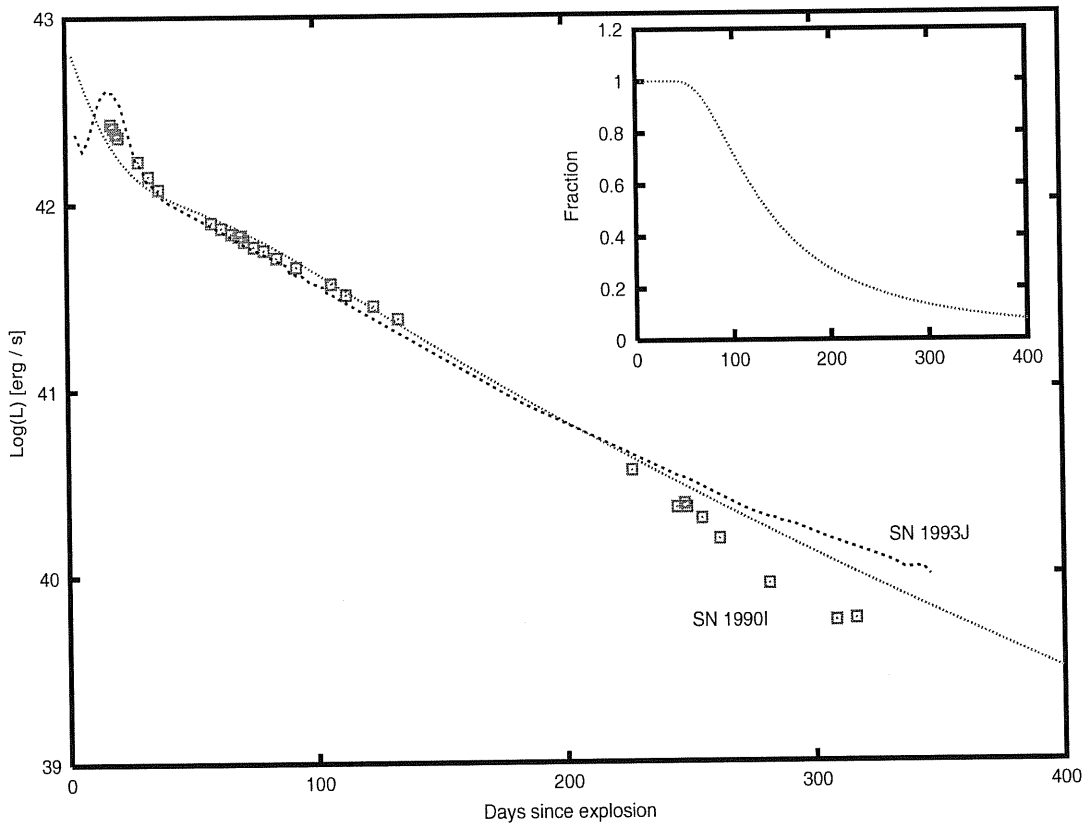

Figure 4.11: The computed $BVRI$ bolometric light curve of SN 1990I together with that of SN 1993J for comparison. SNe 1990I and 1993J luminosities are shifted upward to account for a JHK contribution of the order of 35%. The best fit with a simplified γ-ray deposition model from ^{56}Ni$\rightarrow^{56}$Co$\rightarrow^{56}$Fe is shown. It corresponds to $M_{ej} \sim 3.7$ $M_\odot$ and M(Ni)$\sim$ 0.11 $M_\odot$. The window displays the evolution of the fraction of the γ-ray luminosity deposited in the envelope corresponding to the best fit.

the slight difference in brightness in favour of SN 1990I in the [90 : 130] d time range, SN 1993J has a slightly smaller ejected mass ($\sim$ 3.4 $M_\odot$ from our best fit to SN 1993J data). The best fit parameters for SN 1993J are in good agreement with those from more complicated light curve calculations ($M(^{56}Ni) = 0.1 - 0.14$ $M_\odot$ and $M_{ej} = 1.9 - 3.5$ $M_\odot$; Young, Baron & Branch. 1995 [60])

We note, however, that owing to the observed higher velocity nature of SN 1990I compared to the Ib SNe sample of Branch et al (2002)[5], a higher kinetic energy might be anticipated though it is not, a priori mandatory. An adopted higher energy of about $E(10^{51}\text{ergs}) = 1.2$ can be compensated with a mass $M_{ej} \simeq 3.95$ $M_\odot$ to keep equal the γ-ray optical depth, in accordance with equation 4.3. Therefore, bearing in mind as well the possible uncertainties in the adopted parameters (i.e. distance and reddening), an ejected mass in the range [3 – 4.5] $M_\odot$ is possible.

4.4 Discussion and conclusions

We have presented and analysed photometric and spectroscopic data of SN 1990I, covering about 400 days of evolution. The classification of the SN as a Type Ib event discovered near maximum light is confirmed .

The optical He I lines are identified in the photospheric spectra of SN 1990I, displaying higher velocities compared to those derived, at similar epochs, from Branch et al. (2002)[5] type Ib sample. The high velocity nature of SN 1990I is confirmed first from photospheric velocities, inferred from Fe II lines, and second from comparing [O I] 6300,64 Å line profiles with those of SNe 1993J and 1998bw. The features in the $6000 - 6500$ Å range during the first 40 days, on the other hand, shows the presence of two absorption features near 6050 Å and 6250 Å . The possible identification of the 6250 Å trough with Hα may point to the presence of a thin hydrogen layer. Deeper investigation of these line identifications requires detailed synthetic spectra.

Entering the nebular phase, SN 1990I shows strong emission features of Mg I], Na I, [O I] and [Ca II], typical for type Ib/c SNe at late epochs. We note the presence of a depletion in the $[-2500 : 0]$ km s^{-1} region of the [O I] 6300,64 Å emission profile in the 315 d and 375 d spectra, which may point to large scale clumps in the oxygen ejecta at late phases.

The low mass of SN 1990I ejecta with respect to SN 1987A is obviously shown through the evolution of [Ca II] to [O I] flux ratio, although it must be kept in mind that in Ib/c SNe there is no hydrogen rich [Ca II] emitting zone as is the case for type II objects. We estimate a lower limit on the ejected oxygen mass to fall in the range $(0.7 - 1.35)$ M$_\odot$, although this estimate is subject to large uncertainties (i.e. density, temperature and fluxes). Clumping of the oxygen materials is indicated on the basis of two independent estimates of the density of oxygen.

The large asymmetry seen, especially, in the oxygen and calcium forbidden lines is a result of radioactive material being distributed asymmetrically. Furthermore we identify possible fine structures superimposed on the top of some strong emission lines. In fact, contrary to SN 1993J where some bumps have been identified on the [O I] 6300,64 Å and O I 5577 Å profiles with similar velocities, two fine structures, on day 107, are found to repeat in the Ca II 8662 Å and [Ca II] 7307.5 Å in SN 1990I. We interpret this to be an indication of different excitation conditions, in space and time, between SN 1990I and SN 1993J.

Interestingly, SN 1990I spectra in addition to asymmetric profiles, display a blueshift change during the time period from 254 d to 275 d ($\Delta t/t \sim 0.1$), seen clearly in the [O I] 6300,64 Å profile with a velocity of $\sim$600 km s^{-1}. Because of the presence of the depletion and poor S/N it is difficult to confirm the blueshift in the last two spectra. On the other hand, [Ca II] 7307.5 Å appears blueshifted at the last two epochs.

A photometric comparison of SN 1990I with other type Ib/c and IIb events, also demonstrates some peculiarities. During the early tail phase SN 1990I shows a decline rate similar to other SNe Ib/c, and faster than that of ^{56}Co decay, indicating a low mass

ejecta that allows the γ-rays to escape with lower deposition. Furthermore, light curves of SN 1990I show a marked change of slope. In fact, around day 230 the "V, R and I" light curves drop suddenly, while the B light curve tends to flatten. A comparison with events that show changes in slope is made introducing the third to second slope ratio as a measure of the how the SN changes its slope at late epochs. SN 1990I behaves in a completely different way compared to SN 1993J.

As a consequence the rapid and sudden drop is also seen in the colour evolution of SN 1990I, at an epoch similar to that of the already reported blueshift in the nebular lines. We interpret this rapid change, photometrically and spectroscopically, to be due to dust condensation in the ejecta of SN 1990I. The dust condensation at a time as early as $\sim$250 d could be due to the rapid cooling and low ejecta in SN 1990I compared to SN 1987A and SN 1999em which show evidence for dust formation around 530 d and 500 d, respectively.

We constructed the "*BVRI*" quasi-bolometric light curve, and compared it to that of SN 1993J, revealing a similarity in the [30 : 100] time interval. After 200 d, the two SNe evolve differently: while SN 1993J tends to flatten, SN 1990I falls dramatically. Then, in order to estimate physical parameters of the SN, we applied a simple γ-ray deposition model. The model allows us to estimate the ejecta and ^{56}Ni masses ($M(^{56}Ni) = 0.11$ M$_\odot$ and $M_{ej} = 3.7$ M$_\odot$).

The sudden fall in luminosity at day 230 results from the fact that the light curve in Fig. 4.11 is not a real bolometric light curve. After day 230 the dust absorbs at shorter wavelengths and re-emits at much longer IR wavelengths, consistent with the dust having an ambient temperature which is probably lower than 1500 K and decreasing with time. This contribution of IR radiation from the dust has not been included. What remains to be understood, however, is why dust has formed in SN 1990I but has not been recorded in other Type Ib/c. Possibly inadequate sampling of light curves and spectra of Type Ib/c at nebular phases is at least partially responsible.

Bibliography

[1] Barbon R. et al. 1990, A&AS, 237, 79

[2] Baron E. 1992, MNRAS, 255, 267

[3] Benetti S., Branch D., Turatto M. et al. 2002, MNRAS, 336, 91

[4] Bessel M. S. 1979, PASP, 91, 589

[5] Branch D., Benetti S., Kasen D. et al. 2002, ApJ, 566, 1005.

[6] Buta R. 1984, IAU Circ., No.3981

[7] Cardelli J. A., Clayton G. C. & Mathis J. S. 1989, ApJ, 345, 245

[8] Chugai N.N. 1994, ApJ, 428, 17

[9] Chugai N. N. 2000, AstL, 26, 797

[10] Clocchiatti A. & Wheeler J. C. 1997, ApJ, 491, 375

[11] Danziger I.J., Bouchet P., Gouiffes C., Lucy L.B. 1989, IAUC 4746

[12] Danziger I.J., Lucy L. B., Bouchet P., Gouiffes C. 1991, in *Supernovae*, p. 69, ed. Woosley S. E., Springer-Vergal, New York.

[13] de Kool M., Li H. & McCray R. 1998, ApJ, 503, 857

[14] Deng J. S., Qiu Y. L., Hu J. Y., Hatano K. & Branch D. 2000, ApJ, 540, 452

[15] Elmhamdi A., Danziger I. J., Chugai N. N. et al. 2003, MNRAS, 338, 939

[16] Ensman L. M. & Woosley S. E. 1998, ApJ, 333, 754

[17] Filippenko A. V., Porter A. C. & Sargent W. 1990, AJ, 100, 1575

[18] Filippenko A. V. 1997, ARA&A, 35, 309

[19] Fransson C., 1987, in ESO Workshop on "*the SN 1987A*", Garching, European Southern Observatory, p. 467

[20] Fransson C., Chevalier R. A. 1987, ApJ, 322, 15

[21] Fransson C., Chevalier R. A. 1989, ApJ, 343, 323

[22] Fransson C. et al. 1993, in "*Supernova and Supernova remnants*", MCCRAY and WANG, Xian, China, Colloquium 145 p.211

[23] Galama T. J. et al. 1998, Nature, 395, 670

[24] Houck J. C. & Fransson C., 1996, ApJ, 456, 811

[25] Jeffery D. J. 1999, Astro-ph/9907015.

[26] Leibundgut B. et al, 1991, ApJ, 372, 531

[27] Lewis J. R. et al. 1994, MNRAS, 266, 27

[28] Lucy L. B., Danziger I.J ., Gouiffes G., Bouchet P., 1989, In "*Structure and dynamics of the Interstellar Medium*", ed. G. Tenorio-Tagle et al., IAU Colloquium No. 120 (Springer-Verlag), p.164

[29] Lucy L. B. 1991, ApJ, 383, 308

[30] McKenzie E. H. & Schaefer B. E. 1999, PASP, 111, 964

[31] Meikle W. P. et al. 1984, IAU Circ., No.4003

[32] Nadyozhin D. K. 1994, ApJS, 92, 527

[33] Nomoto K., Filippenko A. V. & Shigeyama T. 1990, A & A, 240

[34] Nomoto K., Maeda K., Nakamura T. et al. 2000, hgrb.symp, 622

[35] Patat F. et al. 2001, AJ, 555, 900

[36] Phillips M. M. 1990, IAUC.5032.

[37] Pizarro O., Miranda J., Pasquini L. et al. 1990, IAUC.5003.

[38] Richmond M. W. et al. 1994, AJ, 107, 1022

[39] Richmond M. W. et al. 1996, AJ, 112, 732

[40] Schlegel E. M. & Kirshner R. P. 1989, AJ, 98, 577

[41] Schlegel D. J., Finkbeiner D. P. & Davis M. 1998, 500, 525

[42] Shigeyama T., Nomoto K., Tsujimoto T., Hashimoto M. 1990, ApJ, 361, 23

[43] Sollerman J., Leibundgut B. & Spyromilio J. 1998, A&A, 337, 207

[44] Sollerman J. et al. 2000, ApJ, 537, 127

[45] Sollerman J. et al. 2002, A&A, 386, 944

[46] Spyromilio J. & Pinto P. A. 1991, In Proc. *ESO/EPIC* Workshop on "*SN 1987A and other Supernovae*", p. 423, ed. Danziger I. J., ESO, Munich.

[47] Spyromilio J. 1994, MNRAS, 266, 61

[48] Suntzeff N. B. & Bouchet P. 1991, In *Supernovae*, p. 12, ed. Woosley S. E., Springer-Vergal, New York.

[49] Swartz D. A. & Wheeler J. C. 1991, ApJ, 379, 13

[50] Tsvetkov D. Y. 1985, Astron.Zhur., 62, 365

[51] Tsvetkov D. Y. 1987, PAZh, 13, 894

[52] Tsvetkov D. Y. 1988, Perem. Zvezdy, 22, 653

[53] Tutukov A. V. & Chugai N. N. 1992, SvAL, 18, 242

[54] Uomoto A. 1986, ApJ, 310, 35

[55] Wheeler J. C. et al. 1987, ApJ, 313, 69

[56] Wheeler J. C. & Harkness R. P. 1990, Rep. Prog. Phys., 53, 1467

[57] Woosley S. E., Hartmann D., Pinto P. A. 1989, ApJ, 346, 395

[58] Woosley S. E., Eastman R. G. & Schmidt B. P. 1999, ApJ, 5167, 88

[59] Yamaoka Y. & Nomoto K. 1991, In Proc. *ESO/EPIC* Workshop on "*SN 1987A and other Supernovae*", p. 193, ed. Danziger I. J., ESO, Munich.

[60] Young. T. R., Baron E. & Branch D. 1995, AJ, 449, 51.

Chapter 5

Conclusions

5.1 Summary of results

In this study we have presented spectra and photometry of core collapse SNe spanning different epochs of evolution. Various effects, imprinted on the spectra and light curves, have been discussed and their physical interpretations are given. In what follows I summarize the main results of this dissertation:

- **Observations:**

The well sampled data of SN 1999em, the best observed type IIP after SN 1987A, are presented and analysed. The quality of the spectra, optical and infrared, provides an opportunity to look deeper in the composition of the ejecta as the SN ages. The presence of He I 5876 Å in the early-time spectra can be indicative of helium enhancement, similar to what was seen in SN 1987A. However, the origin of these helium lines at this early phase remains unknown. During the photospheric phase, the identified lines are typical in type IIP events (prominent Hα P-Cygni profile). The nebular phase spectra, on the other hand, display clear evidence for Na I, [O I], Hα, [Ca II], O I and Ca II lines. Interestingly, the [Ca II] 7392,7324 Å doublet is unusually dominating over Hα in the +465, +510 and +642 days spectra. This fact has not been reported in the well sampled event SN 1987A. Indeed, even at very late-time, e.g. +606 and +718 days spectra, SN 1987A displays a dominating Hα compared to [Ca II] 7392,7324 Å line. This particular behaviour of SN 1999em still requires an explanation, while in SN 1987A Li & McCray (1993 ApJ, 405, 730) showed that the strength of Ca II features could be explained without requiring newly synthesized calcium. The two available infrared spectra, at +20 and +440 days, are combined with similar phase optical ones to get extended "*bolometric*" spectra. We argued for the presence of the He I 10830 Å line, blended with Pγ, in the +20 spectrum. This early evidence of He I 10830 Å line may be a result of of the non-thermal excitation due to the presence of ^{56}Ni in the outer layers of the ejecta.

We have analysed as well the photospheric and nebular spectra of SN 1990I. We

clearly identified the presence of optical helium lines in the photospheric phase spectra. The Ca II IR triplet is the most prominent feature at this epoch. The photospheric velocity, inferred from Fe II 5169 Å line, is found to be greater with respect to values derived from a SNe Ib sample. At the nebular phase, the prominent features are due to Mg I], Fe II, [Fe II], Na I, [O I] and [Ca II] lines.

Photometrically, we study the broad-band light curves of SNe 1999em and 1990I. Their absolute V−light curves are compared with a selected sample of type IIP and type Ib/c, respectively. The colour evolution is described, and the pseudo-bolometric light curves are recovered, allowing us to estimate the ^{56}Ni and ejecta masses. Furthermore, the constructed *"pseudo − bolometric"* light curves show deviations at late epochs, more dramatic in SN 1990I than in SN 1999em, that we interpret as a consequence of dust condensation in their ejecta.

Furthermore, the available observations were used to determine the distance to SN 1999em and its explosion time by means of the "EPM". The derived results are in good agreement with what was found by other studies.

• **Asymmetry and clumping:**

SN IIP 1999em reveals clear indications for asymmetry and clumping in its spectra. The complicated structure of the Hα profile at the photospheric phase, reminiscent of the "Bochum event" in SN 1987A, has been discussed, indicating real asymmetry of the hydrogen excitation owing to the mixing and clumping of radioactive material into the outer envelope. This was, in fact, analysed in terms of two models: 1. two-sided ^{56}Ni jets, 2. one-sided ^{56}Ni ejection combined with a non-monotonic behaviour of the Hα optical depth. The second case is found to be supported by the red shift seen in both Hα and He I 10830 Å at the nebular phase. We propose that SN 1999em is similar to SN 1987A in the way the ^{56}Ni is distributed, namely biased to one side with more in the far hemisphere.

SN 1990I, a type Ib event, is as well found to show evidence for asymmetry and clumping. This is clearly indicated, first from two independent estimates of the oxygen material density (a filling factor $\geq 10^{-2}$), and second by the presence of some fine structures. The large asymmetry results from the mixing and the non-uniform distribution of the radioactive material.

The study of these two events, i.e. SNe 1999em and 1990I, provides further observational indications of asymmetry and clumping effects in core collapse SNe.

• **Nucleosynthesis and yields:**

The general belief about the ^{56}Ni production in type II SNe, i.e. all eject $\sim 0.07\ M_{\odot}$, is really changed by the emergence of the extremely faint and bright events. In fact, analyzing a selected sample of type IIP SNe, we derive a large range in the synthesized ^{56}Ni mass (i.e. $[0.003 - 0.13]\ M_{\odot}$). This has been done using SN 1987A radioactive tail as a template to fit the sample SNe late photometry. We adopt a simple method to estimate the ejected oxygen mass in this class of objects (Appendix A). The oxygen

and iron yields in type IIP SNe are then compared with similar element yields from type Ib/c SNe by means of the oxygen over iron ratio.

• **Progenitors:**

Understanding the progenitor star properties (i.e. nature, evolution & explosion mechanisms) is surely one of the hottest topics in SNe field. We found different observational facts that tend to reinforce the idea of type IIP SNe having massive ejected envelopes compared for example to type Ib/c events. In particular two properties are highly indicative when analysing type IIP sample: 1. the plateau phase duration which reflects the time taken by the hydrogen recombination wave to move, inward in mass, and hence indicates massive ejecta ($\sim 8\ M_{\odot}$), 2. during the tail phase, SNe IIP have a decline rate close to the ^{56}Co $e-$folding time, indicative of massive envelopes able to trap the $\gamma-$rays. The contrary is seen in type Ib/c photometry, namely a short duration peaks and faster decline rates, reflecting the smaller ejecta masses with greater $\gamma-$ray escape. In fact various derived pieces of evidence indicated that SN 1999em had a main sequence progenitor mass of $11-14\ M_{\odot}$. Further indications about the progenitor natures of core collapse SNe could be provided by the "$[O/Fe]$ .vs. M_{ms}" plot (Appendix A), although at present these determinations suffer from different sources of uncertainties, not least of which is the still arbitrary choice of mass-cut (or fall back) in theoretical models.

• **Dust formation:**

Following the evolution of SN 1999em, spectroscopically and photometrically, we argued for dust condensation in its ejecta around day 500. It is the second case of dust formation after SN 1987A, showing distinctive characteristics in manifesting the same phenomenon. The main differences can be summarized as follows: 1. dust in SN 1999em condenses earlier than in 1987A. This can be due to the lower ^{56}Ni mass and, accordingly, lower temperature earlier in SN 1999em. 2. a clear cut difference is the demonstrated large optical depth of the dusty zone in SN 1999em ($\tau \gg 10$) with respect to SN 1987A ($\tau \sim 0.5$), which may possibly result from the more homogeneous distribution of dust or be due to the greater number of the opaque dusty clumps in SN 1999em.

We interpret as well the detected rapid transformation in some nebular line profiles, especially the [O I] 6330,64 Å line, as indicative of dust formation in the ejecta of SN 1990I around day 250. This finding is supported by the dramatic fall in luminosity and the $(B-V)$ colour evolution. We believe this is the first event belonging to type Ib/c SNe that shows evidence for dust condensation in its ejecta. This may be due only to inadequate sampling of spectra and light curves at nebular phases. Deeper investigations are needed once we possess high quality and well covered type Ib/c samples.

• **Correlations:**

Different correlations are found throughout the present work. Improved statistical samples and better sampled data are surely needed to have a firmer confirmation of these correlations. They can be summarized as follows: 1. a "second plateau" feature is seen in some faint IIP objects (i.e. SNe 1999em, 1991G, 1997D and 1999eu) immediately after the steep decline from the main plateau phase. A correlation is hinted at between the

duration of this behaviour and the amount of the ejected ^{56}Ni: the lower is the ^{56}Ni mass the longer is the "second plateau" duration. 2. we confirm and quantify the correlation found first by Hamuy (2003) between the absolute plateau V−magnitude and the ^{56}Ni mass in type IIP SNe. A consequent correlation between the plateau and the radioactive tail magnitudes (apparent or absolute) is given after introducing two new parameters namely, the steepness and the inflection time. 3. the Hα luminosity is found to be a good indicator of the ejected ^{56}Ni mass in SNe IIP at the nebular phase. Using then the SN 1987A Hα luminosity as a template in the $200 - 400$ d time range, it is possible to recover the amount of the ejected ^{56}Ni within an uncertainty of $\sim$20%. 4. the steepness is found to anticorrelate with the ^{56}Ni mass in type IIP events. This provides an unique possibility, independent of the adopted distance and extinction, to determine the ^{56}Ni mass from the light curve shape. 5. a correlation between the peak-to-tail contrast and the peak width in type Ib/c SNe light curves is hinted, and if confirmed it may provide a light-curve-shape-based classification to differentiate type Ib SNe from Ic events.

These kinds of analyses demonstrate how large sample analyses in SNe studies can provide robust results and correlations with their consequent impact for our understanding of SNe physics.

5.2 Future plans

My research plan and interest is mainly addressed to the study and analysis of Core Collapse SNe (CCSNe; II and Ib/c SNe), both photometrically (multi-bands and bolometric) and spectroscopically. Studying these events is interesting in many aspects, namely to test our understanding of the nature of their progenitors and whether for example there is a correlation between the progenitor nature (e.g. mass, radius) and evolution (e.g. mass loss, binary systems) on one side and the classification on the other side as it is indicated by the presence (or not) of helium or even hydrogen lines in Ib SNe (Ic).

I am planning to devote part of my time to make a more detailed study on IIP SNe, since we have had recently an understanding with Mario Hamuy (Carnegie Observatories) for a collaboration and the use of his unpublished data base (both photometry and spectroscopy) to enlarge our SN IIP sample. In principle, the extended sample analysis will be dedicated to check and test the recent correlations found for this class of events (A. Elmhamdi, N. N. Chugai and I. J. Danziger. 2003, A&A, 404, 1077), displaying a high degree of homogeneity making them promising as cosmological probes. Furthermore such a study will allow us to enlarge on the subject of whether there are two groupings of SN IIP with and without fall-back, giving respectively small and large iron production.

Another important issue concerns features in the $6000 - 6500$ Å region of the early spectra in Ib/c SNe. Indeed one may argue for the presence of Hα indicating a thin hydrogen layer above the helium layer with high velocity which disappears or is overwhelmed by C II 6580 Å as Hα optical depth decreases as a consequence of the envelope expansion. The presence of Hα at early phases in the spectra of Ib SNe is an interesting

point to treat.

An additional interesting point investigate at as well for these classes of events (CC-SNe: II and Ib/c) is the amount of oxygen produced by the explosion. This will provide a deeper view of the oxygen to iron ratios in these objects and how it changes as a function of the type of SN and hence make a possible classification on the basis of this yield. One may study the impact of these yields on the chemical evolution models of galaxies, especially for metal-poor halo stars which are heavily dependent on theoretical nucleosynthesis yields of CCSNe. Although in the present work we give preliminary results concerning this issue (Appendix A), we believe that deeper and more accurate investigations are needed to draw conclusions concerning both absolute and ratio yields of oxygen and iron peak elements.

Appendix A

Oxygen yields in Core Collapse SNe

(Possible diagnostics for the future.)

As discussed previously in Chap. 2, we adopt the simple approach used to estimate the ejected oxygen mass of SN 1999em for a sample of type IIP supernovae. The sample's main parameters are reported in Table 3.1 (Chap. 3). In Fig. A.1 we report the measured [O I] 6300,64 Å luminosities of the sample. The spectra have been corrected for reddening and have been flux calibrated with the photometry (when needed).

The method is based on the fact that the luminosity of [O I] doublet at the epoch of $\sim$ 1 year is powered by the γ-ray deposition and by ultraviolet emission arising from the deposition of γ-rays in oxygen-poor material. One may write the [O I] doublet luminosity as:

$$L([\text{O I}]6300,64) = \eta \frac{M_{\text{O}}}{M_{\text{ex}}} L(^{56}\text{Co}), \tag{A.1}$$

where M_{O} is the mass of oxygen, M_{ex} is the "excited" mass in which the bulk of radioactive energy is deposited, and η is the efficiency of transformation of the energy deposited in oxygen into the [O I] doublet radiation. L(^{56}Co), on the other hand, refers to the radioactive decay energy input ($L = L_0 \times (M_{\text{Ni}}/M_{\odot}) \text{e}^{-t/\tau_{\text{Co}}}$, with $L_0 \simeq 1.32 \times 10^{43}$ ergs s^{-1} and $\tau_{\text{Co}} = 111.23$ d).

Assuming that all supernovae have similar η and M_{ex} (which may not be precise), we derive rough estimates of the oxygen mass for the events of the sample adopting [O I] 6300,64 Å light curve of SN 1987A as template. The oxygen mass in SN 1987A is estimated to be in the range $1.5 - 2\ M_{\odot}$ (Fransson & al. 1993 [3]; Chugai 1994 [2]).

In Table A.1 we report the amounts of the ejected oxygen mass derived adopting the simple approach described above. The range for each reflects only the range for the template SN 1987A. Clearly a larger uncertainty must obtain owing to the simplicity of the assumed model.

We compute the [O/Fe][1] yield for each IIP event. A value about $log_{10}(O/Fe)_{\odot} = 0.82$ dex, taken from Anders & Grevesse (1989)[1], is adopted. The recovered amounts are reported in Figure A.2 (horizontal lines) as function of the initial mass according to the

[1] $[A/B] = log_{10}(A/B)_{\star} - log_{10}(A/B)_{\odot}$

Table A.1: ^{56}Ni and oxygen mass estimates.

SN name	$M_{\rm Ni}^{\ddagger}$ ($M_\odot$)	$M_{\rm Oxy}$ ($M_\odot$)
1987A	0.075	$1.5 - 2$
1988A	0.088	$1.02 - 1.35$
1988H	0.033	$0.79 - 1.07$
1990E	0.043	$0.94 - 1.3$
1991G	0.021	$0.36 - 0.49$
1992H	0.123	$1.10 - 1.46$
1997D(a)	0.0065	$0.92 - 1.24$
1997D(b)	0.0036	$1.32 - 1.77$
1999em*	0.027	$0.4 - 0.55$

‡ From Table 3.2 (Chap. 3).

* We are using 8.8 Mpc as distance (See Chap. 3)

core collapse SN models by Woosley & Weaver 1995 [8] (long dashed line), Thielemann, Nomoto & Hashimoto 1996 [7] (short dashed line) and Nomoto et al. 1997 [5] (dotted line). Also plotted in Fig. A.2 are the [O/Fe] estimates for SNe 1984L(Ib), 1990I(Ib), 1993J(IIb) (Chap. 3) and a typical value of about $[O/Fe] \simeq -0.37$ dex argued from photometric data modeling of SNe 1983I(Ic) and 1983N(Ib) by Shigeyama et al. (1990)[6].

The shaded box in Fig. A.2 defines the concentration region (within errors) of type IIP objects (except for SN 1997D). This zone provides constraints on the progenitor mass of type IIP. According to Thielemann, Nomoto & Hashimoto (1996)[7] and Nomoto et al. (1997)[5] models, one obtains a progenitor mass range of $16 - 23\ M_\odot$, while Woosley & Weaver (1995)[8] model gives higher masses, especially for $[O/Fe] \geq 0.4$ dex. SN 1997D, on the other hand, is clearly deviating from the location of *"normal"* type IIP SNe. We expect 97D–like SNe (i.e. very faint objects like SNe 1999br & 1999eu) to cluster closer to SN 1997D location, indicating the high mass nature of their progenitors. These events could be the condidates for black hole formation due to a significant fallback.

Furthermore, an important issue that one may read out from Fig. A.2 is that the reported type Ib/c are found to be located at the bottom of type IIP SNe. Within the core collapse models of type Ib/c SNe, two scenarios are argued: *first* a high mass star ($M_{ms} \geq 35\ M_\odot$) exploding as Wolf-Rayet star after an episode of strong stellar wind, and *second* a less massive stars ($M_{ms} \sim 13 - 18\ M_\odot$) in binary systems. The position of type Ib/c events in the "$[O/Fe]$ *.vs.* M_{ms}" plot, according to Fig. A.2, could therefore be taken as an observational support of the intermediate massive stars in binary systems being favoured as progenitors of this class of objects. A typical value for type Ia SNe is as well reported (Nomoto et al. 1984[4]), which shows the nature of type Ia SNe being iron producers. The oxygen mass alone should in principle act as a diagnostic of progenitor mass. Table A.1 therefore does not indicate the same trend as suggested by the O/Fe

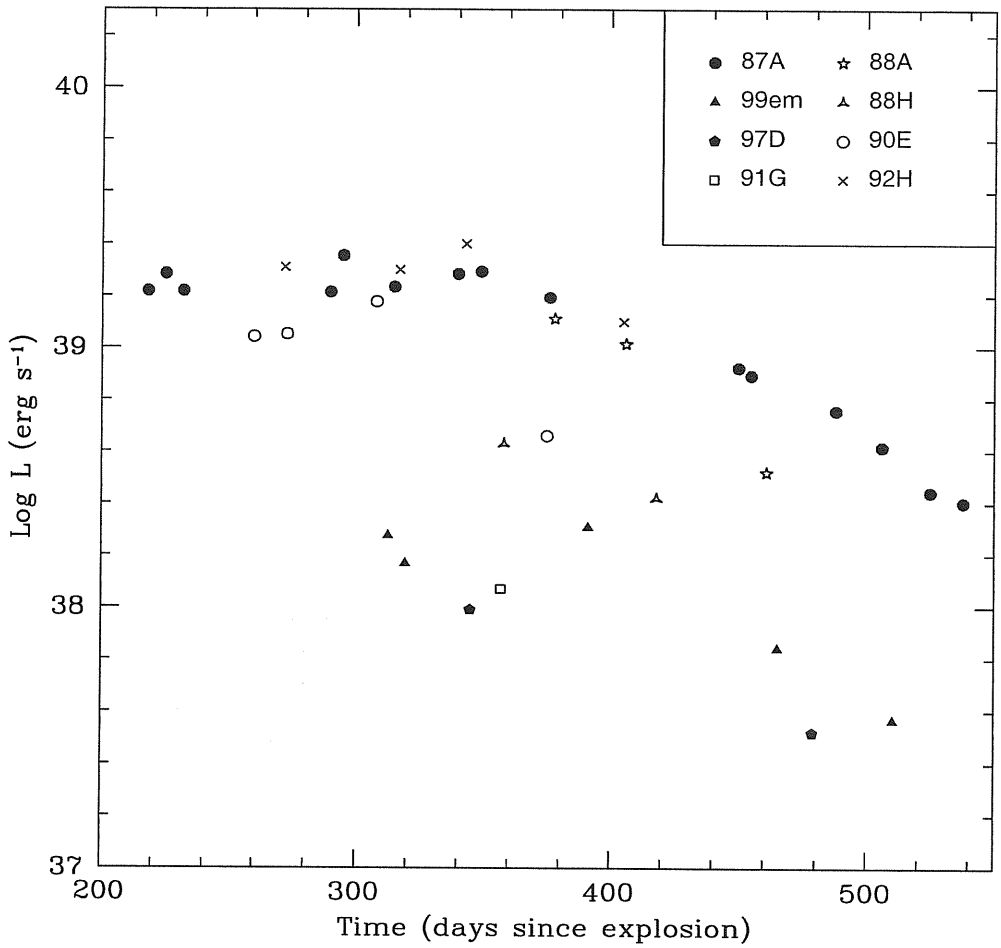

Figure A.1: The temporal evolution of the [O I] 6300,64 Å luminosity. The adopted parameters are reported in Table 3.1 (Chapter 3).

yields. This undoubtedly reflects the large uncertainties in the oxygen masses.

Although the uncertainties in the determination of oxygen yields, both in type IIP and Ib/c events, make present correlations unreliable, Fig. A.2 provides a way to elucidate the progenitor nature of core collapse SNe. However, extended samples and more reliable determinations of oxygen abundances are clearly needed to draw more accurate conclusions and deeper view on the oxygen to iron ratio and how it changes as function of the type of SN.

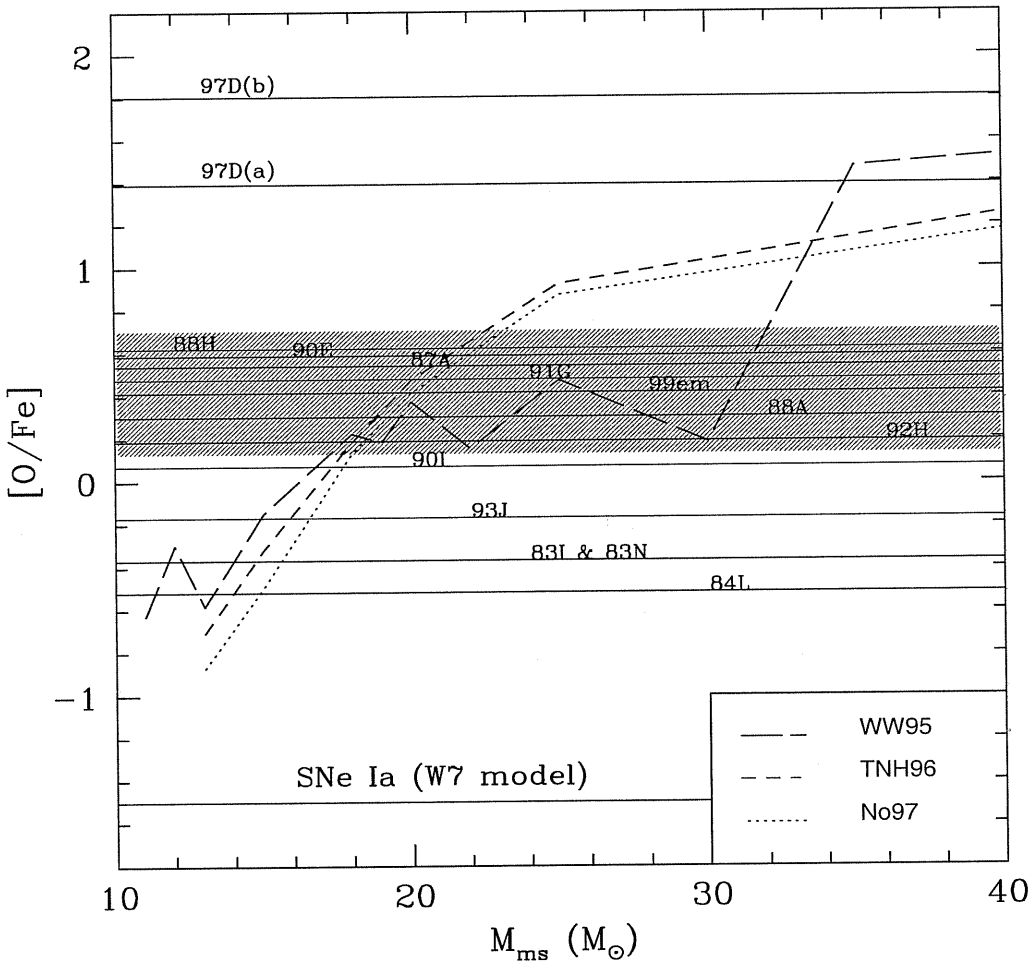

Figure A.2: The [O/Fe] ratio as a function of the initial mass according to the models by Woosley & Weaver 1995 (long dashed line), Thielemann, Nomoto & Hashimoto 1996 (short dashed line) and Nomoto et al. 1997 (dotted line). The estimated [O/Fe] yields for core collapse SNe are also shown (continuous horizontal lines). Typical value for thermonuclear SNe is also reported for comparison [4]

References

[1] Anders E. & Grevesse N. 1989, Geochimica et cosmochimica Acta, 53, 197

[2] Chugai N.N. 1994, ApJ, 428, 17

[3] Fransson C. et al. 1993, in Supernova and Supernova remnants, MCCRAY and WANG, Xian, China, Colloquium 145 p.211

[4] Nomoto K. et al. 1984, ApJ, 286, 644

[5] Nomoto K. et al. 1997, Nucl. Phys., A161, 79c13

[6] Shigeyama T., Nomoto K., Tsujimoto T., Hashimoto M. 1990, ApJ, 361, 23

[7] Thielemann F.K., Nomoto K. & Hashimoto M. 1996, ApJ, 460, 408

[8] Woosley S.E. & Weaver T.A., 1995, ApJ, 101, 181